2011-04-12

Fluorescence Switching with Photochromic Oxazines

Erhan Deniz
University of Miami, denizerhan@yahoo.com

UNIVERSITY OF MIAMI

FLUORESCENCE SWITCHING WITH PHOTOCHROMIC OXAZINES

By

Erhan Deniz

A DISSERTATION

Submitted to the Faculty
of the University of Miami
in partial fulfillment of the requirements for
the degree of Doctor of Philosophy

Coral Gables, Florida

May 2011

UNIVERSITY OF MIAMI

A dissertation submitted in partial fulfillment of
the requirements for the degree of
Doctor of Philosophy

FLUORESCENCE SWITCHING WITH PHOTOCHROMIC OXAZINES

Erhan Deniz

Approved:

_____ Françisco M. Raymo, Ph.D. Professor of Chemistry	_____ Terri A. Scandura, Ph.D. Dean of the Graduate School
_____ Vaidhyanathan Ramamurthy, Ph.D. Professor of Chemistry	_____ Angel E. Kaifer, Ph.D. Professor of Chemistry
_____ Anthony J. Hynes, Ph.D. Professor of Marine and Atmospheric Chemistry	

ERHAN DENIZ (Ph.D., Chemistry)
Fluorescence Switching with Photochromic Oxazines. (May 2011)

Abstract of a dissertation at the University of Miami.

Dissertation supervised by Professor Françisco M. Raymo.
No. of pages in text. (136)

Fluorescence microscopy offers the opportunity to image noninvasively biological samples in real time. However, the phenomenon of diffraction limits the resolution of conventional fluorescence microscopes to submicrometer dimensions in both the horizontal and vertical directions. This limitation can be overcome by photoswitchable fluorescent probes able to undergo reversible saturable optically linear fluorescence transitions (RESOLFT).

In this study, firstly, a photoswitchable fluorescent probe based on BODIPY fluorophore and Spiropyran photochrome were designed and its photophysical and photochemical properties were investigated in organic and aqueous environments. Also, its imaging with patterned illumination was showed by trapping them in PMMA matrix.

Secondly, photochromic [1,3]oxazines with different substituents as well as polymers incorporating them were synthesized and their photochemical and photophysical properties were investigated.

Thirdly, to improve the switching speeds and fatigue resistance of the BODIPY-Spiropyran conjugate, the photochromic part was replaced by [1,3]oxazines and dyads incorporating BODIPY fluorophore and [1,3]oxazine photochromes were synthesized.

Lastly, a new strategy was designed to switch the fluorescence of fluorophores by a modular approach. It is based on photoinduced elongation of the absorption wavelength of a fluorescent chromophore with the aid of an appended photochromic auxochrome.

To my family.

Acknowledgements

First of all, I would like to thank my research advisor, Professor Françisco M. Raymo, for his support, advice and infinite patience throughout these productive years.

I thank the members of my committee, Professor Angel Kaifer, Professor Vaidyanathan Ramamurthy and Professor Anthony J. Hynes for their valuable time.

I wish to thank Professor Engin Akkaya, my previous professor for his encouragement to pursue a Ph.D. in Chemistry.

I would like to thank Dr. Salvatore Sortino for his laser flash photolysis measurements

I would also like to extend my gratitude to my friends and colleagues, Massimiliano Tomasulo, Ibrahim Yildiz, Janet Cusido, Stefania Impellizzeri and Mutlu Battal for all their help and cooperation. Special appreciation goes to the faculty and staff of the Department of Chemistry.

Lastly, I offer my regards and blessings to all of those who supported me in any respect during the completion of this thesis.

TABLE OF CONTENTS

List of Tables and Figures

CHAPTER 1

FLUORESCENT SWITCHES BASED ON PHOTOCHROMIC COMPOUNDS

1.1. Photochromism

1.1.1. History and Definitions.

The term "photochromism" was introduced in the early 1950's to indicate the photoinduced and reversible change in color of certain compounds.[1] Since then, the number of publications on photochromism has increased exponentially and, eventually, this area has evolved into a mature and active research field.[2–6] Indeed, numerous families of photochromic compounds have been developed and investigated over the past five decades and their unique properties have led to the realization of a diversity of photochromic materials for various applications.[7–9]

The term photochromism derives from the Greek words "phos" and "chroma", which mean light and color respectively, and indicates literally a photoinduced change in color.[10] When restricted to the molecular world, however, this term implies a *reversible* color change under illumination. In most instances, photochromic processes actually involve the photoinduced interconversion of a colorless state into and colored one. The photoinduced transformation of a colored form into a colorless one is also possible, but is definitely less common. In order to distinguish these two classes of photochromic processes, the terms "positive photochromism" and "negative photochromism" are used to indicate photoinduced colorations and decolorations respectively. In both instances, the photogenerated state must be able to revert to the original form. In general, two broad classes of photochromic compounds can be distinguished on the basis of the nature of the

reverse process. Thermally-reversibly photochromic compounds switch back to the original state when stored in the dark. Thermally-irreversible photochromic compounds revert to the original form under irradiation at a different wavelength.

1.1.2. Photochromic Compounds.

Photochromic transformations are generally based on unimolecular or bimolecular reactions.[2–6] The unimolecular processes are definitely more common than their bimolecular counterparts and involve the interconversion of two isomers. For example, the spiropyran **1a** (Figure 1.1) ring opens to the merocyanine **1b** upon ultraviolet irradiation with a quantum yield of 0.1 in MeCN.[11] The photogenerated and colorless isomer **1b** has a lifetime of *ca.* 400 s and eventually reverts to the colorless state **1a** after thermal ring closing. Similarly, the colorless diarylethene **2a** (Figure 1.1) ring closes to the colored isomer **2b** upon ultraviolet irradiation with a quantum yield of 0.46 in hexane.[12] In this instance, however, the photogenerated isomer is thermally stable and reverts to the original and colorless state only after visible irradiation with a quantum yield of 0.015. Other common photochromic compounds based on ring opening and closing steps are the dihydroazulenes (*e.g.*, **3a** in Figure 1.1),[13] the spiroindolizines (*e.g.*, **4a**),[14,15] the dihydropyrans (*e.g.*, **5a**)[16] and the fulgides (*e.g.*, **6a**).[17] In alternative to ring opening and closing reactions, photoinduced *cis/trans* isomerizations can also be exploited to implement photochromic transformations. For example, the colorless *trans*-azobenzene **7a** switches to the colored *cis* isomer **7b** upon ultraviolet irradiation with a quantum yield of 0.1 in cyclohexane.[18,19] The photogenerated isomer has a lifetime of *ca.* 5000 s and reverts to the original species after a thermal *cis* $\rightarrow$ *trans* isomerization.

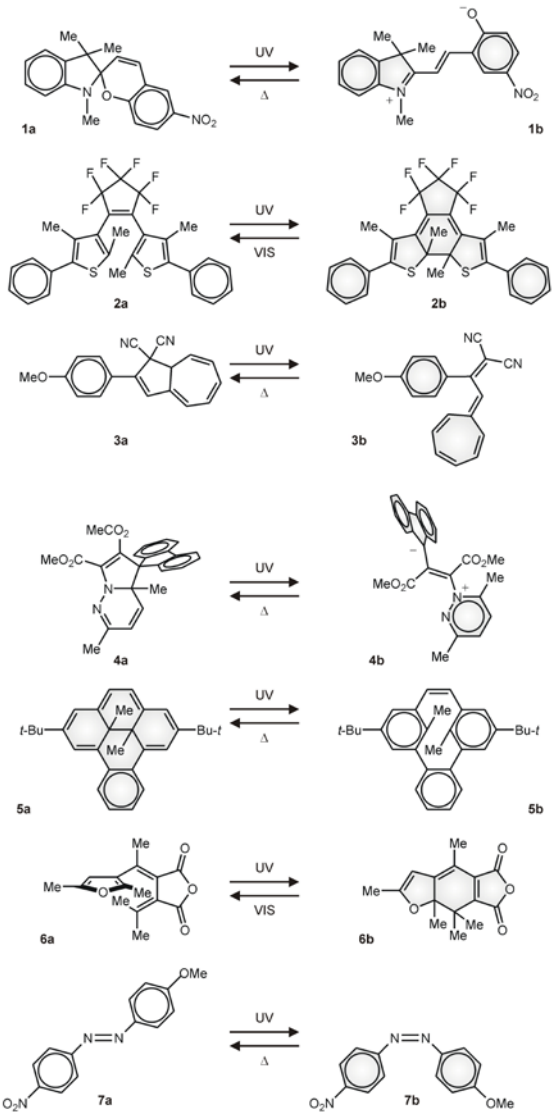

Figure 1.1 The photoinduced (UV and VIS) and thermal (Δ) transformations of representative photochromic compounds.

1.1.3. Properties of Photochromic Compounds.

The photoinduced interconversion of one state of a photochromic compound into another is generally accompanied by significant structural and electronic transformations.[2–6] For example, the colorless isomer **1a** (Figure 1.1) combines an indole and benzopyran fragments within its molecular skeleton. The spirocenter joining the two heterocyclic fragments imposes an orthogonal arrangement on them. As a result, there is

no electronic communication between them and **1a** absorbs only in the ultraviolet region of the electromagnetic spectrum. The ultraviolet excitation of this compound, however, cleaves the [C–O] bond at the spirocenter and, after the *cis* → *trans* isomerization of the adjacent double bond, generates the colored isomer **1b**. Indeed, the extended π-system of this species absorbs strongly in the visible region of the electromagnetic spectrum. Thus, the profound structural and electronic changes associated with the photoinduced isomerization from **1a** to **1b** alter drastically the spectroscopic response of the photochromic system and ensure coloration. In addition to the absorbance changes in the visible region, the transformation from **1a** to **1b** alters also the dipole moment and molecular polarizability of the photochromic system.[20] For example, AM1 calculations estimate an increase of *ca.* 4 D in the dipole moment with the formation of **1b**.[21] The photoinduced and reversible changes of these *molecular properties* in turn translate into significant modifications of *macroscopic properties*. In fact, the interconversion of a photochromic system within a liquid solution, a rigid polymer or even in a crystal alters the color and refractive index of the overall material. Hence, photonic materials with unique behavior can be designed around the photoresponsive properties of photochromic compounds.[7–9]

1.2. Fluorescence Modulation

1.2.1. Fluorescent and Photochromic Compounds.

The structural and electronic modifications that accompany the interconversion of photochromic compounds often translate also into significant changes in fluorescence quantum yield.[8b,21,22] For example, the spiropyran **1a** (Figure 1.1) and the

dihydroazulene **3a** do not emit electromagnetic radiations.[13,23] Instead, their photogenerated isomers **1b** and **3b** fluoresce in the visible region. Similarly, the spiroindolizine **4a** and the dihydropyran **5a** are fluorescent, while their photogenerated isomers **4b** and **5b** are not.[14–16] Thus, the photoinduced and reversible interconversion of these four pairs of isomers results in the modulation of their fluorescence intensity.

An alternative approach to modulate fluorescence with photochromic compounds relies in the interaction of fluorescent and photochromic components within the same molecular skeleton. In the resulting systems, the photoinduced isomerization of one component regulates the emissive behavior of the other. Diverse mechanisms can be invoked to implement these operating principles. For example, changes in either the conjugation or the polarity of the photochromic switch can affect the fluorescence quantum yield[24–32] and/or wavelength[33,34] of the fluorescent partner. The two molecular dyads **8a** (Figure 1.2) and **9a** are representative examples of these mechanisms for fluorescence modulation.[25,29] The dyad **8a** (Figure 1.2) combines an emissive tungsten complex with a diarylethene photochrome through a pyridyl ligand. The luminescence quantum yield for this isomer, however, is only 0.03. Upon ultraviolet irradiation, the diarylethene component undergoes ring closing with a significant change in electronic structure. As a result of the change in conjugation across the photochromic system, the luminescence quantum yield for the tungsten complex increases to 0.15. The process can be reversed by irradiating the dyad with visible light. Indeed, the original diarylethene isomer is regenerated and the luminescence quantum yield returns to the initial low value. Furthermore, similar operating principles can be extended from fluorophore–photochrome dyads to fluorophore–photochrome–fluorophore triads.[26,35–37]

The molecular dyad **9a** (Figure 1.2) integrates an oxazine fluorophore with a fulgide switch within its molecular skeleton. The photochromic component ring closes upon ultraviolet irradiation. The zwitterionic character of the photogenerated isomer translates into a significant enhancement in dipole moment with the isomerization from **9a** to **9b**. The process, however, can be reverted simply by irradiating with visible light. The photoinduced changes in dipole moment alter the local polarity around the adjacent oxazine fluorophore. As a result, the fluorescence quantum yield decreases by 80% with the transformation of **9a** into **9b** and returns to the original value after the photoinduced re-isomerization.

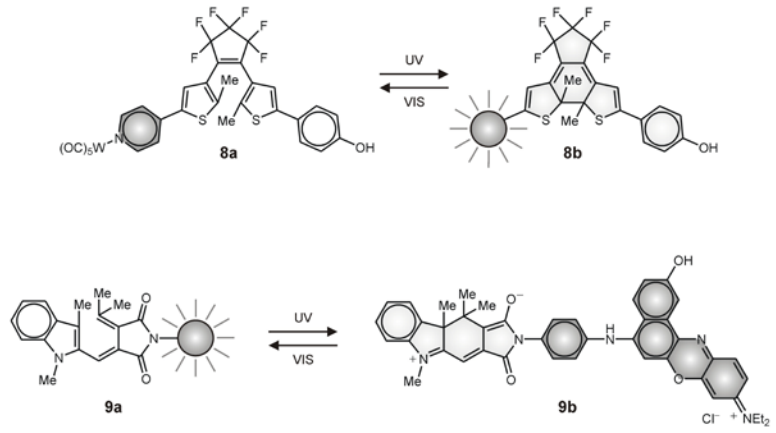

Figure 1.2. The photoinduced and reversible interconversion between **8a** and **8b** and between **9a** and **9b** results in the modulation of their luminescence quantum yield.

1.2.2. Electron Transfer.

The emissive behavior of a fluorescent component appended to a photochromic switch can also be modulated on the basis of photoinduced electron transfer.[21,38] In fact, the two states of a photochrome often differ in their redox potentials. As a result, the photoinduced and reversible change in either the oxidation or the reduction potential of the photochromic component can be exploited to activate or suppress intramolecular

electron transfer pathways in fluorophore–photochrome assemblies.[39–42] For example, the molecular dyad **10a** (Figure 1.3) incorporates a porphyrin fluorophore and a spiroindolizine photochrome. The local excitation of the porphyrin at 650 nm is followed by intense emission at 720 nm. After ultraviolet irradiation, however, the spiroindolizine photochrome ring opens to the corresponding zwitterionic isomer. This transformation is accompanied by a shift in the reduction potential of the photochromic component by *ca.* –0.48 V. Under these conditions, the transfer of electrons from the excited porphyrin to the photochrome becomes thermodynamically favorable. Consistently, the porphyrin fluorescence is effectively quenched. After visible irradiation, the zwitterionic state of the photochrome switches back to the original form, suppressing the electron transfer pathway and restoring the initial fluorescence intensity. Thus, the emission of one component can be modulated by operating the other with ultraviolet and visible inputs.

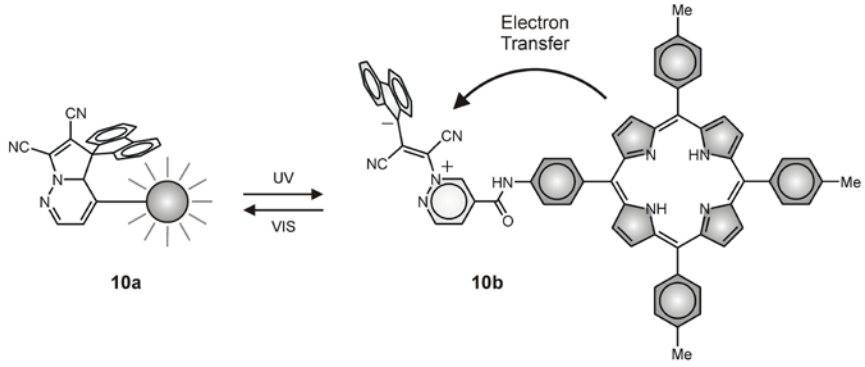

Figure 1.3. The photoinduced interconversion of **10a** into **10b** activates an electron transfer pathway quenching the fluorescence of the porphyrin appendage.

The photoinduced and reversible interconversion of a photochromic compound can also be exploited to regulate the physical separation between an electron donor and a complementary acceptor.[43–48] In the resulting systems, the efficiency of electron transfer varies with the state of the photochrome, even although the interconverting component is

not directly involved in the electron transfer process. For example, the triad **11a** (Figure 1.4) incorporates two porphyrin fluorophores and an azobenzene photochrome. In this molecular assembly, the fluorinated porphyrin can donate electrons to its nonfluorinated counterpart upon excitation. The distance between the two porphyrin units, however, changes with the state of the azobenzene bridge. Specifically, the photoinduced isomerization of the azobenzene from a *trans* to a *cis* configuration shortens significantly the physical separation between the electron donor and the acceptor. As a result, the efficiency of electron transfer increases dramatically and the fluorescence quantum yield drops by *ca.* 50%. After the thermal re-isomerization of the *cis*-azobenzene to the *trans* state, the original distance between donor and acceptor is restored with the concomitant recovery of the initial emission intensity.

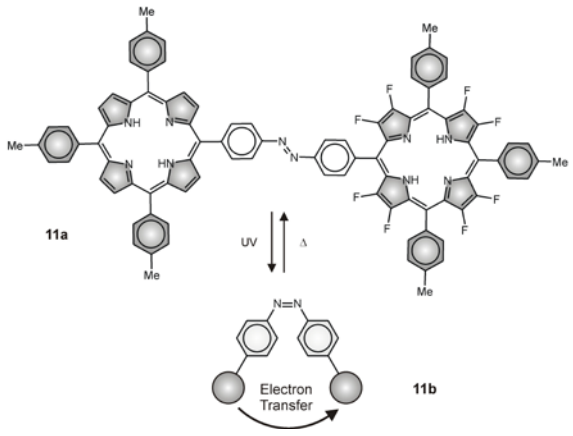

Figure 1.4. The photoinduced interconversion of **11a** into **11b** activates an electron transfer pathway quenching the emission of the porphyrin fluorophores.

1.2.3. Energy Transfer.

The emissive behavior of fluorophore–photochrome dyads can also be regulated on the basis of energy transfer.[49–56] Indeed, only one of the two interconvertible states of the photochromic component can be designed to absorb in the wavelength range where the

fluorescent component emits. Under these conditions, the photoinduced and reversible interconversion of the photochrome controls the intramolecular transfer of the excitation energy of the fluorophore from one component to the other. For example, the dyad **12a** (Figure 1.5) incorporates an anthracene fluorophore and a diarylethene photochrome.[51d] The ultraviolet irradiation of this molecular assembly induces the ring closing of the diarylethene switch with the formation of the isomer **12b**. The photogenerated state of the photochrome absorbs in a range of wavelengths where the anthracene fluorophore emits. As a result, the transformation of **12a** into **12b** activates an energy transfer pathway from the fluorophore to the photochrome with a concomitant decreases in fluorescence quantum yield from 0.73 to 0.001. After visible irradiation, the photochromic component ring opens to regenerate the original isomer **12a** with the concomitant recovery of the initial fluorescence intensity.

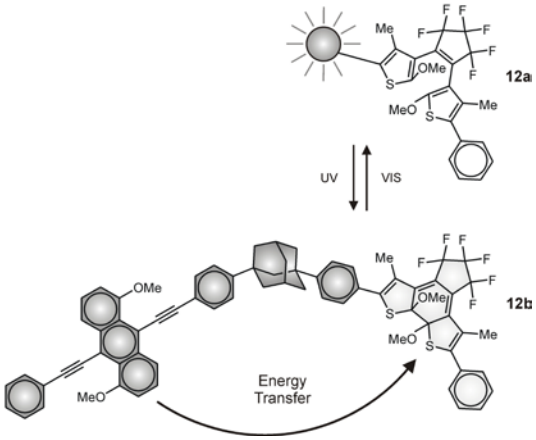

Figure 1.5. The photoinduced interconversion of **12a** into **12b** activates an energy transfer pathway quenching the fluorescence of the anthracene appendage.

The operating principles regulating the emissive behavior of the fluorophore–photochrome dyad **12a** can be extended to fluorophore–photochrome–fluorophore[57–61] and photochrome–fluorophore–photochrome[62,63,64] triads. Instead, the molecular triad

13a (Figure 1.6) operates according to a different mechanism also based on energy transfer.[65] This molecule incorporates an anthracene donor, a coumarin acceptor and a fulgide photochrome. The local excitation of the anthracene donor is followed by the transfer of excitation energy to the coumarin acceptor, which then emits in the visible region. After ultraviolet irradiation, the fulgide photochrome ring closes to generate the isomer **13b**. The photochromic component of **13b** can accept the excitation energy of the anthracene donor, preventing the transfer of energy to the coumarin acceptor. As a result, the photoinduced interconversion of **13a** into **13b** results in a significant decrease in the fluorescence intensity of the coumarin appendage. The process can be reversed by irradiating with visible light. Under these conditions, the fulgide photochrome ring opens to regenerate the original state with the concomitant recovery of the initial fluorescence intensity.

1.3. Nanostructured Constructs

1.3.1. Polymers.

Photochromic compounds can be integrated within or appended to the main chains of a diversity of polymers.[66] After their incorporation in these macromolecular constructs, they generally retain their characteristic photochemical behavior and can still be switched back and forth between their two interconvertible states under the influence of optical inputs. In few representative examples, one of the two states can emit electromagnetic radiations upon excitation and, hence, the photochemical transformations associated with these polymeric assemblies offer the opportunity to modulate fluorescence.[67,68] More commonly, however, fluorescent components are incorporated together with

photochromic elements within the same macromolecular construct to implement the operating principles for fluorescence modulation. In some systems, the fluorescent and photochromic components are both integrated within the polymer main chain.[69–71]

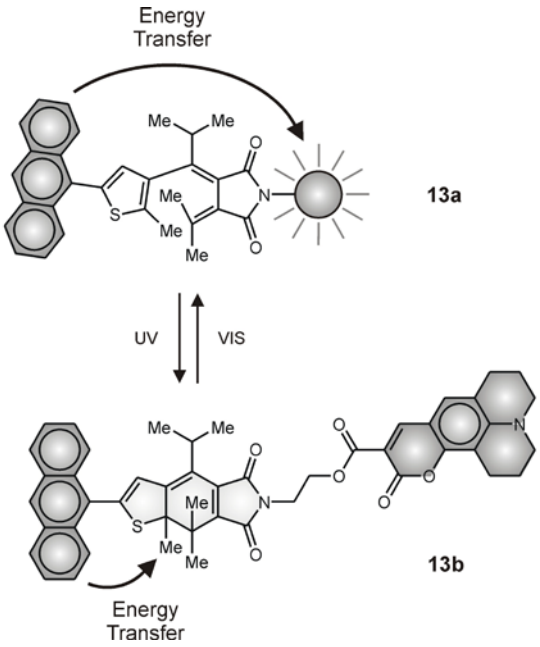

Figure 1.6. The photoinduced interconversion of **13a** into **13b** turns the photochromic component into an energy acceptor and affects the intramolecular energy transfer pathway.

In others, the polymer backbone itself is the fluorescent component and the photochromic elements are in side chains[72,73] Alternatively, independent fluorophores and photochromes are appended to a common polymer chain.[74] Similarly, a fluorescent component can first be attached to a photochromic switch and then the resulting fluorophore–photochrome dyad can be appended to a polymer backbone.[75] In the resulting macromolecular constructs, the photoinduced interconversion of the photochromes results in the efficient modulation of the emission intensity associated with the fluorophores.

1.3.2. Nanoparticles.

Photochromic compounds can be attached to luminescent inorganic nanoparticles and the emission of the resulting assemblies can be regulated with optical stimulations.[76–81] Alternatively, photochromic ligands, able to emit electromagnetic radiations in one of their two interconvertible states only, or fluorophore–photochrome dyads can be conjugated to nanostructured inorganic scaffolds.[82,83] Once again, the photoinduced interconversion of the photochromic components of the resulting nanostructured materials results in the effective modulation of the emission intensity. The nanoscaled construct **14a** (Figure 1.7) is a representative example of these functional assemblies.[79a] It incorporates an emissive CdSe core, surrounded by a protective ZnS shell and pendant photochromic ligands. Upon excitation, this luminescent nanostructured emit at 554 nm (***a*** in Figure 1.7) in dichloroethane, where the colorless state of the photochromic components does not absorb. After ultraviolet irradiation, however, a fraction of the spiropyran ligands switches to the corresponding merocyanines with the concomitant appearance of their characteristic absorption band at 592 nm. This band overlaps the emission of the inorganic components and, as a result, energy can be transferred from the excited CdSe core to the photogenerated state of the photochromes. Consistently, the emission intensity of this nanostructured assembly decreases significantly with the photoinduced transformation of **14a** into **14b** (***b*** in Figure 1.7). Nonetheless, the colored state of the photochromic ligands has a lifetime of 250 s and, eventually, reverts to the colorless state with first-order kinetics upon storage in the dark. In fact, the original luminescence intensity of the CdSe core is fully restored after the thermal reisomerization of **14b** back to **14a**. Thus, the luminescence of this nanostructured construct can

repeatedly be switched between high and low values simply by turning an ultraviolet source on and off.

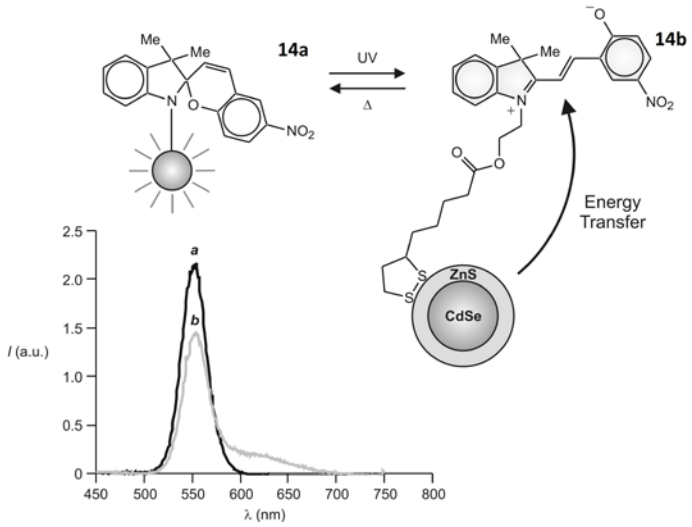

Figure 1.7. Emission spectra (0.7 μM, dichloroethane, 25°C, λ_{Ex} = 380 nm) of the nanostructured construct **14a** before (***a***) and after (***b***) ultraviolet irradiation.

Fluorescent and photochromic components can also be incorporated within organic nanoparticles to build nanostructured constructs with photoswitchable fluorescence. In fact, some photochromic compounds tend to assemble spontaneously into nanostructured aggregates without losing their photochemical character.[84–87] When only one of the two states of these photochromic compounds is fluorescent, their photoinduced transformations result in the effective modulation of the emission intensity of the overall assembly. Alternatively, independent fluorescent and photochromic components can be trapped within the hydrophobic interior[88–90] or covalently linked to the macromolecular backbone[91,92] of cross-linked polymer nanoparticles. For example, the nanostructured construct **15a** (Figure 1.8) can be assembled by co-polymerizing perylene diimide fluorophores and spiropyran photochromes together with *N*-*i*-propylacrylamide, divinylbenzene and styrene in aqueous environment.[91b] In the resulting assembly, the

fluorescent and photochromic components are integral part of the cross-linked covalent skeleton. Upon excitation, the perylene diimide fluorophores emit at 530 nm, where the spiropyran photochromes do not absorb. After ultraviolet irradiation, the spiropyrans switch to the corresponding merocyanines to form **15b** with the concomitant appearance of their characteristic absorption at 588 nm. The overlap between the emission of the fluorophores and the absorption of the photogenerated state of the photochromes encourages the transfer of energy from one component to the other. Consistently, the perylene diimide emission decreases significantly in intensity. The hydrophobic environment of this nanostructured construct, however, facilitates the radiative deactivation of the excited merocyanines. As a result, the energy transferred from the perylene diimide to the merocyanines components is released in the form of electromagnetic radiations. In fact, the decrease in the perylene diimide fluorescence at 530 nm is paralleled by the growth of an emission band at 670 nm, corresponding to the merocyanine fluorescence.

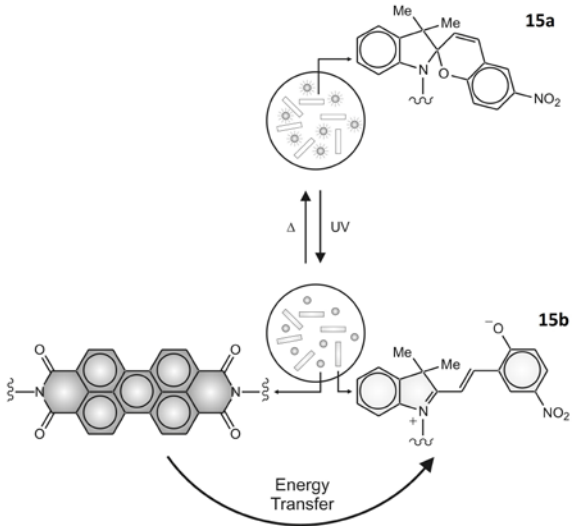

Figure 1.8. The photoinduced transformation of the spiropyran photochromes, entrapped within the cross-linked polymer nanoparticle **15a**, activates an energy transfer process and quenches the emission of the perylene diimide fluorophores.

Upon storage in the dark, the photogenerated state of the photochromes reverts to the colorless form, preventing the intercomponent energy transfer process and restoring the original emission spectrum. Hence, the emission intensity can be modulated at two different wavelengths in parallel under the influence of ultraviolet inputs and on the basis of energy transfer with these functional organic nanoparticles.

1.3.3. Biomolecules.

The photoinduced interconversion between the non-emissive and emissive states of certain photochromic compounds can be exploited to probe living cells,[93,94] image biological samples with improved resolution[95] and develop immunoassays.[96] In addition, fluorophore–photochrome dyads can be conjugated to proteins and the emission intensity of the resulting assemblies can be modulated with optical stimulations on the basis of intercomponent energy transfer.[97] Similarly, photochromic components can be appended to fluorescent proteins in order to control the biomolecule emission within living cells under the influence of optical stimulations.[98] For example, the green fluorescent protein (GFP) was labeled with a photochromic spiropyran inside Swiss 3T3 cells to generate the construct **16a** (Figure 1.9). Under these conditions, the GFP component emits at *ca.* 510 nm upon excitation, where the colorless state of the photochromes does not absorb. After ultraviolet irradiation, the spiropyran switches to the corresponding merocyanine to generate **16b**. The photogenerated state of the photochromic component absorbs at *ca.* 540 nm. The pronounced degree of overlap between the GFP emission and the merocyanine absorption results in efficient energy transfer with a concomitant fluorescence quenching. The visible irradiation of **16b**, however, switches the photochromic component back to the original and colorless state, suppressing the energy

transfer pathway and restoring the original fluorescence intensity. Thus, the emission of this particular system can be switched multiple times between high and low values inside living cells simply by illuminating the biological samples with ultraviolet and visible inputs.

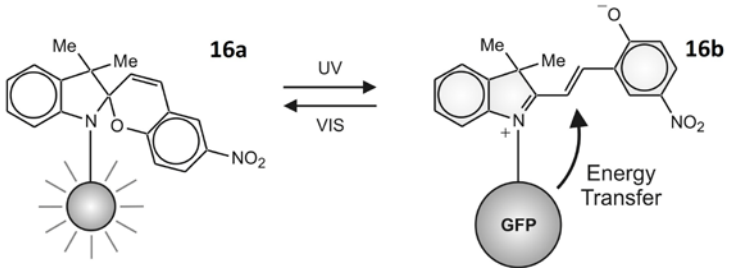

Figure 1.9. The photoinduced interconversion of the photochromic component of **16a** activates an energy transfer process and quenches the emission of the green fluorescent protein (GFP).

Fluorescent and photochromic components can also be connected through an oligonucleotide strand in order to assemble fluorophore–photochrome dyads with photoswitchable emission.[99] In particular, a fluorescein fluorophore and a merocyanine photochrome were attached to the ends of a cytosine-rich oligonucleotide strand to generate the construct **17a** (Figure 1.10). At a pH of 5.5, this particular oligonucleotide folds into a compact conformation to bring its two ends in close proximity. Under these conditions, the photochromic component is preferentially in its colored state and, consistently, the absorption spectrum shows a band centered at 520 nm. This band overlaps the emission of the fluorescein component and, as a result, the excitation of the fluorophore is followed by the transfer of the excitation energy to the adjacent merocyanine with a concomitant fluorescence quenching. Upon visible irradiation, the photochromic component switches form its colored state to its colorless form to generated **17b**.

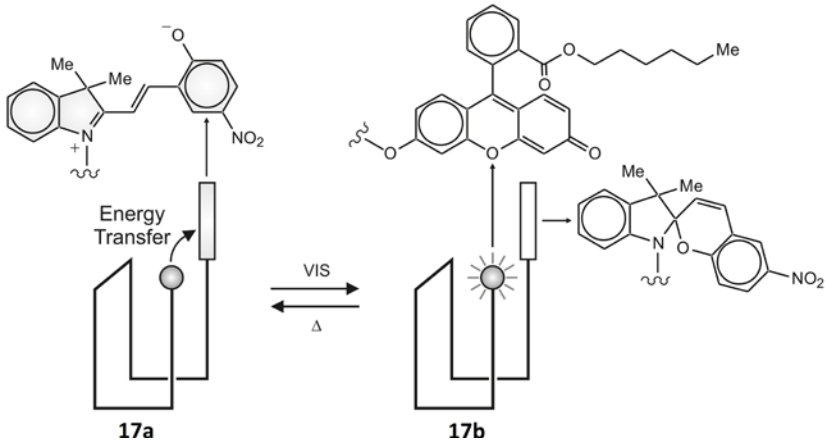

Figure 1.10. The photoinduced transformation of the photochromic component of **17a** prevents the energy transfer process and restores the emission of the fluorescent component.

This species does not absorb in the range of wavelengths where the fluorophore emits and, hence, it cannot accept its excitation energy. Thus, the visible irradiation of this fluorophore–photochrome dyad causes a significant enhancement in emission intensity. Upon storage in the dark, the colorless state of the photochromic component switches to the colored one over the course of several hours and the emission intensity returns to its original low values. In fact, the alternation of visible irradiation and storage in the dark can be exploited to turn the emission intensity of this particular system from low to high an *vice versa*.

1.4.Summary

The photoinduced and reversible interconversion between the two states of a photochromic compound can be exploited to modulate fluorescence. Intrinsically-fluorescent photochromes differ in the luminescence quantum yield of their interconvertible states and, as a result, the transformation of one of their states into the other alters the emission intensity. Alternatively, photochromic switches can be attached covalently to fluorescent partners. In the resulting molecular assemblies, the

photoinduced interconversion of one component modulates the emissive behavior of the other on the basis of changes in conjugation, local polarity, electron transfer or energy transfer. The electron transfer mechanisms rely on either a change in the redox potential of the photochromic component or in a change of the separation between an electron donor and an electron acceptor with the interconversion of the photochrome. In both instances, the efficiency of electron transfer and, as a result, the fluorescence quantum yield vary with the state of the photochrome. The energy transfer mechanisms are based on a change in the overlap between the emission band of a fluorescent component and the absorption bands of a photochromic component with the interconversion of the latter. The overall result is a change in energy transfer efficiency and, as a consequence, in emission intensity. Strategies to modulate the fluorescence of an emissive component with a photochromic element can also be extended from the intramolecular to the intermolecular level. Once again the overlap between the emission band of a fluorophore and the absorption bands of a complementary photochrome can be invoked to implement these operating principles. Furthermore, these strategies can be extended to the modulation of multiple fluorophores in parallel within the same or different solution or even within rigid matrices. Similarly, these mechanisms for fluorescence modulation can be adapted to nanostructured constructs. In fact, fluorescent and photochromic components can be incorporated within linear and cross-linked polymers, attached to nanostructured inorganic scaffolds or conjugated to biomolecules. Alternatively, photochromic ligands can be connected to luminescent inorganic nanoparticles. In all these nanostructured constructs, the interconversion of the photochromic components controls the emission of the luminescent components. Thus, the investigation of these

fascinating systems can advance our understanding of the subtle factors regulating the photochemical and photophysical properties of inorganic and organic compounds as well as lead to the development of novel materials for the manipulation of optical signals. Indeed, the realization of devices for information storage and of luminescent probes for biomedical application can ultimately be envisaged.

CHAPTER 2

PHOTOSWITCHABLE FLUORESCENT ASSEMBLIES BASED ON BODIPY-SPIROPYRAN CONJUGATES

2.1. Overview

Fluorescence imaging[100] offers the opportunity to localize targets non-invasively in biological samples, relying on the ability of appropriate chromophoric labels[101] to emit electromagnetic radiations upon excitation. The phenomenon of diffraction,[102] however, limits the resolution of conventional microscopes to hundreds of nanometers in both the horizontal and vertical directions. As a result, the factors regulating biological structures and processes at the molecular level cannot be appreciated with this convenient analytical technique.

Recently, clever operating principles to record fluorescence images of biological preparations with sub-diffraction resolution have been identified and demonstrated experimentally.[103–109] They are based on either the patterned illumination of the specimen or the sequential localization of individual labels, but require photoswitchable fluorescent probes. In particular, compounds able to undergo reversible saturable optically-linear fluorescence transitions (RESOLFT) permit the acquisition of images with nanoscaled resolution by irradiating the sample with pairs of beams at different wavelengths (λ_{Ex} and λ_{OFF}). The beam at λ_{Ex} is designed to produce a circular spot on the focal plane of the specimen and excite the labels to encourage fluorescence. That at λ_{OFF} is engineered to generate a doughnut-shaped spot, overlapped and concentric with the circular one, and deactivate the excited state of the labels to switch fluorescence off. Under these conditions, fluorescence is confined within the nanoscaled hole of the

doughnut and images with subdiffraction resolution can be recorded by scanning the overlapped spots over the entire sample.

RESOLFT images can be recorded with synthetic dyes on the basis of stimulated emission depletion[110] (STED) or intersystem crossing[110o,111] (ISC). Both mechanisms ensure fluorescence suppression upon illumination of the sample at λ_{OFF} and offer the opportunity to overcome diffraction. Nonetheless, the high irradiation intensities required for STED and the reactivity of triplet states, populated after ISC, complicate the experimental implementation of these operating principles. In addition, ISC can sensitize the generation of singlet oxygen and damage biological specimens. In principle, these limitations can be overcome with the design of photochromic transformations, instead of STED or ISC, to suppress fluorescence upon illumination at λ_{OFF}.[112] Indeed, the photoinduced and reversible interconversion of photochromic compounds[2-6] can be exploited to modulate fluorescence under the influence of optical stimulations.[113] In fact, images of photochromic proteins expressed in *Escherichia coli*,[114] fluorescent and photochromic dopants entrapped in a polymer matrix[115] and fluorophore–photochrome dyads attached to silica particles[116] have already been recorded with subdiffraction resolution.

In search of viable structural designs to control fluorescence with photochromic compounds, I synthesized a photoswitchable fluorescent assembly, consisting of a boron dipyrromethane (BODIPY) fluorophore covalently connected to a photochromic spiropyran. Next, I copolymerized a similar BODIPY-spiropyran conjugate with a monomer bearing a pendant polyethylene glycol chain to make it water soluble. Lastly, I

prepared poly(methyl methacrylate) (PMMA) films of the conjugate by spin coating. In this chapter, I report the synthesis, photochemical and photophysical properties of these hydrophilic and fluorescent molecular switches and preparation of the PMMA films as well as its spectroscopic and imaging with patterned illumination.

2.2. Results and Discussion

2.2.1. BODIPY-Spiropyran Conjugate

2.2.1.1. Design and Synthesis

The colorless spiropyran **18a** (Figure 2.1) switches to the colored merocyanine **18b** upon ultraviolet irradiation.[117] The photoinduced transformation of **18a** into **18b** is accompanied by the appearance of an intense band in the visible region of the absorption spectrum (***a*** and ***b*** in Figure 2.2). This band is positioned in the same region of wavelengths where the BODIPY fluorophore **19** emits (***c*** in Figure 2.2) and disappears with the thermal reisomerization of **18b** back to **18a**. As a result, the excited fluorophore can transfer energy to the colored state of the photochrome, if the two components are sufficiently close to each other, but not to the colorless one. On the basis of these considerations, we have designed the BODIPY–spiropyran conjugate **20a** (Figure 2.1) and prepared this compound in one step, starting from **18a** and **21**, with a yield of 54%.

2.2.1.2. Absorption Spectroscopy

The absorption spectrum (***d*** in Figure 2) of the fluorophore–photochrome conjugate **20a** resembles the sum (***f*** in Figure 2.2) of those associated with the fluorophore **19** and photochrome **18a**. Upon ultraviolet irradiation, the photochromic component of **20a**

switches to its colored state and forms **20b** with the concomitant appearance of the characteristic absorption (***e*** in Figure 2.2) in the visible region. However, this band is centered at 570 nm for **20b** and 563 nm for **18b**.[123] In both instances, the photogenerated isomer reverts thermally to the original one and the absorbance in the visible region decays monoexponentially (***a*** in Figure 2.3).

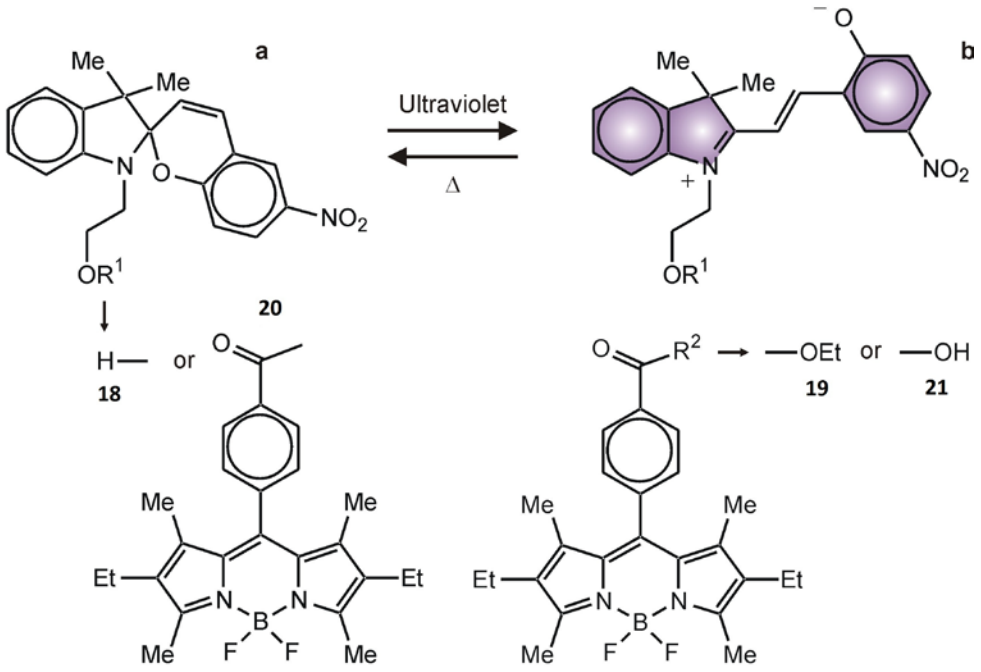

Figure 2.1. Photoinduced interconversion between **18a** and **18b** as well as between **20a** and **20b** and structures of the model fluorophore **19** and precursor **21**.

The nonlinear curve fitting of the absorbance profile indicates the lifetime of **20b** to be 2.7×10^2 s in acetonitrile at 25°C, while it is 1.9×10^2 s for **18b** under the same conditions.[123 b] Thus, the photochromic component can be operated effectively even when it is covalently connected to the BODIPY fluorophore. Nonetheless, the latter has some influence on the spectroscopic signature and reisomerization kinetics of the former.

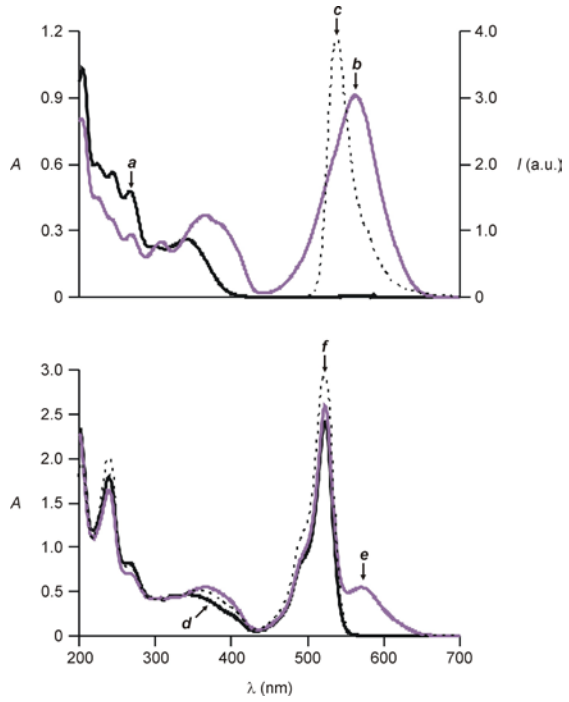

Figure 2.2 Absorption spectra of a solution of **18a** (0.1 mM, MeCN, 25°C) before (***a***) and after (***b***) ultraviolet irradiation (254 nm, 0.5 mW cm^{-2}, 5 min) and emission spectrum (***c***) of **19** (0.01 mM, MeCN, 25°C, 480 nm). Absorption spectra of a solution of **20a** (0.1 mM, MeCN, 25°C) before (***d***) and after (***e***) ultraviolet irradiation (254 nm, 0.5 mW cm^{-2}, 5 min) and sum (***f***) of the absorption spectra of **18a** and **19** (0.1 mM, MeCN, 25°C).

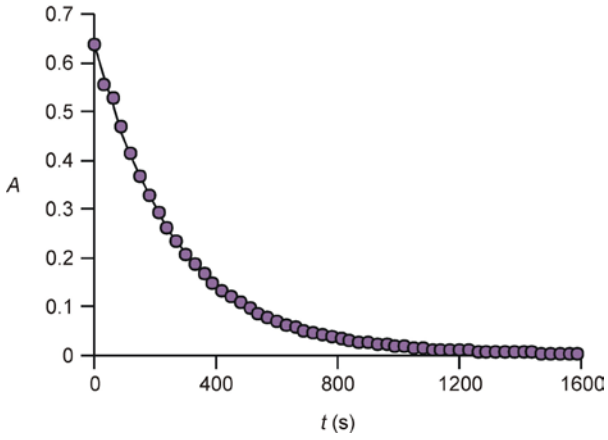

Figure 2.3. Absorbance decay for a solution of **20a** (0.1 mM, MeCN, 25°C, 570 nm) maintained in the dark after ultraviolet irradiation (254 nm, 0.5 mW cm^{-2}, 5 min).

2.2.1.3. Emission Spectroscopy

The emission spectrum (***a*** in Figure 2.4) of the fluorophore–photochrome conjugate **20a** resembles that (***c*** in Figure 2.2) of the model fluorophore **19**. Both spectra show a band at 539 nm. However, the fluorescence quantum yield of **20a** is 0.8, while that of **19** is 1.0. Thus, the covalent attachment of the spiropyran photochrome to the BODIPY fluorophore has a depressive effect on the quantum yield. Presumably, photoinduced electron transfer from the photochrome to the excited fluorophore is responsible for the decrease in quantum yield. Indeed, the redox potentials of **18a** and **19** (Table 2.1) suggest that the electron transfer process is exoergonic with a free energy change of –0.18 eV.[118] Upon ultraviolet irradiation, **20a** switches to **20b** and the emission intensity decreases to 44% of the original value at the photostationary state (***b*** in Figure 2.4).[119]

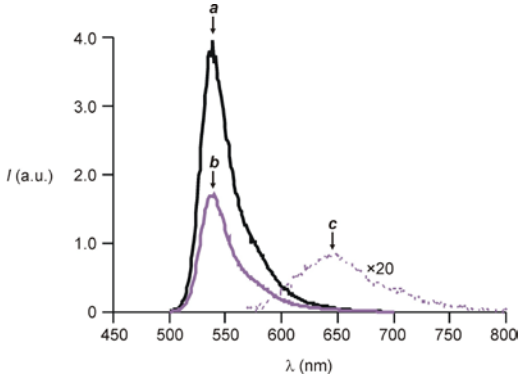

Figure 2.4. Emission spectra of a solution of **20a** (0.01 mM, MeCN, 25°C, 480 nm) before (***a***) and after (***b***) ultraviolet irradiation (254 nm, 0.5 mW cm^{-2}, 5 min) and emission spectrum (***c***) of a solution of **18a** (0.01 mM, MeCN, 25°C, 560 nm) after ultraviolet irradiation (254 nm, 0.5 mW cm^{-2}, 5 min).

Indeed, the photoinduced interconversion of the photochromic component can activate an energy transfer pathway and lead to a partial fluorescence quenching. Nonetheless, the emission spectrum of **20b** does not show the characteristic fluorescence

for the photogenerated state of the photochrome, which is positioned at 646 nm (***c*** in Figure 2.4) for **18b**. The lack of sensitized fluorescence suggests that the transfer of energy from the excited fluorophore to the colored state of the photochrome is not particularly efficient. Thus, the pronounced decrease in emission intensity with the formation of **20b** cannot exclusively be a consequence of energy transfer. In fact, the examination of the redox potentials (Table 2.1) of **18b** and **19** indicates that the photoinduced transfer of one electron from the excited fluorophore to the photochrome is exoergonic with a free energy change of –0.42 eV.[124] Presumably, this electron transfer process contributes to the nonradiative deactivation of the excited fluorophore together with the anticipated energy transfer pathway.

Table 2.1. Oxidation (E_{Ox}) and reduction (E_{Red}) potentials of the model fluorescent and photochromic components [a].

	E_{Ox} (V)	E_{Red} (V)
18a	+0.72	–1.54
18b	—	–1.23
19	+0.77	–1.52

[a] E_{Ox} and E_{Red} were determined by cyclic voltammetry in a MeCN solution of Bu_4NPF_6 (0.1 M), using a glassy carbon working electrode, a nonaqueous Ag/Ag^+ reference electrode and a platinum counter electrode.

In any case, the original emission intensity of the BODIPY component is restored after the thermal reisomerization of **20b** back to **20a**. In fact, the fluorescence of this particular fluorophore–photochrome dyad can be switched between high (***a–f*** in Figure

2.5) and low values (***g*–*k*** in Figure 2.5) simply by turning on and off an ultraviolet source. While the change in emission intensity associated with each switching step remains approximately constant, however, the fluorescence measured before and after each step tends to decrease with the number of switching cycles. This trend is, presumably, a result of the gradual photodegradation of the BODIPY–spiropyran conjugate.

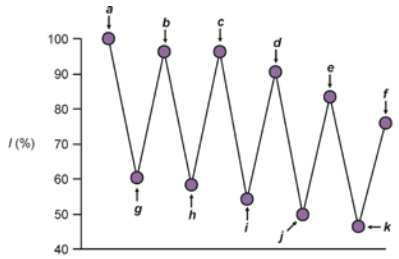

Figure 2.5. Relative emission intensity of a solution of **20a** (0.01 mM, MeCN, 25°C, 480 nm) measured at 539 nm before (***a***) and after consecutive ultraviolet irradiation (***g*–*k***, 254 nm, 0.5 mW cm^{-2}, 1 min) and storage in the dark (***b*–*f***, 30 min).

2.2.2. Polymer Incorporating BODIPY-Spiropyran Conjugates

2.2.2.1. Design and Synthesis

The spectroscopic analysis of **20a** demonstrates that the photoinduced interconversion of the spiropyran component can be exploited to modulate the fluorescence of the BODIPY component. However, this compound is rather hydrophobic and cannot be operated in aqueous environments. In order to overcome this limitation, we have envisaged the possibility of attaching a similar BODIPY–spiropyran conjugate to a polymer backbone with pendant hydrophilic chains. Specifically, we have synthesized the photochromic monomers **22a** and **23a** (Figure 2.6) and reacted them with the

hydrophilic monomer **24**, under the assistance of first-generation Grubbs' catalyst,[120] to generate the co-polymers **25a** and **26a** respectively.

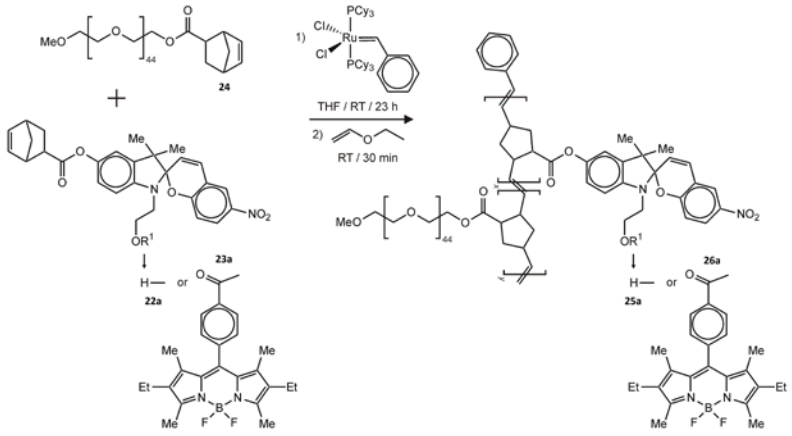

Figure 2.6. Synthesis of the photochromic polymers **25a** and **26a**.

2.2.2.2. Absorption Spectroscopy

The polyethylene glycol chains appended to the main backbone of **25a** impose aqueous solubility on the overall macromolecular construct. Consistently, the photochromic component of this polymer can be operated in aqueous environments with optical stimulations, as observed for **18a** and **20a** in organic solvents. Specifically, the absorption spectra (***a*** and ***b*** in Figure 2.7) of a solution of **25a** in sodium phosphate buffer (pH = 7.0) show the appearance of a band at 522 nm upon ultraviolet irradiation. This band corresponds to the colored state of the photochromic component and is indicative of the photoinduced formation of **25b**. In addition, this absorption overlaps the emission of the model fluorophore **21** (***c*** in Figure 2.7). Thus, the photogenerated state of the photochromic polymer can, in principle, accept the excitation energy of this particular fluorophore, if the two components are sufficiently close to each other.

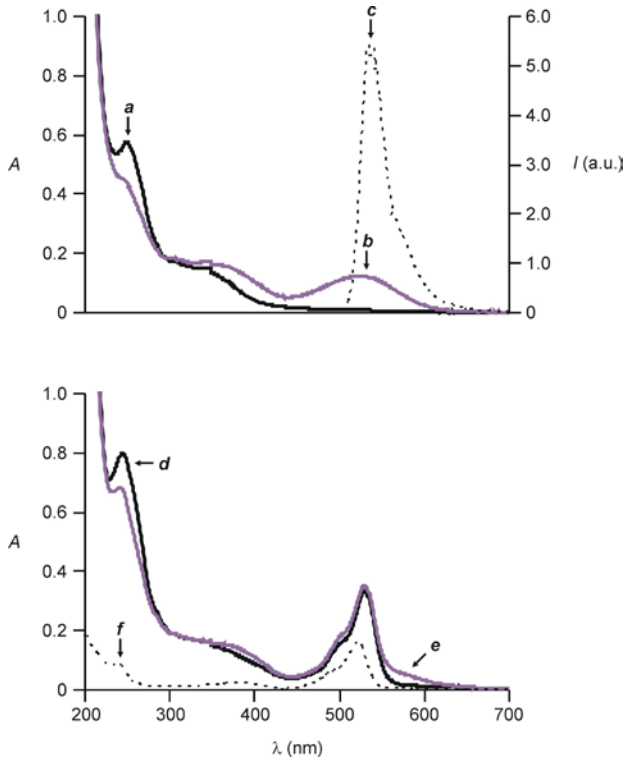

Figure 2.7. Absorption spectra of a solution of **25a** (4.7 mg mL^{-1}, sodium phosphate buffer, pH = 7.0, 25°C) before (***a***) and after (***b***) ultraviolet irradiation (254 nm, 0.5 mW cm^{-2}, 4 min) and emission spectrum (***c***) of **21** (0.05 mM, MeCN, 25°C, 480 nm). Absorption spectra of a solution of **26a** (1.5 mg mL^{-1}, sodium phosphate buffer, pH = 7.0, 25°C) before (***d***) and after (***e***) ultraviolet irradiation (254 nm, 0.5 mW cm^{-2}, 4 min) and absorption spectrum (***f***) of **21** (0.05 mM, sodium phosphate buffer, pH = 7.0, 25°C).

The polymer **26a** combines BODIPY, spiropyran and polyethylene glycol components in its macromolecular skeleton. As observed for **25a**, the polyethylene glycol chains ensure solubility in aqueous environments and the photochromic component can be operated with optical stimulations under these conditions. Indeed, the absorption spectra (***d*** and ***e*** in Figure 2.7) of **26a** show the appearance of a band in the visible region upon ultraviolet irradiation. This band corresponds, once again, to the colored state of the photochrome and is consistent with the photoinduced transformation of **26a** into **26b**. In addition, both absorption spectra show a band for the BODIPY component, which resembles the one for the model fluorophore **21** (***f*** in Figure 2.7).

However, this band is centered at 530 nm for **26a** and 522 nm for **21**, while essentially no difference is observed between the position of the absorption of the model BODIPY **19** and the monomeric BODIPY–spiropyran conjugate **20a** (***d*** and ***f*** in Figure 2.2). Thus, the elongation of the absorption wavelength of the fluorophore with the transition from **21** to **26a** is, presumably, a result of the incorporation of the BODIPY component within the polymeric construct.

The photogenerated states of both polymers revert to the original forms upon storage in the dark. Consistently, the absorption band in the visible region fades with the thermal reisomerization of **25b** to **25a** and **26b** to **26a**. As observed for **18b** and **20b** (Figure 2.3) in organic solvents, the absorbance of **25b** and **26b** decays monoexponentially (***a*** and ***b*** in Figure 2.8). The nonlinear curve fittings of the absorbance profiles indicate the lifetimes of **25b** and **26b** to be 2.0×10^4 and 0.9×10^4 s respectively in sodium phosphate buffer (pH = 7.0) at 25°C. These values are approximately two orders of magnitude greater than those of **18b** and **20b** in acetonitrile at the same temperature.

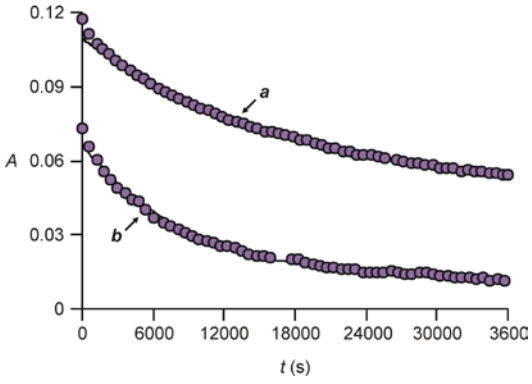

Figure 2.8. Absorbance decays for solutions (sodium phosphate buffer, pH = 7.0, 25°C) of **25a** (***a***, 4.7 mg mL^{-1}, 526 nm) and **26a** (***b***, 1.5 mg mL^{-1}, 572 nm) maintained in the dark after ultraviolet irradiation (254 nm, 0.5 mW cm^{-2}, 4 min).

2.2.2.3. Emission Spectroscopy

The emission spectrum of **26a** (***a*** in Figure 2.9) in sodium phosphate buffer (pH = 7.0) resembles that of the model fluorophore **21** (***c*** in Figure 2.7) recorded under the same conditions. Both show an intense band centered at 545 nm for **26a** and 539 nm for **21**. However, the quantum yield for **26a** is only 1.1×10^{-2}, while that for **21** is 8.7×10^{-2}. The decrease in quantum yield with the transition from the model BODIPY **21** to the polymeric BODIPY–spiropyran assembly **26a** is, presumably, a consequence of photoinduced electron transfer from the photochrome to the excited fluorophore in **26a**. Once again, the redox potentials in Table 1.1 suggest that this process is exoergonic with a free energy change of –0.18 eV.[124] Upon ultraviolet irradiation, **26a** switches to **26b** and the emission intensity decreases to 60% of the original value at the photostationary state (***b*** in Figure 2.9).[125] In addition to the fluorescence of the BODIPY component at 545 nm, the emission spectrum (***b*** in Figure 2.9), recorded after ultraviolet irradiation, shows also the fluorescence of the photogenerated state of the photochromic component at 623 nm. This band is essentially identical to that observed after the ultraviolet irradiation of **25a** (***c*** in Figure 2.9) and then excitation of the photostationary state at the very same wavelength used for **26a**. Thus, this emission appears to be mainly a result of the direct excitation of the photogenerated state of the photochromic component, rather than a consequence of energy transfer form the excited BODIPY. Presumably, the pronounced decrease in the emission intensity of the BODIPY component with the transformation of **26a** into **26b** is mainly a result of photoinduced electron transfer. In fact, the redox potentials in Table 1.1 suggest that the transfer of one electron from the

excited fluorophore to the photogenerated state of the photochrome is exoergonic with a free energy change of –0.42 eV.[124]

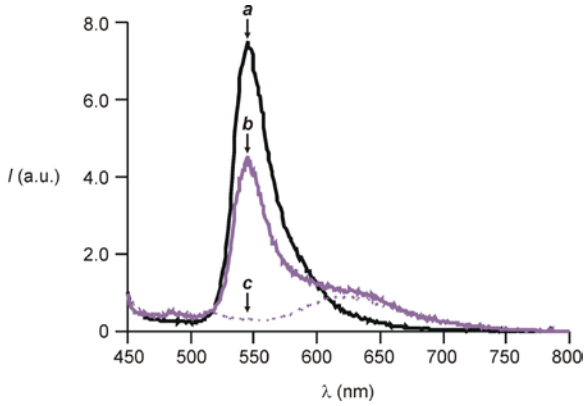

Figure 2.9. Emission spectra of a solution of **26a** (1.5 mg mL^{-1}, sodium phosphate buffer, pH = 7.0, 25°C, 440 nm) before (***a***) and after (***b***) ultraviolet irradiation (254 nm, 0.5 mW cm^{-2}, 4 min) and emission spectrum (***c***) of a solution of **25a** (4.7 mg mL^{-1}, sodium phosphate buffer, pH = 7.0, 25°C, 440 nm) after ultraviolet irradiation (254 nm, 0.5 mW cm^{-2}, 4 min).

Upon storage in the dark, **26b** switches back to **26a** with a concomitant increase in the emission intensity of the BODIPY component. However, this process is significantly slower than the reisomerization of **20b** back to **20a** and the original emission intensity is almost completely restored only after 12 h (***a*** and ***b*** in Figure 2.10). Additional switching cycles can be performed by alternating ultraviolet irradiation and storage in the dark. Nonetheless, the emission intensity (***b***–***f*** in Figure 2.10) measured after the thermal reisomerization tends to decrease with the number of switching cycles. This depressive effect on the emission of the BODIPY fluorophore suggests that the photoinduced interconversion of the spiropyran photochrome is, presumably, accompanied by a significant degradation of the fluorophore–photochrome assembly.

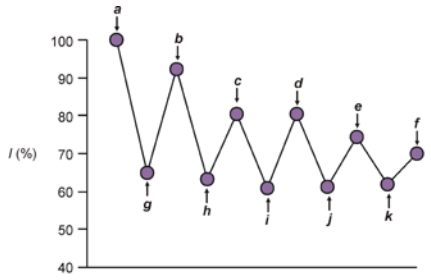

Figure 2.10. Relative emission intensity of a solution of **26a** (1.5 mg mL^{-1}, sodium phosphate buffer, pH = 7.0, 25°C, 440 nm) measured at 543 nm before (***a***) and after consecutive ultraviolet irradiation (***g–k***, 254 nm, 0.5 mW cm^{-2}, 1 min) and storage in the dark (***b–f***, 12 h).

2.2.3. PMMA films of BODIPY-Spiropyran Conjugate

2.2.3.1. Spectroscopy

The absorption and emission spectra (***a*** and ***d*** in Figure 2.11) of a PMMA film doped with the model fluorophore **19** (Figure 2.1) show bands at 526 and 554 nm respectively. In this region of wavelengths, the model photochrome **18a** (Figure 2.1) does not absorb. Indeed, the absorption spectrum of a PMMA film doped with **18a** shows bands only in the ultraviolet region (***b*** in Figure 2.11). Upon irradiation at 341 nm, **18a** switches to **18b** (Figure 2.1) with the concomitant appearance of a band at 563 nm in the absorption spectrum (***c*** in Figure 2.11). This band overlaps the emission of **19**, suggesting that the photogenerated state of the photochrome can accept the excitation energy of the fluorophore. Furthermore, the redox potentials of **19** and **18b** also suggest that the transfer of one electron from the excited fluorophore to the photogenerated state of the photochrome is exoergonic with an estimated free energy change of *ca.* –0.42 eV.[124] Thus, electron and energy transfer processes can quench the excited state of the fluorophore and suppress fluorescence.

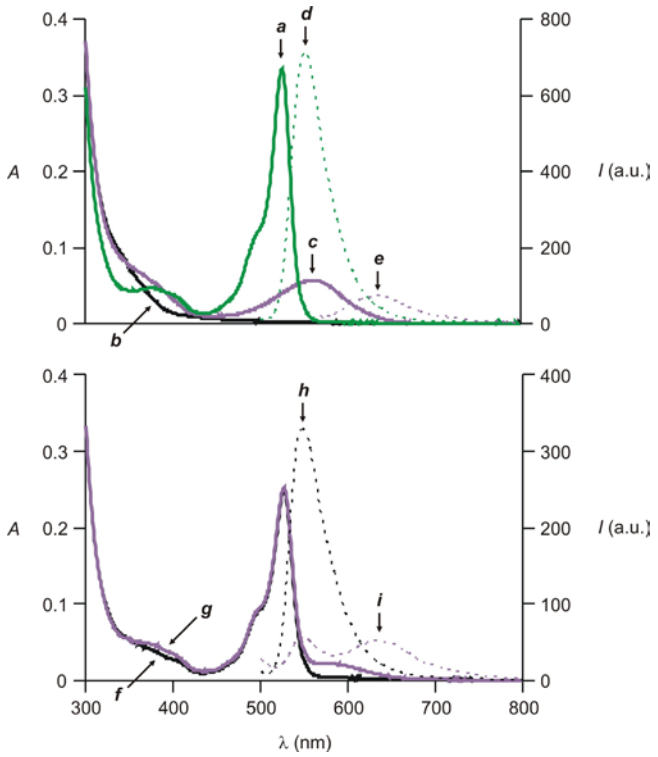

Figure 2.11 Absorption spectra of PMMA films (2% w/w, 6 μm, 20°C) doped with **19** (***a***), **20a** before (***b***) and after (***c***) irradiation, **18a** before (***f***) and after (***g***) irradiation. Emission spectra of the very same films doped with **19** (***d***), **20a** after irradiation (***e***), **18a** before (***h***) and after (***i***) irradiation. The samples were irradiated at 341 nm (35 μW cm^{-2}) for 10 min. The excitation wavelength was 480 nm in ***d***, ***h*** and ***i*** and 560 nm in ***e***.

The absorption spectrum (***f*** in Figure 2.11) of a PMMA film doped with the dyad **20a** shows the characteristic band of the BODIPY component at 527 nm. Upon irradiation at 480 nm, the fluorescent fragment of **20a** is selectively excited and its characteristic fluorescence appears at 548 nm in the emission spectrum (***h*** in Figure 2.11). Illumination at 341 nm, however, switches the photochromic component to generate **20b**. As a result, the characteristic absorption of the photogenerated merocyanine appears at 563 nm (***g*** in Figure 2.11). In addition, the emission of the BODIPY component decreases significantly with the photoisomerization and a new band appears at 640 nm (***i*** in Figure 2.11). This emission resembles that (***e*** in Figure 2.11) of the model merocyanine **18b** and is indicative of the transfer of energy from the excited BODIPY to the adjacent

photochrome within **20b**. Upon storage in the dark, the photogenerated isomer **18b** reverts to the original species **18a** with first-order kinetics. Fitting the temporal absorbance profile to a monoexponential decay function indicates the lifetime of **18b** to be *ca.* 1.4×10^3 s (*cf.*, 1.2×10^3 s for **20b**). Similarly, illumination at 560 nm encourages the reisomerization of **18b** back to **18a**. As a result, the emission intensity of the BODIPY component at 550 nm can be modulated by alternating ultraviolet and visible irradiation (Figure 2.12). However, the initial emission intensity is not fully restored after the first switching cycle. Thus, a significant fraction of molecules remains in the nonemissive form **18b** at the photostationary state reached upon visible irradiation. Nonetheless, subsequent switching cycles indicate that the emission intensity can be modulated reproducibly between *ca.* 10 and 35% of the original intensity.

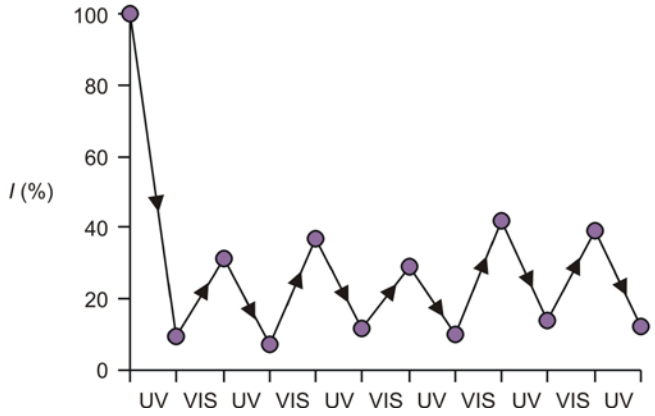

Figure 2.12 Emission intensity at 550 nm of PMMA films (2% w/w, 6 μm, 20°C) doped with **20a**, measured upon excitation at 480 nm, before and after sequential irradiation steps of 10 min at 341 (UV, 35 μW cm^{-2}) and 560 nm (VIS, 870 μW cm^{-2}).

2.2.3.2. Imaging

Illumination of a PMMA film doped with **20a** at 351 nm (λ_{OFF}), using a laser able to produce a doughnut-shaped spot of *ca.* 1 mm in diameter on the sample, results in the formation of **20b** only within the irradiated region. Consistently, an image (***a*** in Figure

2.13) of the resulting substrate, recorded with wide-field illumination at 480 nm (λ_{Ex}), shows a dark doughnut-shaped pattern against a green background, corresponding to the BODIPY fluorescence. The emission profile (Figure 2.14) across the patterned sample reveals the intensity at the doughnut center to be approximately four times greater than that measured in the dark region.

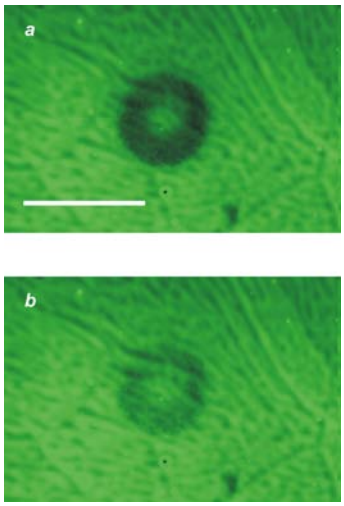

Figure 2.13 Wide-field fluorescence images (scale bar = 1 mm) of PMMA films (2% w/w, 6 μm, 20°C) doped with **20a**, recorded upon excitation at 480 nm, after irradiation at 351 nm (26 mW cm^{-2}) with a beam producing a doughnut-shaped spot (***a***) and subsequent storage in the dark for 15 min (***b***).

Thus, the interplay between λ_{Ex} and λ_{OFF}, in combination with the photochemical and photophysical response of the fluorophore–photochrome dyad, can, indeed, be exploited to confine fluorescence within the hole of a doughnut-shaped pattern. Upon storage of the doped PMMA film in the dark, the nonemissive species **20b** gradually reverts to the emissive form **20a** and the wide-field image (***b*** in Figure 2.13), recorded after 15 min, shows the fading of the dark doughnut. This behavior confirms that the contrast between dark and green regions is definitely a consequence of the interconversion between **20a** and **20b**.

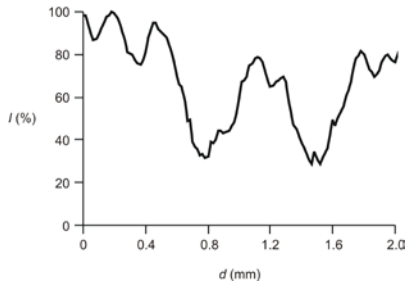

Figure 2.14 Profile of the emission intensity across the doughnut-shaped pattern in ***a*** of Figure 2.13.

2.3. Conclusions

BODIPY fluorophores can be connected covalently to spiropyran photochromes to construct photoswitchable fluorescent assemblies. Indeed, the photoinduced transformation of the spiropyran component of the resulting constructs into the corresponding merocyanine isomer causes a decrease in the emission intensity of the BODIPY component. Specifically, the emission intensity of the fluorophore decreases to 44% of the original value at the photostationary state in acetonitrile. The photogenerated isomer reverts thermally to the original one with monoexponential kinetics and a lifetime of 2.7×10^2 s. As a result, the original emission intensity is fully restored and the alternation of ultraviolet irradiation and storage in the dark can be exploited to switch repeatedly the emission intensity between high and low values. However, the fluorophore–photochrome dyad has a modest fatigue resistance and the emission intensity decreases by 24% after five switching cycles.

A norbornene fragment can be attached to the BODIPY–spiropyran conjugate and the resulting compound can be co-polymerized with a monomer incorporating a polyethylene glycol chain. The product of this reaction is a macromolecular assembly with an average of 15 hydrophilic chains per photochromic component. The polyethylene glycol

appendages of this construct impose solubility in aqueous environments and its photochromic components can be operated with optical stimulations in neutral buffer. In particular, the photoinduced isomerization of the photochrome causes a decrease of the emission intensity of the fluorophore to 60% of the original value at the photostationary state. The original species is regenerated, once again, upon storage in the dark. However, the lifetime of the photogenerated state of the polymer in aqueous environments is approximately two orders of magnitude longer than that of the monomeric BODIPY–spiropyran dyad in acetonitrile. Thus, the fluorescence of this polymeric assembly can be modulated alternating ultraviolet irradiation and storage in the dark. Nonetheless, its fatigue resistance is relatively poor and the emission intensity drops by 30% after five switching cycles.

Also, the BODIPY-Spiropyran conjugate can be trapped within a PMMA matrix and its fluorescence can be modulated under these conditions, relying on the interplay of two exciting beams of different wavelengths (λ_{OFF} and λ_{Ex}). As a result of this behavior, the patterned illumination of the doped PMMA film at λ_{OFF} can be exploited to imprint fluorescent patterns on the sample. In particular, irradiation at λ_{OFF} with a laser producing a doughnut-shaped spot confines the fluorescent molecules in the doughnut hole. Thus, the design logic behind the photochemical and photophysical response of this particular molecular switch can evolve into valuable operating principles for the realization of photoswitchable probes for super-resolution imaging schemes based on reversible fluorescence photodeactivation.

CHAPTER 3

PHOTOCHROMIC OXAZINES WITH DIFFERENT SUBSTITUENTS

3.1. Overview

Nitrospiropyrans are members of one of the most common families of photochromic compounds.[121–125] These molecules switch from a colorless form to a colored state upon ultraviolet irradiation and back to the original species in the dark. Their photocoloration involves the opening of a benzopyran ring followed by a *cis* → *trans* isomerization and occurs on a microsecond timescale. Their thermal decoloration requires a *trans* → *cis* isomerization in the ground state and is fairly slow. In fact, a full switching cycle, from colorless to colored and back, can only be completed on timescales of several minutes. In addition to slow switching speeds, these photochromic compounds have also poor fatigues resistances, mostly because of the participation of their triplet state in the photoisomerization process. In search of strategies to improve the switching speeds and fatigues resistance of nitrospiropyrans, a new family of photochromic compounds were developed based on the photoinduced opening and thermal closing of [1,3]oxazine rings.[126] In acetonitrile, these molecules switch from colorless to colored forms on a subnanosecond timescale and revert to the original species on nanosecond to microsecond timescales. Furthermore, they tolerate thousands of switching cycles with no sign of degradation, even in the presence of molecular oxygen. In principle, all-optical logic gates,[127–131] optical limiters,[132–136] photoresponsive filters[137] and photoswitchable probes[138–141] can all be designed around the unique properties of these thermally-reversible photochromic compounds. Each one of these applications, however, demands

stringent photochemical and photophysical requirements to be satisfied. Specifically, the excitation wavelength of the photochromic switch, the color of the photogenerated state, the efficiency of the photochemical transformation and the timescales of the photoinduced and thermal interconversions must all be adjusted to the specific application of choice. On the basis of these considerations, we explored structural modifications of the native [1,3]oxazine skeleton. In this chapter, I report the synthesis of eight new members of this class of photoresponsive molecules together with a detailed characterization of their photochemical and photophysical properties.

3.2. Results and Discussions

3.2.1. Design and Synthesis

The ultraviolet excitation of **27a** (Figure 3.1) opens its [1,3]oxazine ring to generate **27b** in less than 6 ns with a quantum yield of 0.10 (Table 3.1) in acetonitrile at 20°C. The photogenerated isomer reverts thermally to the original state with first-order kinetics and a lifetime of 25 ns. The photoinduced transformation of **27a** into **27b** is accompanied by the appearance of a band at 440 nm in the absorption spectrum. This band corresponds to a ground-state absorption of the 4-nitrophenolate chromophore of **27b** and decays monoexponentially with the thermal reisomerization of this species back to **27a**. In principle, the introduction of substituents in the *para* (R^1) and *ortho* (R^2) positions, relative to the nitrogen atom, of the 3*H*-indole fragment of **27a** or on its chiral center (R^3) can be exploited to control the rate of the decoloration process. Indeed, electron donating groups should stabilize the 3*H*-indolium cation of the corresponding photogenerated isomer and delay its thermal reisomerization, while electron withdrawing groups should

encourage the opposite effect. In addition, the nature of R^3 can also be exploited to regulate the absorption characteristics of the 3*H*-indolium cation of the photogenerated isomer. In fact, the photoinduced opening of the [1,3]oxazine ring brings R^3 in conjugation with the 3*H*-indolium cation. Thus, an extended π-system able to absorb in the visible region, in addition to the 4-nitrophenolate fragment, can be generated with a careful choice of R^3. On the basis of these considerations, we designed the eight [1,3]oxazines **27a**–**35a** (Figure 3.1).

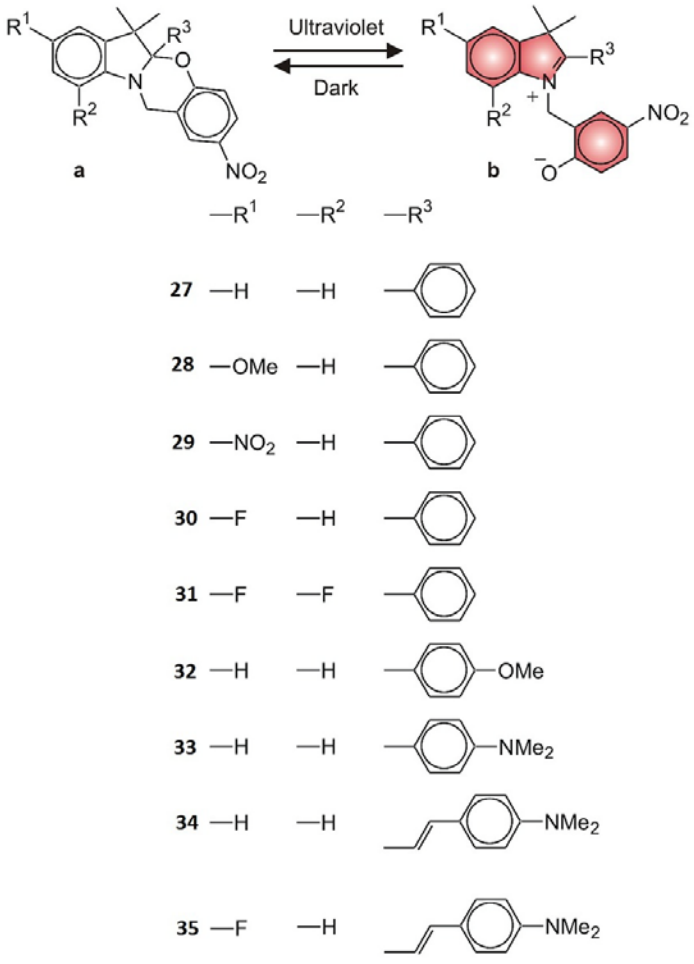

Figure 3.1. Photoinduced transformation of the [1,3]oxazines **27a**–**35a** into the zwitterions **27b**–**35b**.

In **28a**–**30a**, R^1 is a methoxy, nitro or fluorine substituent, R^2 is a hydrogen atom and R^3 is a phenyl ring. In **31a**, R^1 and R^2 are fluorine atoms and R^3 is a phenyl ring. In **32a**–**34a**, R^1 and R^2 are hydrogen atoms and R^3 is a 4-methoxyphenyl, 4-dimethylaminophenyl or 2-(4-dimethylaminophenyl)ethylene group. In **35a**, R^1 is a fluorine atom, R^2 is a hydrogen atom and R^3 is a 2-(4-dimethylaminophenyl)ethylene group.

I synthesized the [1,3]oxazines **28a**–**33a** in one step starting from the corresponding 3*H*-indoles **36**–**41** (Figure 3.2). Specifically, I *N*-alkylated these precursors with 2-chloromethyl-4-nitrophenol and isolated **28a**–**33a** in yields ranging from 18 to 57%, after the spontaneous cyclization of their [1,3]oxazine rings.

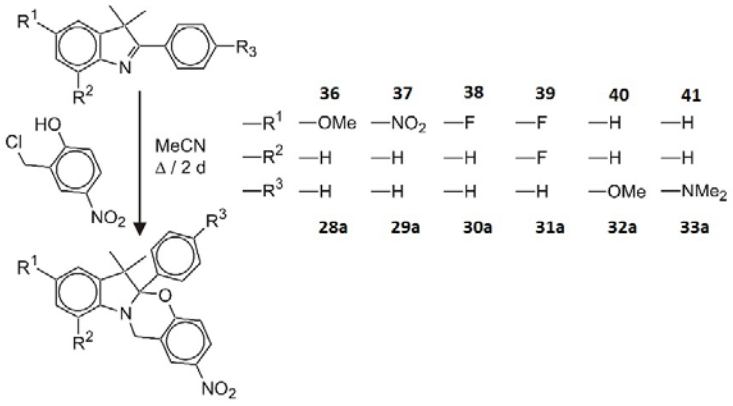

Figure 3.2. Synthesis of the [1,3]oxazines **28a**–**33a**.

I prepared **34a** in one step starting from the preformed [1,3]oxazine **42a** (Figure 3.3). In particular, I condensed this compound with 4-dimethylaminobenzaldehyde in the presence of trifluoroacetic acid and isolated **34a** in a yield of 47%.

Table 3.1. Spectroscopic data [*a*] for the [1,3]oxazines **27a**–**35a** and their model compounds **44**–**56**.

	λ (nm)	ε (mM^{-1} cm^{-1})	Φ	τ
27a	316	11.0	0.10	25 ns
28a	308	13.4	—	—
29a	346	15.3	—	—
30a	304	11.2	0.29	31 ns
31a	309	12.6	0.09	31 ns
32a	304	11.3	0.11	21 ns
33a	310	12.5	0.01	10 μs
34a	305	30.3	0.07	2 μs
35a	306	21.4	0.10	2 μs
44	302	3.9	—	—
45	354	9.9	—	—
46	292	2.8	—	—
48	297	3.8	—	—
47	281	3.9	—	—
49	333	12.6	—	—
50	373	6.5	—	—
51	298	10.8	—	—
52	295	13.1	—	—
53	342	12.2	—	—
54	438	15.5	—	—
55	552	60.8	—	—
56	540	64.0	—	—

[*a*] The absorption wavelength (λ), molar extinction coefficient (ε) at λ, quantum yield (Φ) for the photochromic transformation and lifetime (τ) of the photogenerated isomer were measured in MeCN at 20°C.

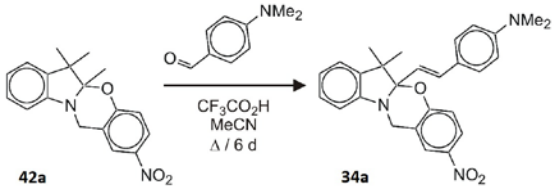

Figure 3.3. Synthesis of the [1,3]oxazine **34a**.

Similarly, I synthesized **35a** (Figure 3.4) by N-alkylation of compound **43** with 2-chloromethyl-4-nitrophenol and isolated **35a** in a yield of 60%.

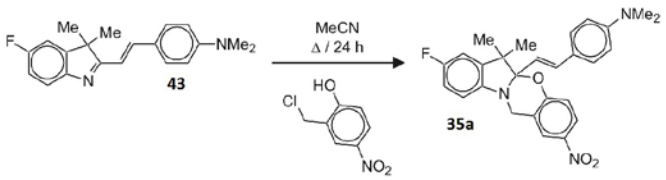

Figure 3.4. Synthesis of the [1,3]oxazine **35a**.

3.2.2. Steady-State Absorption Spectroscopy

The steady-state absorption spectra of **28a**–**33a** (***a*** in Figure 3.5, 3.6, 3.7, 3.8, 3.9 and 3.10) show a band at 304–346 nm (Table 3.1) with a molar extinction coefficient of 11.2–15.3 mM^{-1} cm^{-1}. In each case, this band is a result of the ground-state absorptions of the 4-nitrophenoxy and 3*H*-indole fragments and, hence, resembles the sum of those (***b*** and ***c*** in Figure 3.5, 3.6, 3.7, 3.8, 3.9 and 3.10) of 4-nitroanisole and the corresponding 3*H*-indole (**44**–**48** in Figure 3.11).

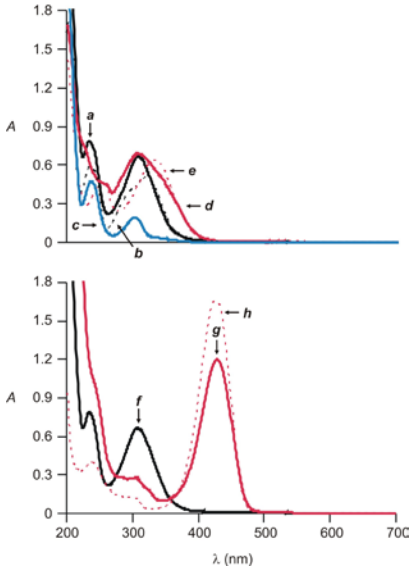

Figure 3.5. Steady-state absorption spectra of solutions (0.1 mM, MeCN, 20°C) of **28a** before (***a*** and ***f***) and after the addition of either CF_3CO_2H (10 eq., ***d***) or Bu4NOH (130 eq., ***g***), 4-nitroanisole (***b***), **44** (***c***), the iodide salt of **49** (***e***) and 4-nitrophenol after the addition of Bu_4NOH (4 eq., ***h***).

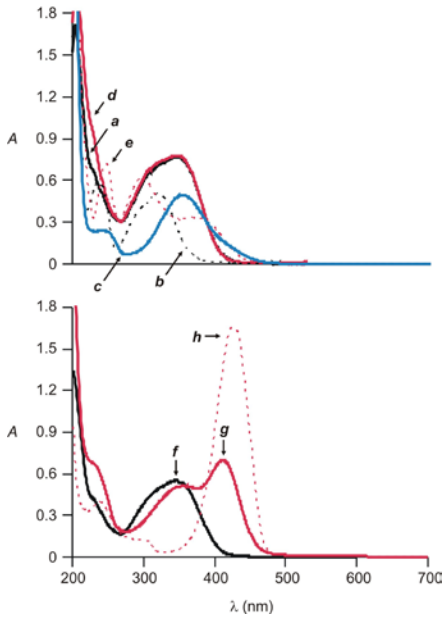

Figure 3.6. Steady-state absorption spectra of solutions (0.1 mM, MeCN, 20°C) of **29a** before (***a*** and ***f***) and after the addition of either CF_3CO_2H (120 eq., ***d***) or Bu_4NOH (50 eq., ***g***), 4-nitroanisole (***b***), **45** (***c***), the iodide salt of **50** (***e***) and 4-nitrophenol after the addition of Bu_4NOH (4 eq., ***h***).

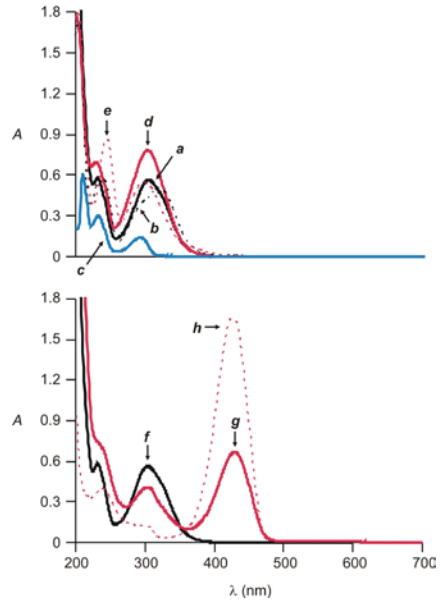

Figure 3.7. Steady-state absorption spectra of solutions (0.1 mM, MeCN, 20°C) of **30a** before (***a*** and ***f***) and after the addition of either CF_3CO_2H (100 eq., ***d***) or Bu_4NOH (10 eq., ***g***), 4-nitroanisole (***b***), **46** (***c***), the iodide salt of **51** (***e***) and 4-nitrophenol after the addition of Bu_4NOH (4 eq., ***h***).

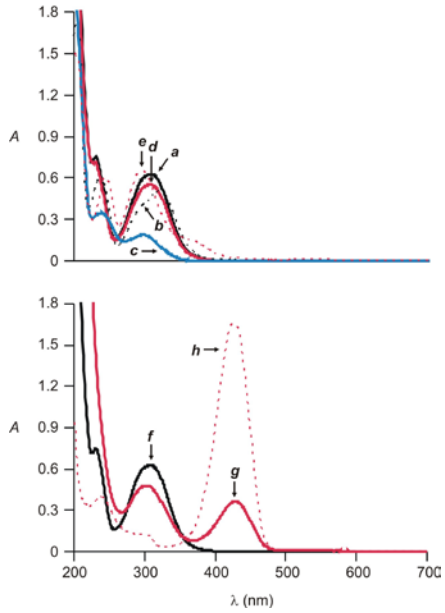

Figure 3.8. Steady-state absorption spectra of solutions (0.1 mM, MeCN, 20°C) of **31a** before (***a*** and ***f***) and after the addition of either CF_3CO_2H (100 eq., ***d***) or Bu_4NOH (100 eq., ***g***), 4-nitroanisole (***b***), **48** (***c***), the iodide salt of **52** (***e***) and 4-nitrophenol after the addition of Bu_4NOH (4 eq., ***h***).

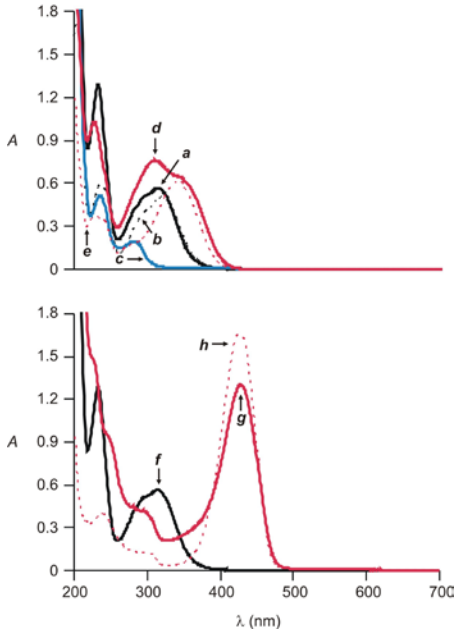

Figure 3.9. Steady-state absorption spectra of solutions (0.1 mM, MeCN, 20°C) of **32a** before (***a*** and ***f***) and after the addition of either CF_3CO_2H (100 eq., ***d***) or Bu_4NOH (100 eq., ***g***), 4-nitroanisole (***b***), **47** (***c***), the iodide salt of **53** (***e***) and 4-nitrophenol after the addition of Bu_4NOH (4 eq., ***h***).

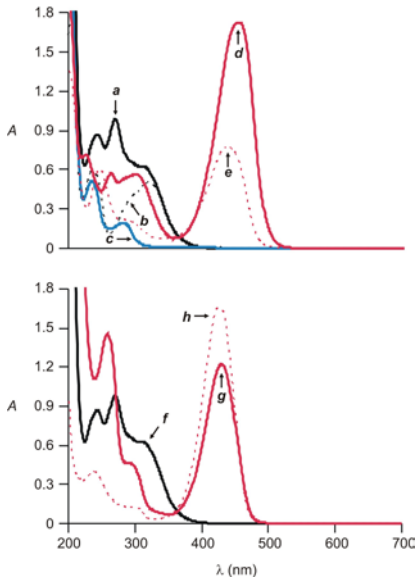

Figure 3.10. Steady-state absorption spectra of solutions (0.1 mM, MeCN, 20°C) of **33a** before (***a*** and ***f***) and after the addition of either CF_3CO_2H (100 eq., ***d***) or Bu_4NOH (100 eq., ***g***), 4-nitroanisole (***b***), **47** (***c***), the iodide salt of **54** (***e***) and 4-nitrophenol after the addition of Bu_4NOH (4 eq., ***h***).

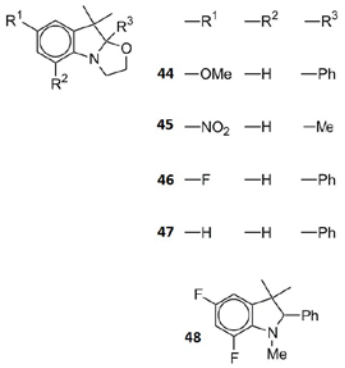

Figure 3.11. Model 3*H*-indoles **44**–**48**.

The spectrum (***a*** in Figure 3.12) of **34a** also shows a band at 305 nm (Table 3.1), but the molar extinction coefficient is 30.3 mM^{-1} cm^{-1}. In fact, the ground-state absorption of 4-vinyl-*N*,*N*-dimethylaniline (***d*** in Figure 3.12) is positioned in the vary same range of wavelengths. Thus, the 2-(4-dimethylaminophenyl)ethylene, 4-nitrophenoxy and 3*H*-indole fragments of **34a** are all responsible for the band at 305 nm. Similarly, the spectrum (Figure 3.13) of **35a** reveals a band centered at 306 nm for the overlapping

absorptions of the 2-(4-dimethylaminophenyl)ethynyl, 4-nitrophenoxy and 3*H*-indole chromophores.

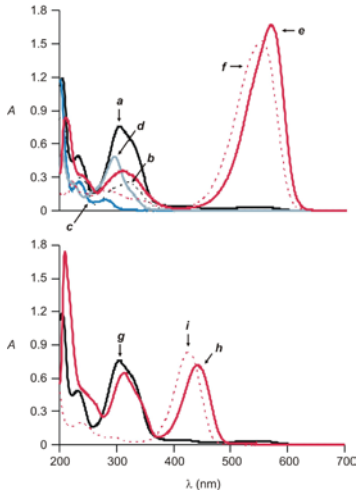

Figure 3.12. Steady-state absorption spectra of solutions (0.05 mM, MeCN, 20°C) of **34a** before (***a*** and ***g***) and after the addition of either CF_3CO_2H (2 eq., ***e***) or Bu_4NOH (51 eq., ***h***), 4-nitroanisole (***b***), **47** (***c***), 4-vinyl-*N*,*N*-dimethylaniline (***d***), the hexafluorophosphate salt of **55** (***f***) and 4-nitrophenol after the addition of Bu_4NOH (4 eq., ***i***).

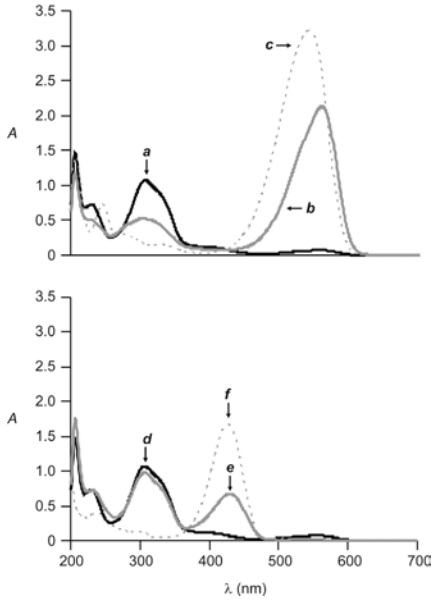

Figure 3.13. Steady-state absorption spectra of solutions (0.1 mM, MeCN, 20°C) of **35a** before (***a*** and ***d***) and after the addition of either CF_3CO_2H (1 eq., ***b***) or Bu_4NOH (5 eq., ***e***), 5**6** (***c***) and 4-nitrophenol after the addition of Bu_4NOH (4 eq., ***f***).

The [1,3]oxazine ring of **28a** and **30a**–**35a** opens upon addition of acid to generate the cations **28c** and **30c**–**35c** (Figure 3.14).

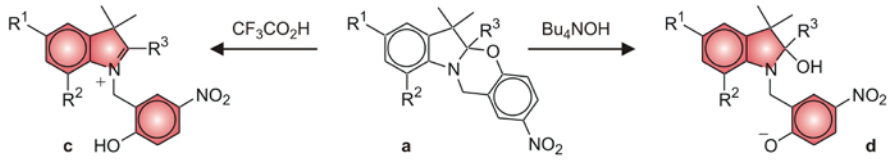

Figure 3.14. Transformation of the [1,3]oxazine **28a**–**35a** into the cations **28c**–**35c** or anions **28d**–**35d** under the influence of acid or base respectively.

These transformations are accompanied by the appearance of bands at 333, 303, 307, 342, 454, 568 and 559 nm respectively in the steady-state absorption spectra. These bands resemble the ground-state absorptions of the model compounds **49** and **51**–**56** (Figure 3.15) and, hence, are associated with the 3*H*-indolium chromophores of **28c** and **30c**–**35c**. In contrast to the behavior of **28a** and **30a**–**35a**, the addition of even a large excess of acid to **29a** causes only negligible changes in the absorption spectrum (***a*** and ***d*** in Figure 3.6), under otherwise identical conditions. Presumably, the electron withdrawing character of the nitro group on the 3*H*-indole fragment of **29a** is responsible for preventing the opening of the [1,3]oxazine ring.

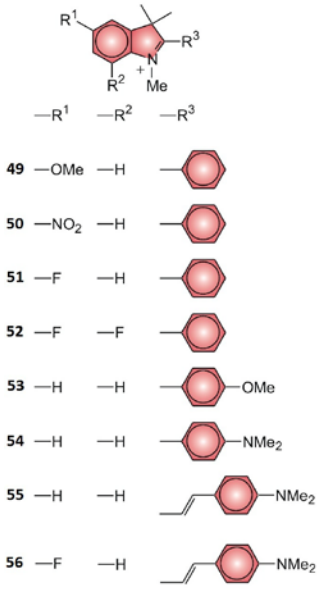

Figure 3.15. Model 3*H*-indolium cations **49**–**56**.

The [1,3]oxazine ring of **28a**–**35a** also opens upon addition of base to generate the anions **28d**–**35d** (Figure 3.14). All these species incorporate a 4-nitrophenolate chromophore and their formation is accompanied by the appearance of a band at 440 nm in the steady-state absorption spectrum. This band resembles the ground-state absorption of tetrabutylammonium 4-nitrophenolate and is associated with the 4-nitrophenolate fragment of **28d**–**35d**.

3.2.3. Transient Absorption Spectroscopy

The local excitation of the 4-nitrophenoxy chromophore of the parent compound **27a** at 355 nm opens its [1,3]oxazine ring to form the zwitterionic isomer **27b** with a quantum yield of 0.10 (Table 3.1) in acetonitrile at 20°C. Consistently, the ground-state absorption of the 4-nitrophenolate chromophore of **27b** can be observed at 440 nm in the transient spectrum recorded several nanoseconds after excitation. The introduction of a methoxy group in the *para* position, relative to the nitrogen atom, of the 3*H*-indole fragment of **27a** has a drastic effect on the photochemical behavior. Indeed, the transient spectra of **28a** do not show any significant signal on a nanosecond timescale, under otherwise identical conditions. By contrast, the presence of a fluorine atom in place of the methoxy group facilitates the photoinduced transformation. In fact, the excitation of **30a** opens the [1,3]oxazine ring with a threefold enhancement in quantum yield (Table 3.1) relative to the parent compound **27a**. Consistently, the transient spectrum (***a*** in Figure 3.16) shows the ground-state absorption of the 4-nitrophenolate chromophore of **30b**. Thus, the nature of the substituent in the *para* position, relative to the nitrogen atom, of the 3*H*-indole fragment has a pronounced influence on the efficiency of photoinduced opening of [1,3]oxazine ring.

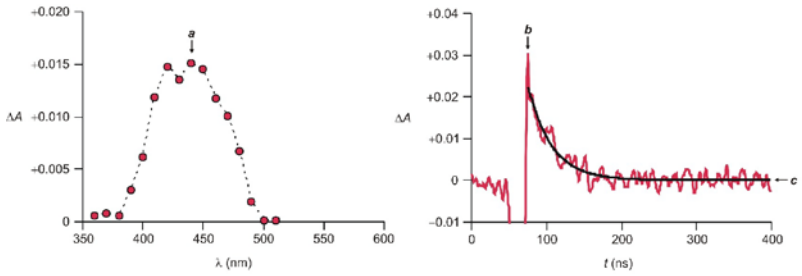

Figure 3.16. Transient absorption spectrum (0.02 mM, MeCN, 20°C) of **30a** (***a***) recorded 40 ns after laser excitation (355 nm, 12 mJ). Temporal evolution of the absorbance at 430 nm (***b***) after excitation and the corresponding monoexponential fitting (***c***).

The introduction of a second fluorine atom in the *ortho* position, relative to the nitrogen atom, of the 3*H*-indole fragment has a modest influence on the photoinduced ring-opening process and the photochemical behavior of **31a** is remarkably similar to that of **30a**. Once again, the ground-state absorption (***a*** in Figure 3.17) of the 4-nitrophenolate chromophore of **31b** can be observed upon excitation.

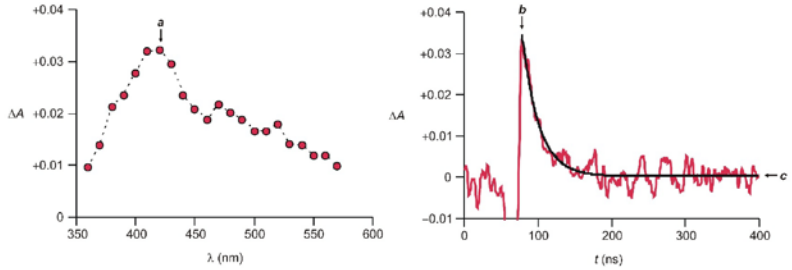

Figure 3.17. Transient absorption spectrum (0.03 mM, MeCN, 20°C) of **31a** (***a***) recorded 40 ns after laser excitation (355 nm, 12 mJ). Temporal evolution of the absorbance at 420 nm (***b***) after excitation and the corresponding monoexponential fitting (***c***).

Instead, the replacement of the fluorine atom of **30a** with a nitro group alters drastically the photochemical response. Indeed, the transient spectra (***a***–***d*** in Figure 3.18) of **29a** show a broad band similar to the one (***g*** in Figure 3.18) observed for the model 3*H*-indolium **50**, under otherwise identical conditions. In both instances, this band

decays with monoexponential kinetics (***e***, ***f*** , ***h*** and ***j*** in Figure 3.18) on a microsecond timescale and the lifetime of the transient species decreases significantly in the presence of molecular oxygen. Presumably, the nitro group on the 3*H*-indole fragment of **29a** facilitates intersystem crossing and encourages the population of the triplet state associated with the 3*H*-indolium chromophore of **29b**.

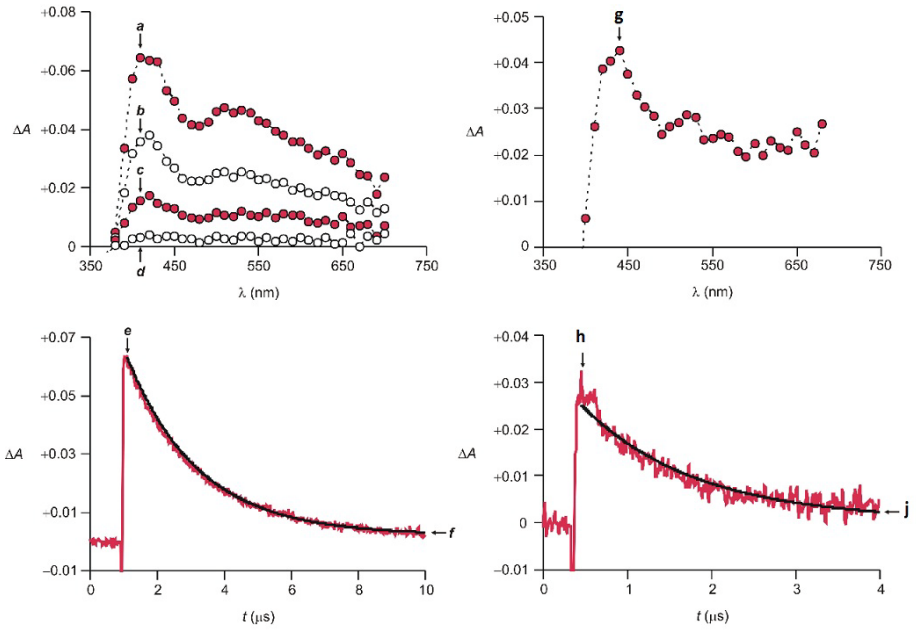

Figure 3.18. Transient absorption spectra (0.03 mM, MeCN, 20°C) of **29a** recorded 0.1 (***a***), 3.0 (***b***), 6.0 (***c***) and 10 μs (***d***) after laser excitation (355 nm, 12 mJ). Temporal evolution of the absorbance at 420 nm (***b***) after excitation and the corresponding monoexponential fitting (***f***). Transient absorption spectrum (0.03 mM, MeCN, 20°C) of the iodide salt of **50** (***g***) recorded 100 μs after laser excitation (355 nm, 12 mJ). Temporal evolution of the absorbance at 420 nm (***h***) after excitation and the corresponding monoexponential fitting (***j***).

The introduction of a methoxy group in the *para* position of the phenyl ring attached to the chiral center of the parent compound **27a** has negligible effects on the photochemical response. In fact, the excitation of **32a** opens its [1,3]oxazine ring to generate **32b** with a quantum yield of 0.11 (Table 3.1) and the transient spectrum (***a*** in

Figure 3.19) shows the characteristic ground-state absorption of the 4-nitrophenolate chromophore.

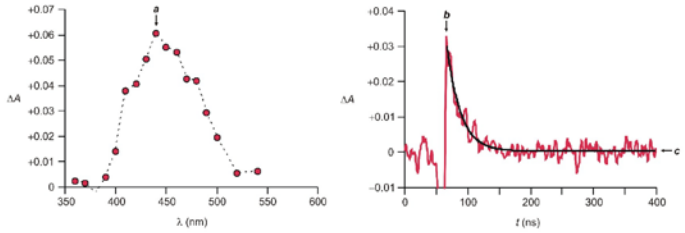

Figure 3.19. Transient absorption spectrum (0.03 mM, MeCN, 20°C) of **32a** (***a***) recorded 50 ns after laser excitation (355 nm, 12 mJ). Temporal evolution of the absorbance at 440 nm (***b***) after excitation and the corresponding monoexponential fitting (***c***).

A similar band is also observed in the transient spectrum (***a*** in Figure 3.20) of **33a**, in agreement with the photoinduced formation of **33b**. In this instance, however, the ground-state absorption of the 3*H*-indolium cation of the photogenerated isomer is positioned in the same region of wavelengths of that associated with the 4-nitrophenolate anion. Thus, the transient band is the sum of the absorptions of the two chromophoric fragments composing **33b**. Nonetheless, the photoinduced ring-opening process is not particularly efficient and the quantum yield for the formation of **33b** is only 0.01 (Table 3.1).

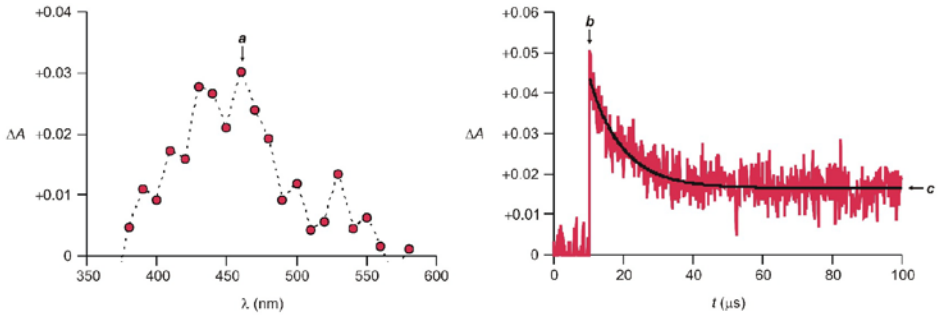

Figure 3.20. Transient absorption spectrum (0.04 mM, MeCN, 20°C) of **33a** (***a***) recorded 100 ns after laser excitation (355 nm, 12 mJ). Temporal evolution of the absorbance at 440 nm (***b***) after excitation and the corresponding monoexponential fitting (***c***).

The steady-state absorption spectrum (***f*** in Figure 3.12) of the hexafluorophosphate salt of the model compound **55** shows that the attachment of a 2-(4-dimethylaminophenyl)ethylene group to the 3*H*-indolium cation translates into the appearance of an intense band at 552 nm. Consistently, the transient spectra (***a–d*** in Figure 3.21), recorded after the excitation of **34a**, reveal a band at 550 nm for the 3*H*-indolium cation of **34b** together with that at 440 nm for the 4-nitrophenolate anion of this zwitterionic species. In agreement with this assignment, the quantum yield (Table 3.1) determined by monitoring the absorbance at 440 nm is essentially identical to that calculated by probing the absorbance at 550 nm.

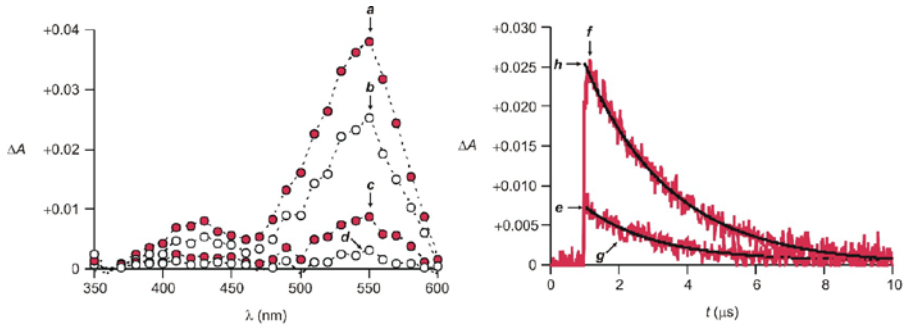

Figure 3.21. Transient absorption spectra (0.01 mM, MeCN, 20°C) of **34a** recorded 0.1 (***a***), 1.0 (***b***), 3.0 (***c***) and 10 μs (***d***) after laser excitation (355 nm, 12 mJ). Temporal evolution of the absorbance at 440 (***e***) and 550 nm (***f***) after excitation and the corresponding monoexponential fittings (***g*** and ***h***).

Similar to **34a**, the laser excitation of **35a** at 355 nm is accompanied by the appearance within 6 ns of two transient bands at 420 and 540 nm (***a*** in Figure 3.22) in the absorption spectrum. They resemble those observed in the steady-state spectra of **35d** and **35c** respectively (***e*** and ***b*** in Figure 3.13) and correspond to ground-state absorptions of the 4-nitrophenolate anion and 3*H*-indolium cation respectively of **35b**. Thus, the [1,3]oxazine ring of **35a** opens upon excitation to generate the bichromophoric isomer

35b, in analogy to the behavior of **34a** and **34b**. However, the transition from **34a** to **35a** results in an increase in quantum yield from 0.07 to 0.10.

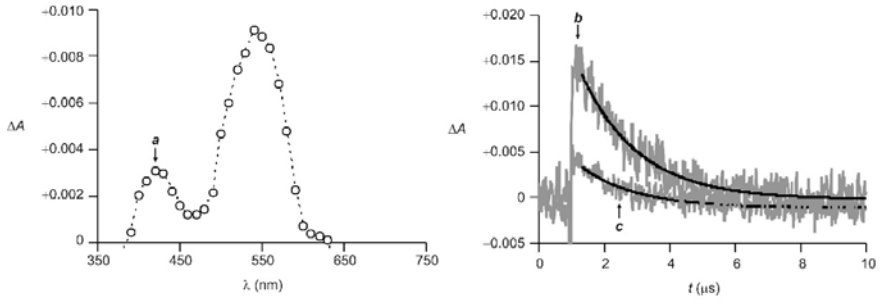

Figure 3.22. Transient absorption spectrum (0.04 mM, MeCN, 20°C) of **35a** (***a***) recorded 0.1 μs after laser excitation (355 nm, 6 ns, 12 mJ Temporal evolution of the absorbance (0.04 mM, MeCN, 20°C) at 440 (***b***) and 540 nm (c) after excitation (355 nm, 6 ns, 12 mJ) of **35a** and the corresponding monoexponential fittings.

The photogenerated isomer **27b** of the parent compound **27a** switches back to the original form in the dark with first-order kinetics and a lifetime of 25 ns (Table 3.1) in acetonitrile at 20°C. The photogenerated species **30b**, **31b** and **32b** show essentially the same behavior. The band of their 4-nitrophenolate chromophore decays monoexponentially on a nanosecond timescale and their lifetime ranges from 21 to 31 ns (Table 3.1). Thus, the introduction of either fluorine atoms on the 3*H*-indole fragment or a methoxy group on the phenyl ring attached to the chiral center has a negligible influence on the reisomerization kinetics.

A similar monoexponential decay is also observed for the band associated with the 4-nitrophenolate chromophore of **33b** as well as for those corresponding to the 4-nitrophenolate anion and 3*H*-indolium cation of **34b** and **35b**. The reisomerization of these compounds, however, occurs on a microsecond timescale and their lifetimes are 10

and 2 μs (Table 3.1) respectively. The relatively long lifetimes of these species are, presumably, a result of the ability of their electron donating substituents to stabilize the 3*H*-indolium cation and, hence, delay the reisomerization process. Thus, all six photochromic compounds can be switched back and forth between their two states with switching rates ranging from 0.1 to 50 MHz. Furthermore, they all have excellent fatigue resistances and survive unaffected thousands of switching cycles in air. Specifically, their steady-state absorption spectra recorded before and after 300 switching cycles are essentially identical, indicating that the photodegradation of these compounds is negligible.

3.3. Conclusions

We investigated the influence of three substituents on the photochromism of heterocyclic compounds fusing 3*H*-indole and nitrobenzooxazine fragments in their molecular skeleton. Specifically, we varied the groups in the *para* (R^1) and *ortho* (R^2) positions, relative to the nitrogen atom, of the 3*H*-indole fragment and that (R^3) attached to the chiral center at the junction of the two heterocycles. Two of them (R^1 and R^3) affect the efficiency of the photochemical process, involving the opening of a [1,3]oxazine ring with the generation of a zwitterionic isomer. One of them (R^3) also dictates the absorption properties of the photogenerated species and the reisomerization kinetics. In particular, the photochromic transformation is completely suppressed when R^1 is a methoxy group, while it is greatly facilitated when R^1 is a fluorine atom. Thus, the ability of R^1 to donate or withdraw electrons to or from the 3*H*-indole heterocycle regulates the quantum yield of the photoinduced ring-opening process. Nonetheless, the nature of R^1 has a negligible influence on the lifetime of the photogenerated isomer,

which is instead dependent on R^3. Indeed, the introduction of dimethylamino or 2-(4-dimethylaminophenyl)ethylene groups at R^3 prolongs the lifetime of the photogenerated isomer from the nanosecond to the microsecond timescale. Presumably, these electron-rich substituents increase the stability of the 3*H*-indolium cation associated with the photogenerated isomer and increase its lifetime. Similarly, R^3 also regulates the absorption properties of the 3*H*-indolium cation and, thus, can be exploited to impose bichromophoric character on these photochromic compounds. When R^3 is a 2-(4-dimethylaminophenyl)ethylene, for example, a band at 550 and 540 nm for the 3*H*-indolium cation of the zwitterionic isomers develops in the transient spectra, together with one at 440 nm for the associated 4-nitrophenolate anion, upon excitation. In addition, these photochromic compounds tolerate hundreds of excitation cycles without decomposing even in the presence of molecular oxygen.

CHAPTER 4

PHOTOCHROMIC POLYMERS BASED ON THE PHOTOINDUCED OPENING AND THERMAL CLOSING OF [1,3]OXAZINE RINGS

4.1. Overview

The excitation of **27a** (Figure 4.1) with ultraviolet radiations opens its [1,3]oxazine ring to generate the zwitterionic isomer **27b** in less than 6 ns with a quantum yield of 0.10 in acetonitrile at 20°C. Under these conditions, the photogenerated isomer has a lifetime of 25 ns and reverts spontaneously back to the original species with first-order kinetics. In fact, a full photoinduced switching cycle, from **27a** to **27b** and back, can be completed on a nanosecond timescale. Furthermore, this photochromic system survives thousands of switching cycles with no sign of degradation, even in the presence of molecular oxygen. Thus, photochromic polymers with fast switching speeds and excellent fatigue resistances can, in principle, be designed around the photochemical properties of these heterocyclic compounds. In search of strategies to append these compounds to polymer backbones, we envisaged the possibility of building macromolecular constructs with photochromic side chains on the basis of ring-opening polymerizations. In this chapter, I report the synthesis of two photochromic polymers, prepared according to these design principles, and a detailed spectroscopic characterization of their photochemical behavior.

4.2. Results and Discussion

4.2.1. Design and Synthesis

In search of strategies to incorporate **27a** into macromolecular constructs, we envisaged the possibility of introducing polymerizable groups in the *para* position (R^1 in

Figure 4.1), relative to the nitrogen atom, of the 3*H*-indole fragment or in the *para* position (R^2) of the phenyl ring at the junction of the two heterocycles. In particular, I attached a norbornene group to both positions through ester linkages in the form of compounds **57a** and **58a** (Figure 4.1) in two synthetic steps, starting from known precursors (Figures 4.2). Then, we reacted **57a** and **58a** with benzylidene-bis(tricyclohexylphosphine)dichlororuthenium and obtained the polymers **59a** and **60a** (Figures 4.3 and 4.4) respectively, after termination with vinyl ethyl ether.

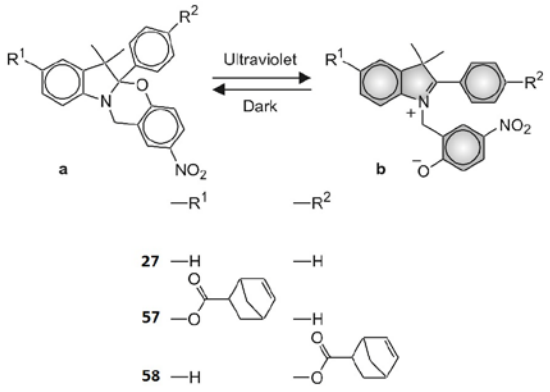

Figure 4.1. Photoinduced transformation of the [1,3]oxazines **27a** and **57a**–**58a** into the zwitterionic isomers **27b** and **57b**–**58b**.

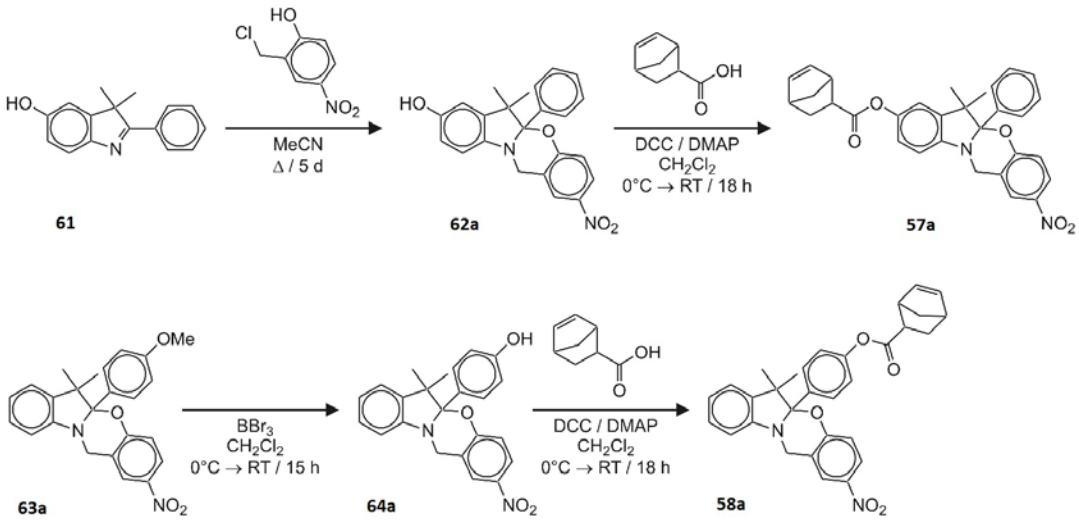

Figure 4.2. Synthesis of the [1,3]oxazine **57a** and **58a**.

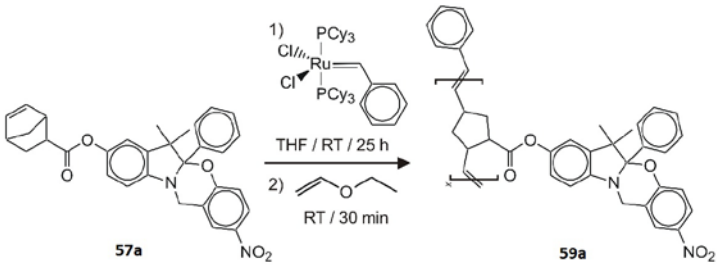

Figure 4.3. Synthesis of the photochromic polymer **59a**.

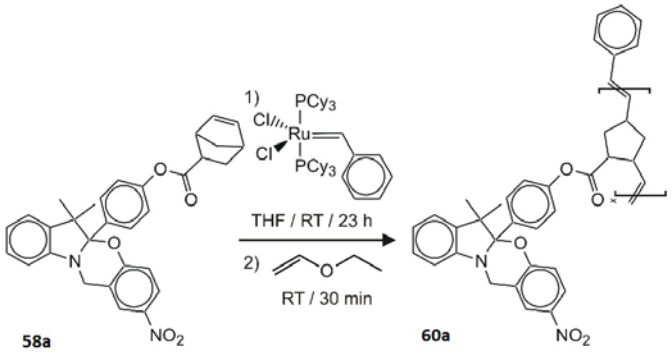

Figure 4.4. Synthesis of the photochromic polymer **60a**.

4.2.2. Steady-State Absorption Spectroscopy

The steady-state absorption spectra (***a*** in Figures 4.5 and 4.6) of the monomers **57a** and **58a** show a band centered at *ca.* 305 nm. This band resembles the one observed in the spectrum (***c*** in Figures 4.5 and 4.6) of 4-nitroanisole and, hence, can be assigned to the 4-nitrophenoxy chromophore of **57a** and **58a**. Upon addition of tetrabutylammonium hydroxide, the [1,3]oxazine ring of **57a** and **58a** opens to generate the hemiaminals **57c** and **58c** respectively (Figure 4.7). As a result of this transformation, a band centered at *ca.* 425 nm appears in the corresponding spectrum (***b*** in Figures 4.5 and 4.6). This band resembles the one observed in the spectrum (***d*** in Figures 4.5 and 4.6) of 4-nitrophenol after the addition of base and, hence, can be assigned to the 4-nitrophenolate chromophore of **57c** and **58c**.

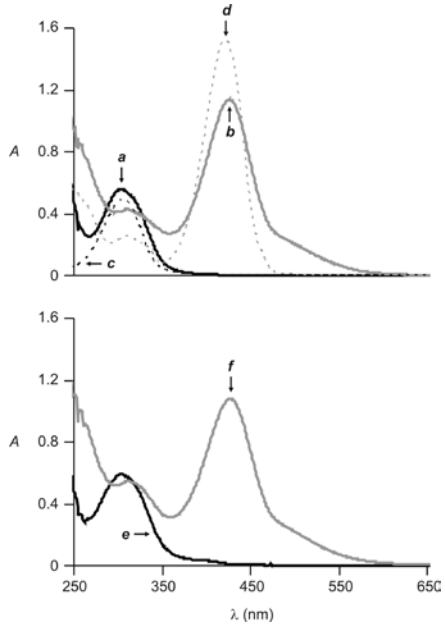

Figure 4.5. Steady-state absorption spectra (THF, 20°C) of **57a** (0.1 mM) before (***a***) and after (***b***) the addition of Bu_4NOH (10 eq.), 4-nitroanisole (0.1 mM, ***c***), 4-nitrophenol (0.1 mM) after the addition of Bu_4NOH (10 eq., ***d***), **59a** (0.1 mg mL^{-1}) before (***e***) and after (***f***) the addition of a THF solution of Bu_4NOH (0.1 M, 100 μL).

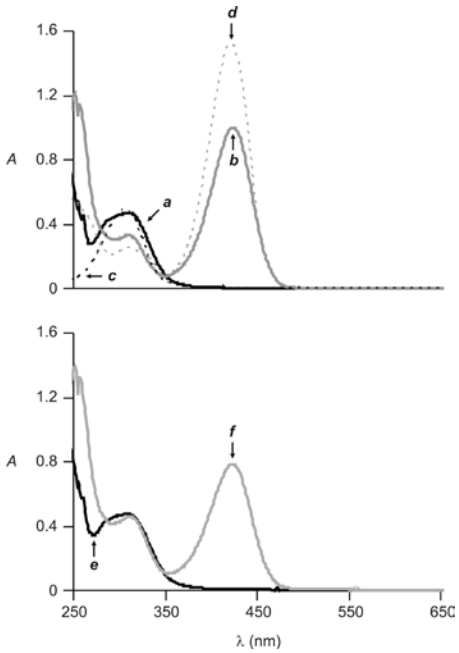

Figure 4.6. Steady-state absorption spectra (THF, 20°C) of **58a** (0.1 mM) before (***a***) and after (***b***) the addition of Bu_4NOH (10 eq.), 4-nitroanisole (0.1 mM, ***c***), 4-nitrophenol (0.1 mM) after the addition of Bu_4NOH (10 eq., ***d***), **60a** (0.1 mg mL^{-1}) before (***e***) and after (***f***) the addition of a THF solution of Bu_4NOH (0.1 M, 100 μL).

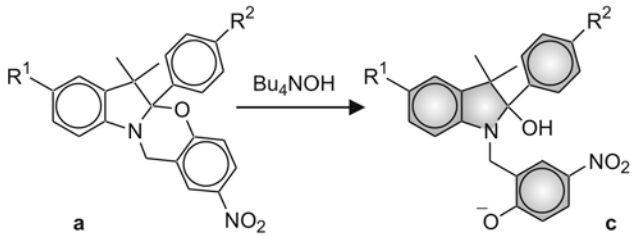

Figure 4.7. Transformation of the [1,3]oxazines **57a**–**60a** into the hemiaminals **57c**–**60c** under the influence of base.

The spectroscopic signature of the polymers **59a** and **60a** is similar to that of the monomers **57a** and **58a**. In both instances, the steady-state absorption spectrum (***e*** in Figures 4.5 and 4.6) shows a band centered at *ca.* 305 nm for the 4-nitrophenoxy fragment. Upon addition of tetrabutylammonium hydroxide, the [1,3]oxazine rings appended to the polymer backbone open to generate the corresponding hemiaminals **59c** and **60c** (Figure 4.7). Consistently, a band centered at *ca.* 425 nm for the 4-nitrophenolate chromophore appears in the corresponding spectra (***f*** in Figures 4.5 and 4.6).

4.2.3. Transient Absorption Spectroscopy

The excitation of the monomers **57a** and **58a** at 355 nm, in the tail of the absorption band corresponding to their 4-nitrophenoxy chromophore, results in the opening of the [1,3]oxazine ring with the formation of the zwitterionic isomers **57b** and **58b** (Figure 4.1) in less than 6 ns. Consistently, the absorption spectra (***a*** and ***b*** in Figure 4.8), recorded 20 ns after laser illumination, reveal the characteristic ground-state absorption of the 4-nitrophenolate chromophore of **57b** and **58b** in the visible region. In both instances, the quantum yield for the photochromic transformation is 0.09.

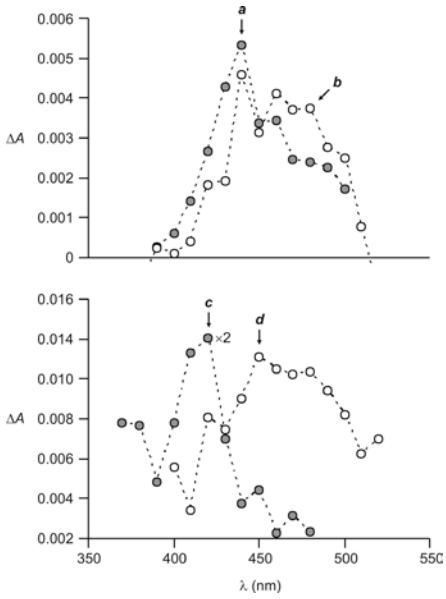

Figure 4.8. Absorption spectra [MeCN/Me_2CO (7:3, v/v), 20°C] of **57a** (0.2 mM, ***a***) and **58a** (0.2 mM, ***b***), recorded 20 ns after laser excitation (355 nm, 6 ns, 15 mJ), and of **59a** (0.08 mg mL^{-1}, ***c***) and **60a** (0.19 mg mL^{-1}, ***d***), recorded 0.1 μs after laser excitation.

The photochemical behavior of the polymers **59a** and **60a** is remarkably similar to that of the corresponding monomers **57a** and **58a**. Once again, excitation in the tail of the 4-nitrophenoxy absorption cleaves the [C–O] bond at the junction of the two heterocyclic fragments to produce the zwitterionic isomers **59b** and **60b**. As a result of these photoinduced transformations, the ground-state absorption of the 4-nitrophenolate chromophore appears in the visible region of the spectra (***c*** and ***d*** in Figure 4.8), recorded 0.1 μs after laser illumination. However, the transient band of **60b** is broader and centered at a longer wavelength than that of **59b**. These spectral differences are, presumably, a result of ground-state interactions between the 4-nitrophenolate chromophores of **60b** and/or the co-existence of subsets of 4-nitrophenolate chromophores in different environments for this particular polymer. Once again, the quantum yield for the photochromic transformation is 0.09. Thus, our compounds retain

their photochromism with comparable quantum efficiency even after covalent attachment to a macromolecular backbone.

The photogenerated isomers **57b** and **58b** revert spontaneously to the original state with first-order kinetics. In concomitance with this thermal transformation, the absorbance of the 4-nitrophenolate chromophore decays mono-exponentially (***a*** and ***e*** in Figure 4.9). Curve fitting of the temporal absorbance profiles (***c*** and ***g*** in Figure 4.9) indicates the lifetimes of **57b** and **58b** to be 21 and 23 ns respectively.

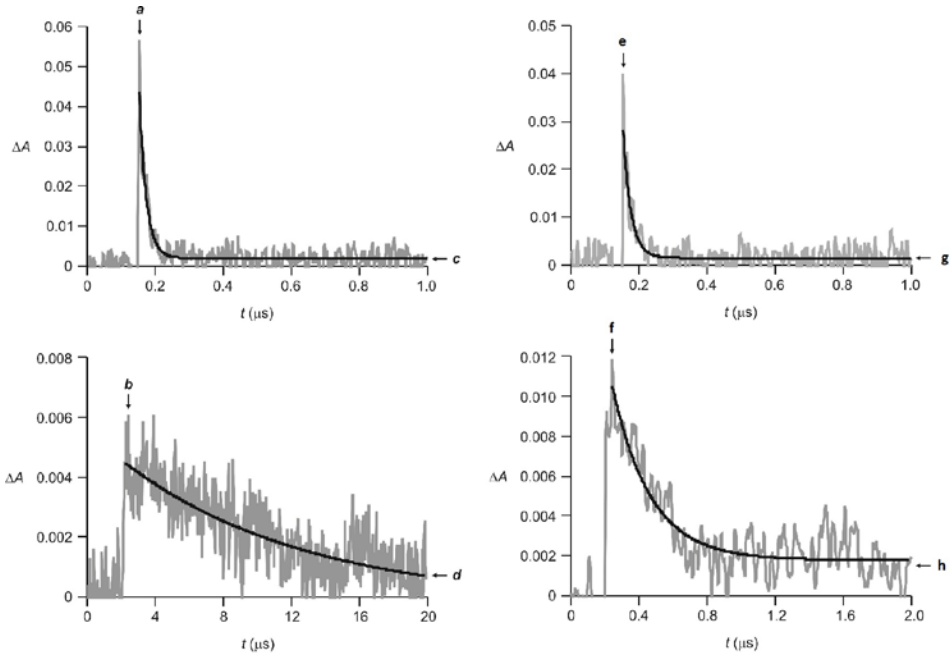

Figure 4.9. Absorbance evolution at 430 nm after the laser excitation (355 nm, 6 ns, 15 mJ) of **57a** (0.2 mM, ***a***) and **59a** (0.08 mg mL^{-1}, ***b***) [MeCN/Me_2CO (7:3, v/v), 20°C] and the corresponding curve fittings (***c*** and ***d***). Absorbance evolution at 430 nm after the laser excitation (355 nm, 6 ns, 15 mJ) of **58a** (0.2 mM, ***e***) and **60a** (0.19 mg mL^{-1}, ***f***) [MeCN/Me_2CO (7:3, v/v), 20°C] and the corresponding curve fittings (***g*** and ***h***).

The absorption spectra of the polymers reveal a similar temporal evolution. Their photogenerated isomers **59b** and **60b** also revert spontaneously to the original state with

first-order kinetics and, concomitantly, the 4-nitrophenolate absorption decays mono-exponentially (***b*** and ***f*** in Figure 4.9). However, the macromolecular backbone tends to delay the reisomerization process and the lifetimes of **59b** and **60b** are 11 and 0.2 μs respectively. Thus, the position of the photochromic element connected to the polymer backbone seems to have a noticeable influence on the stability of the photogenerated species and, as a result, on the reisomerization kinetics. In any case, both photochromic polymers can be switched back and forth between their two interconvertible states on a microsecond timescale. Furthermore, they survive hundreds of switching cycles with no sign of degradation even in the presence of molecular oxygen. Indeed, the 4-nitrophenolate absorbance of **59b** and **60b** (***a*** and ***b*** in Figure 4.10) does not change even after 200 excitation cycles, demonstrating that these photochromic polymers have outstanding fatigue resistances.

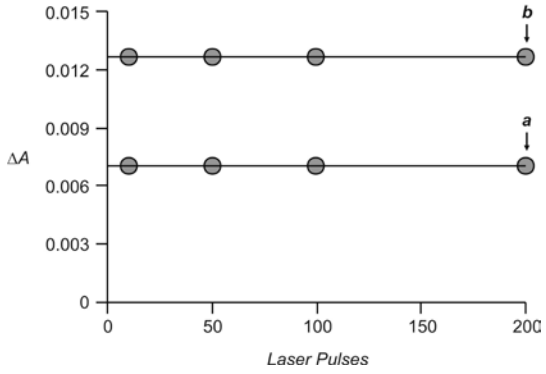

Figure 4.10. Evolution of the transient absorbance at 420 and 450 nm for solutions [MeCN/Me_2CO (7:3, v/v), 20°C] of **59a** (0.08 mg mL^{-1}, ***a***) and **60a** (0.19 mg mL^{-1}, ***b***) respectively with the number of laser pulses (355 nm, 6 ns, 15 mJ).

4.3. Conclusions

Photochromic [1,3]oxazines can be incorporated within macromolecular constructs by ring-opening polymerization of norbornene appendages. The photochromic

components in the side chains of the resulting polymers retain their photochemical behavior with comparable quantum efficiencies to those of the corresponding monomers. In all instances, ultraviolet irradiation opens the [1,3]oxazine rings of the photochromic components in less than 6 ns with a quantum yield of 0.09 in solution. The photogenerated species of the monomers and their polymers revert spontaneously to the original form with first-order kinetics. However, the macromolecular backbone delays considerably the reisomerization kinetics. In fact, the lifetime of the photogenerated species increases from *ca.* 20 ns up to 11 μs with the transition from monomers to polymers. All systems tolerate hundreds of excitation cycles and can be switched back and forth between their interconvertible states with no sign of degradation, even in air. Thus, our results can translate into valuable operating principles for the realization of photochromic polymers with fast switching speeds and excellent fatigue resistances.

CHAPTER 5

HYDROPHILIC AND PHOTOCHROMIC SWITCHES BASED ON THE OPENING AND CLOSING OF [1,3]OXAZINE RINGS

5.1. Overview

Photochromic compounds based on the photoinduced opening and thermal closing of [1,3]oxazine rings switch from colorless to colored forms on a subnanosecond timescale and revert to the original species on nanosecond to microsecond timescales. Furthermore, they tolerate thousands of switching cycles with no sign of degradation, even in the presence of molecular oxygen. In principle, their outstanding photochemical behavior could be used to photoregulate the properties and functions of bimolecular systems. First, however, it is necessary to establish if the photochromic performance of these compounds can survive the transition from organic to aqueous environments necessary for biological applications. On the basis of these considerations, we envisaged the possibility of preparing hydrophilic analogs of these oxazines and studying their photochemical properties in aqueous solutions. In this chapter, I report the synthesis of three hydrophilic and photochromic systems and their spectroscopic characterization.

5.2. Results and Discussion

5.2.1. Design and Synthesis

Once again, compound **27a** has an excellent photochromic properties in terms of switching speeds and fatigue resistance. However, it is not soluble in water and, as a result, its photochromic behavior in aqueous environments could not be tested. In principle, the introduction of a hydrophilic tail in the *para* position, relative to the

nitrogen atom, of its 3*H*-indole fragment can be exploited to impose aqueous solubility on the overall assembly and permit spectroscopic investigations in water. On the basis of these considerations, we designed the oxazines **65a** and **66a** (Figure 5.1) with pendant oligo(ethylene glycol) tails and the co-polymer **67a** with photochromic and hydrophilic fragments attached to a common polymer backbone.

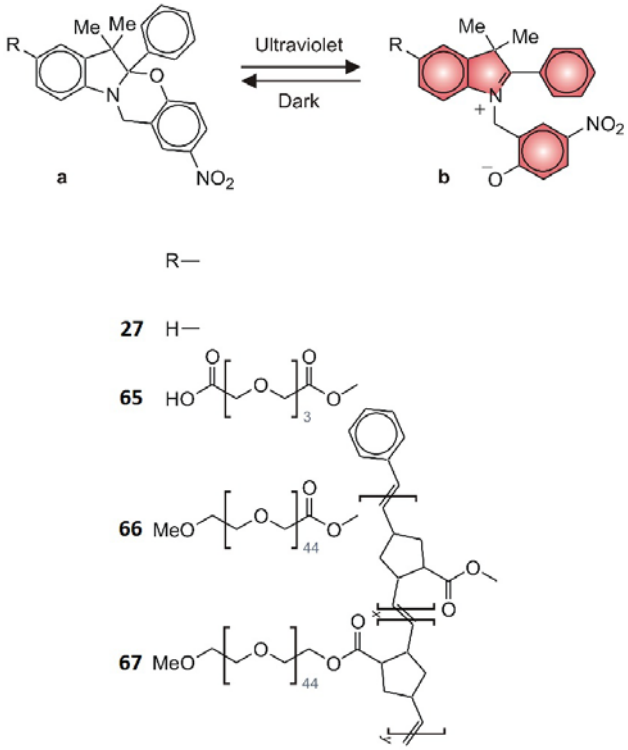

Figure 5.1. Photoinduced transformation of the [1,3]oxazines **27a** and **65a**–**67a** into the zwitterionic isomers **27b** and **65b**–**67b**.

I synthesized the hydrophilic compounds **65a** and **66a** in one step, starting from the pre-formed [1,3]oxazine **62a** (Figure 5.2). In particular, I reacted **62a** with either 3,6,9-trioxaundecanedioic acid or methoxy-PEG-2000-carboxylic acid, in the presence of *N*,*N*'-dicyclohexylcarbodiimide (DCC) and 4-dimethylaminopyridine (DMAP), to generate **65a** or **66a** in yields of 57 and 15% respectively.

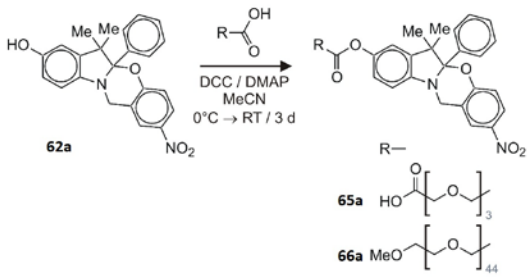

Figure 5.2. Synthesis of the [1,3]oxazines **65a** and **66a**.

Similarly, I prepared the co-polymer **67a** in one step, starting from the preformed [1,3]oxazine **57a** (Figure 5.3). Specifically, I co-polymerized **57a** and **68**, in the presence of benzylidene-bis(tricyclohexylphosphine)dichlororuthenium, to produce **67a**, after the addition of vinyl ethyl ether. The ^{1}H nuclear magnetic resonance (NMR) spectrum of **67a** indicated this co-polymer to incorporate an average of 1.5 photochromic units per hydrophilic chain. In addition, gel permeation chromatography (GPC) revealed the number average molecular weight (M_n) of **67a** to be 19,000 with a polydispersity index (PDI) of 1.13.

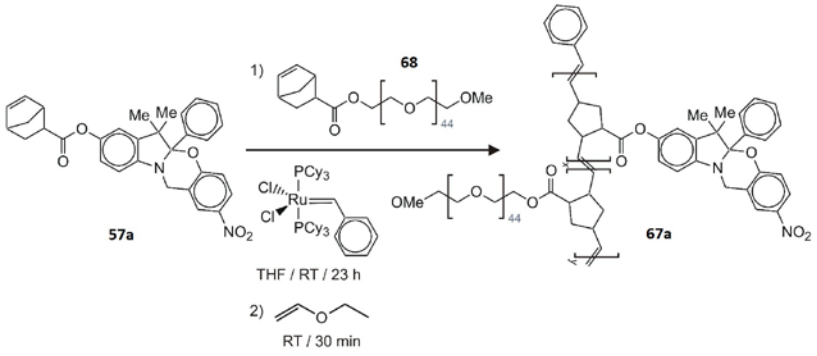

Figure 5.3. Synthesis of the polymer **67a**.

5.2.2. Steady-State Absorption Spectroscopy

The oligo(ethylene glycol) tail of **65a** is not sufficiently long to impose aqueous solubility on the heterocyclic fragment. However, this compound readily dissolves in a

mixture of acetonitrile and water (1:1, v/v). Under these conditions, the steady-state absorption spectrum (***a*** in Figure 5.4) shows a band centered at 309 nm with a molar extinction coefficient of 10.4 mM^{-1} cm^{-1}. This band resembles that of 4-nitroanisole (***c*** in Figure 5.4) and can be assigned to the 4-nitrophenoxy chromophore of **65a**. Upon addition of base, the [1,3]oxazine ring of **65a** opens to generate the hemiaminal **65c** (Figure 5.5). This transformation is accompanied by the appearance of a band centered at 401 nm (***b*** in Figure 5.4). This absorption resembles that of tetrabutylammonium 4-nitrophenolate (***d*** in Figure 5.4) and corresponds to the 4-nitrophenolate anion of **65c**.

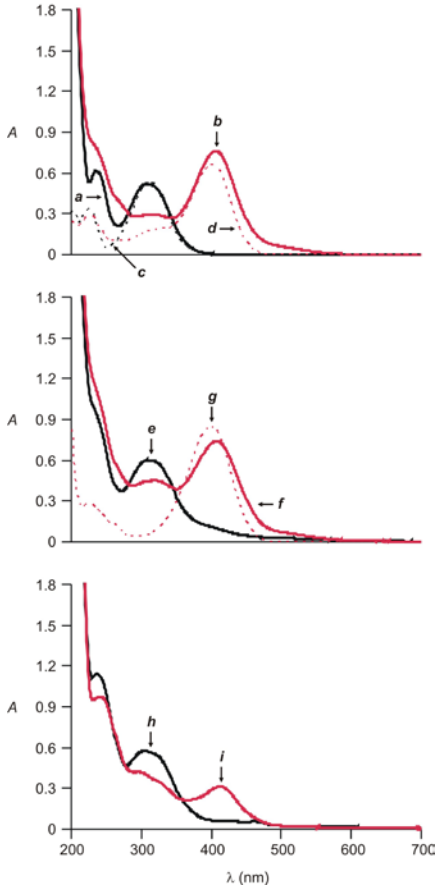

Figure 5.4. Steady-state absorption spectra (20°C) of **65a** before (***a***) and after (***b***) the addition of Bu_4NOH (100 eq.), 4-nitroanisole (***c***), 4-nitrophenol after the addition of Bu_4NOH [1 eq. (***d***) or 10 eq. (***g***)], **66a** before (***e***) and after (***f***) the addition of Bu_4NOH (10 eq.), **67a** before (***h***) and after (***i***) the addition of aqueous Bu_4NOH (160 µL, 1.5 M). The concentration was 0.1 mM in ***a***–***g*** and 1.7 mg mL^{-1} in ***h*** and ***i***. The solvent was MeCN/H_2O (1:1, v/v) in ***a***–***d*** and H_2O in ***e***–***i***.

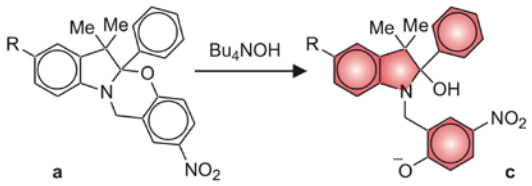

Figure 5.5. Transformation of the [1,3]oxazines **65a**–**67a** into the hemiaminals **65c**–**67c** under the influence of base.

The poly(ethylene glycol) chains of **66a** and **67a** impose aqueous solubility on both compounds. The corresponding spectra (***e*** and ***h*** in Figure 5.4), recorded in water, show a band centered at *ca.* 305 nm for the 4-nitrophenoxy fragment, as observed for **65a** (***a*** in Figure 5.4) in acetonitrile/water. Upon addition of base, the [1,3]oxazine rings of **66a** and **67a** open to generate the hemiaminals **66c** and **67c** (Figure 5.5). As a result of this transformation, a band at *ca.* 400 nm appears in the corresponding spectra (***f*** and ***i*** in Figure 5.4). This absorption resembles that of tetrabutylammonium 4-nitrophenolate (***g*** in Figure 5.4), recorded under the same conditions, and corresponds to the 4-nitrophenolate chromophores of **66c** and **67c**.

The spectra of **66a** and **67a** recorded in sodium phosphate buffer at neutral pH are essentially identical to those recorded in water (***e*** and ***h*** in Figure 5.4) and do not change even after up to six days. Thus, both compounds are stable under these conditions for prolonged periods of time. However, the spectrum of **66a** recorded at a pH of 8.0 reveals a weak band for the hemiaminal **66c**, while that of **67a** remains unaffected even after increasing the pH up to 9.0. Presumably, the rather hydrophobic macromolecular backbone of **67a** prevents the formation of **67c** under these conditions and this species can only be observed after the addition of a large excess of base (***i*** in Figure 5.4).

5.2.3. Transient Absorption Spectroscopy

In acetonitrile/water, the laser excitation of **65a** at 355 nm opens its [1,3]oxazine ring in less than 6 ns to generate the zwitterionic isomer **65b**. As a result, the absorption spectrum (***a*** in Figure 5.6), recorded 0.1 μs after excitation, reveals a band centered at 400 nm for a ground-state absorption of the 4-nitropholate chromophore of the photogenerated isomer **65b**. Indeed, this band resembles that observed in the steady-state absorption spectrum of tetrabutylammonium 4-nitrophenolate (***d*** in Figure 5.4). This photochemical behavior is analogous to that of **27a** in acetonitrile. However, the transition to a mixture of acetonitrile and water has a depressive effect on the quantum yield for the ring opening process. In fact, this parameter is only 0.03 for **65a** in acetonitrile/water, while it is 0.10 for **27a** in acetonitrile.

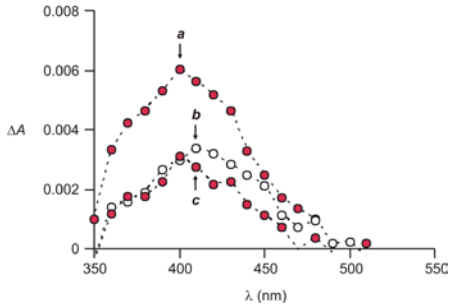

Figure 5.6. Absorption spectra (20°C) of **65a** (***a***), **66a** (***b***) and **67a** (***c***) recorded 0.1 μs after laser excitation (355 nm, 6 ns, 12 mJ). The concentration was 0.1 mM in ***a*** and ***b*** and 1.1 mg mL^{-1} in ***c***. The solvent was MeCN/H_2O (1:1, v/v) in ***a*** and H_2O in ***b*** and ***c***.

The photogenerated isomer **65b** reverts spontaneously back to the original species **65a** with first-order kinetics. Concomitantly, the absorbance at 400 nm decays monoexponentially. Curve fitting of the absorbance decay (***a*** in Figure 5.7) indicates the lifetime of **65b** to be 2 μs.

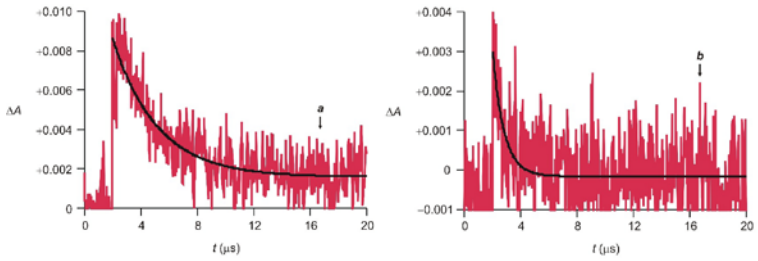

Figure 5.7. Temporal evolution (20°C) of the absorbance at 400 nm for solutions of **65a** (***a***) and **67a** (***b***) after laser excitation (355 nm, 6 ns, 12 mJ). The concentration was 0.1 mM in ***a*** and 1.1 mg mL^{-1} in ***b***. The solvent was MeCN/H_2O (1:1, v/v) in ***a*** and H_2O in ***b***.

The photochemical response of **66a** and **67a** in water is similar to that of **65a** in acetonitrile/water. Once again, laser excitation at 355 nm opens the [1,3]oxazine ring of **66a** and **67a** to generate the zwitterionic isomers **66b** and **67b** with a quantum yield of 0.02 in both instances. The photoinduced transformation causes the appearance of the ground-state absorption of the 4-nitrophenolate chromophore of **66b** and **67b** at 400 nm in the corresponding spectra (***b*** and ***c*** in Figure 5.6). This band decays monoexponentially with essentially identical kinetics for both systems, as **66b** and **67b** revert spontaneously back to **66a** and **67a** respectively. Curve fitting of the temporal absorbance profile (***b*** in Figure 5.7) reveals the lifetime of **66b** and **67b** to be 1 μs. Thus, a full switching cycle can be completed in few microseconds for both photochromic systems. Furthermore, they tolerate hundreds of switching cycles with no sign of degradation. In fact, the steady-state absorption spectra of **66a** and **67a**, recorded before and after 200 cycles, are essentially identical, indicating that both systems do not decompose under these irradiation conditions.

5.3. Conclusions

The introduction of a sufficiently-long oligo(ethylene glycol) chain in the *para* position, relative to the nitrogen atom, of the 3*H*-indole fragment of photochromic

oxazines imposes water solubility on them. Alternatively, hydrophilic character can be ensured by appending these photochromic compounds to a polymer backbone together with multiple poly(ethylene glycol) chains. The resulting hydrophilic oxazines retain their photochromic behavior in aqueous environment. In particular, the laser excitation of these molecules with ultraviolet wavelengths opens their [1,3]oxazine rings in less than 6 ns to generate zwitterionic isomers able to absorb in the visible region of the electromagnetic spectrum. The transition from organic solvents to water, however, has a depressive effect on the quantum efficiency of the ring-opening process. Approximately a five-fold decreases in quantum yield is observed on going from acetonitrile to water. The nature of the solvent has also a significant influence on the reisomerization kinetics. Both in organic and aqueous environments, the photogenerated isomers reverts spontaneously back to the original species with first-order kinetics. However, their lifetime increases from the nanosecond to the microsecond regime with the transition from acetonitrile to water. In any case, these photochromic systems can be switched back and forth between their two interconvertible states hundreds of times with no sign degradation. Thus, the compatibility of our photochromic oxazines with aqueous environments can offer the opportunity to photomodulate biological structures and functions with microsecond switching times and excellent fatigue resistances.

CHAPTER 6

PHOTOSWITCHABLE FLUORESCENT DYADS INCORPORATING BODIPY AND [1,3]OXAZINE COMPONENTS

6.1. Overview

The photoinduced transformation of **20a** into **20b (**Figure 2.1**)** activates electron and energy transfer pathways, which culminate in the effective quenching of the BODIPY fluorescence. The photogenerated species **20b** has a lifetime of 270 s in acetonitrile at 25 °C and eventually reverts to **20a** with first-order kinetics. Thus, the fluorescence of this particular system can be switched off and on simply by turning on and off respectively an ultraviolet source. However, the relatively slow reisomerization kinetics and poor fatigue resistance of this system are not compatible with RESOLFT imaging. Indeed, a full switching cycle from **20a** to **20b** and back can only be completed on a timescale of several minutes and 25 % of the original fluorescence is lost after only five cycles. Thus, the fatigue resistances and switching speeds of this fluorophore–photochrome dyad must be improved significantly in view of possible applications in superresolution imaging, which require microsecond switching times and the ability to tolerate tens of switching cycles. In this chapter, I report the synthesis of two novel dyads with improved performance and the characterization of their photochemical and photophysical properties with a combination of steady-state and time-resolved spectroscopic measurements.

6.2. Results and Discussion

6.2.1. Design and Synthesis

The [1,3]oxazine ring of **34a** (Figure 6.1) opens in less than 6 ns to generate **34b** with a quantum yield of 0.07 in acetonitrile at 20 °C upon ultraviolet irradiation. The

photogenerated isomer **34b** has a lifetime of 2 μs under these conditions and eventually reverts to **34a** with first-order kinetics. Thus, a full switching cycle can be completed on a microsecond timescale with this photochromic system. Furthermore, this species survives unaffected hundreds of switching cycles even in the presence of molecular oxygen. Thus, the introduction of this photochromic oxazine within **20a** in place of the spiropyran component should translate into the generation of fluorophore–photochrome dyads with switching speeds and fatigue resistances compatible with RESOLFT imaging. On the basis of these considerations, we designed the BODIPY–oxazine dyads **69a** and **70a** and synthesized these compounds in three to five steps starting from commercial and known precursors.

Table 6.1. Photochemical and photophysical parameters [a] of the fluorophore–photochrome dyads **69a**–**70a** and their model compounds **19** and **77-79**.

	λ_{Em} [b] (nm)	ϕ_F [b]	χ [b, c]	ϕ_P	τ [d] (μs)
34a	—	—	—	0.07	2
69a	541	0.12	4.5	0.05	1
70a	542	0.07	4.9	—	—
19	543	0.40	—	—	—
77a	542	0.34	0.9	—	—
78	542	0.02	—	—	—
79	543	0.01	—	—	—

[a] All parameters were measured in MeCN at 20 °C. [b] The emission wavelength (λ_{Em}), fluorescence quantum yield (ϕ_F) and contrast ratio (χ) were determined from the spectra in Figures 6.4, 6.6 and 6.8. [c] χ is the ratio between the ϕ_F measured before and that determined after the addition of acid. [d] The lifetime of the photogenerated isomers were determined form the temporal absorbance evolutions in Figure 6.10.

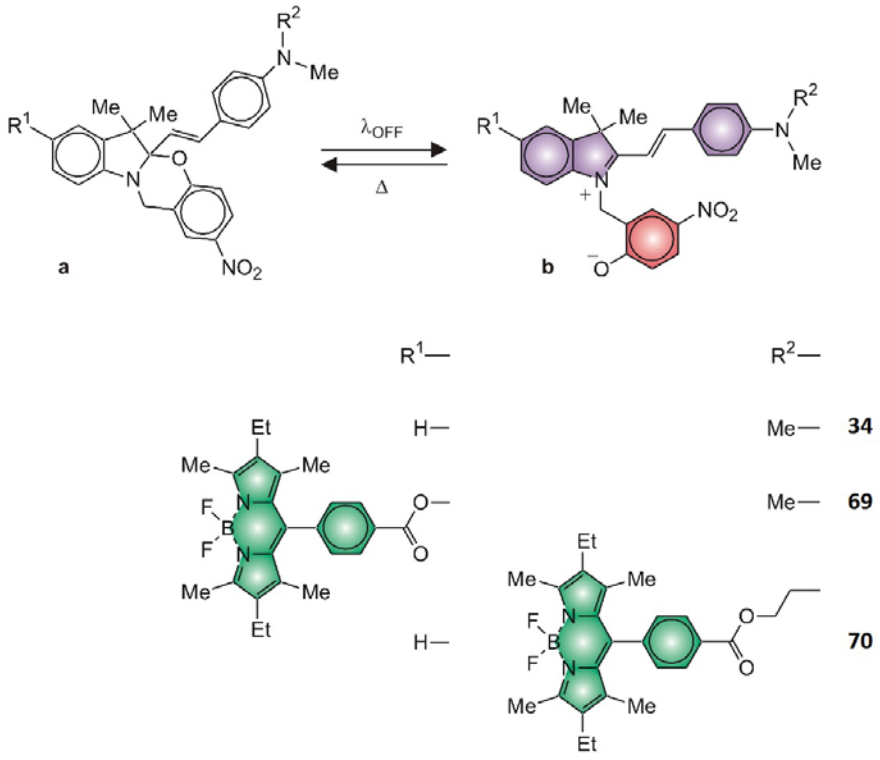

Figure 6.1. Photoinduced and reversible transformation of **34a**, **69a** and **70a** into **34b**, **69b** and **70b**.

I prepared the fluorophore–photochrome dyad **69a** in five steps, starting from 4-methoxyphenyl hydrazine (Figure 6.2). In particular, I condensed this precursor with 3-methyl-2-butanone, in the presence of *p*-toluene sulfonic acid (PTSA), to generate the 3*H*-indole **71**. Then, I condensed **71** with 4-dimethylamino benzaldehyde, in the presence of hydrogen bromide and trifluoroacetic acid (TFA), to produce the extended 3*H*-indole **72**. After the cleavage of the methoxy group with boron tribromide, I reacted the resulting compound **73** with **21**, under the assistance of *N*,*N*'-dicyclohexylcarbodiimide (DCC) and 4-dimethylaminopyridine (DMAP), to produce **74**. Finally, I condensed **74** with 2-chloromethyl-4-nitrophenol to yield the target molecule **69a**.

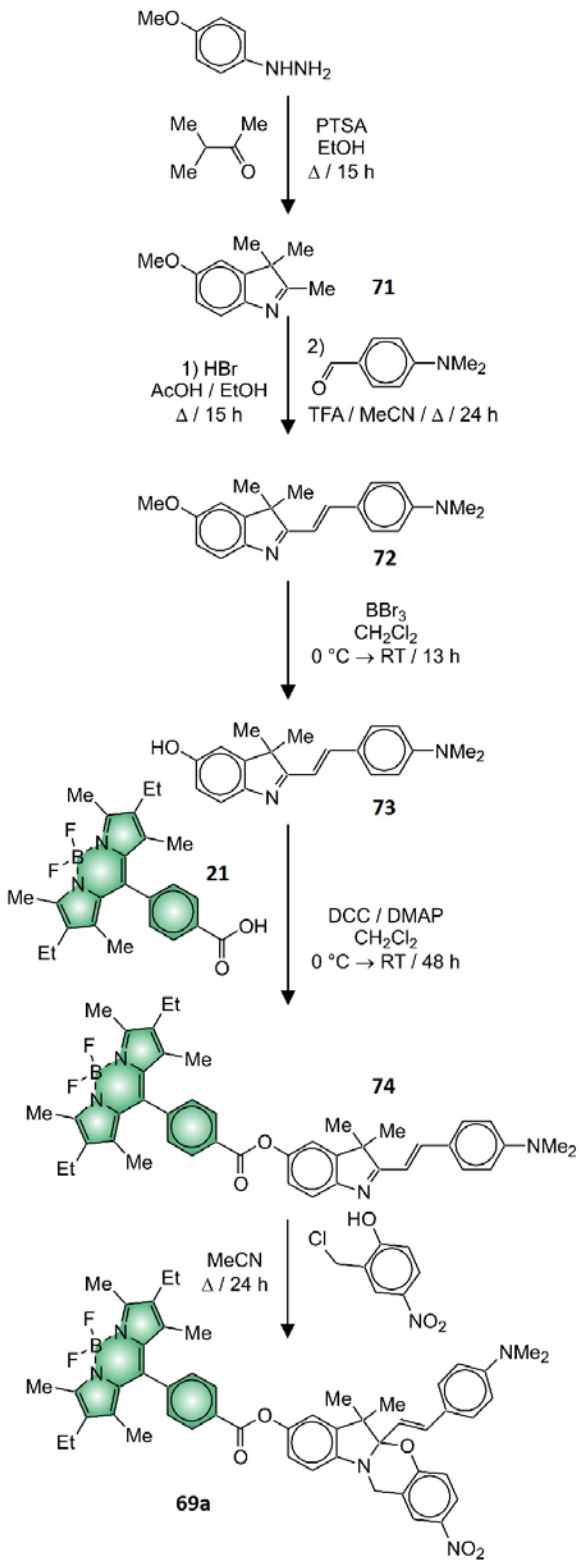

Figure 6.2. Synthesis of the fluorophore–photochrome dyad **69a**.

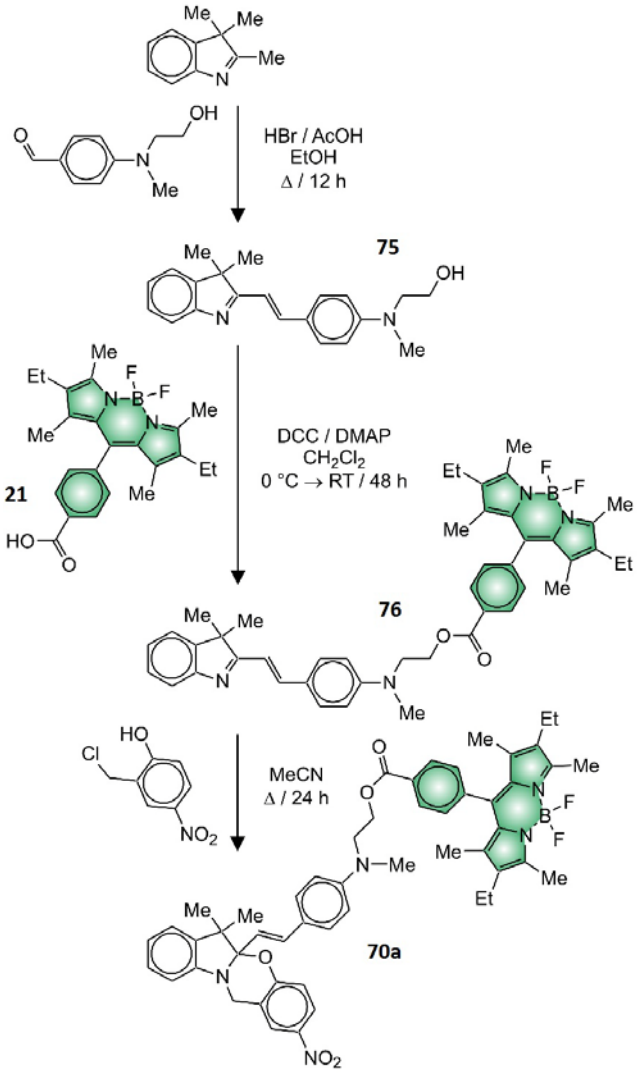

Figure 6.3. Synthesis of the fluorophore–photochrome dyad **70a**.

I synthesized the fluorophore–photochrome dyad **70a** in three steps, starting from 2,3,3-trimethyl-3*H*-indole (Figure 6.3). Specifically, I condensed this precursor with *N*-methyl-*N*-(2-hydroxyethyl)-4-aminobenzaldehyde, in the presence of hydrogen bromide, to generate the extended 3*H*-indole **75**. Then, I reacted **75** with **21**, under the assistance of DCC and DMAP, to produce **76** and condensed this compound with 2-chloromethyl-4-nitrophenol to yield the target molecule **70a**.

6.2.2. Steady-State Absorption Spectroscopy

The steady-state absorption spectrum of the model photochrome **34a** shows a band centered at 305 nm (***a*** in Figure 6.4). The model fluorophore **19** (Figure 6.5) instead reveal a band at *ca.* 520 nm (***c*** in Figure 6.4). Both absorptions can also be observed in the spectra of the fluorophore–photochrome dyads **69a** and **70a** (***a*** and ***c*** in Figure 6.6), suggesting that their fluorescent and photochromic components have negligible ground-state interactions, even if they are integrated within the same molecular skeleton.

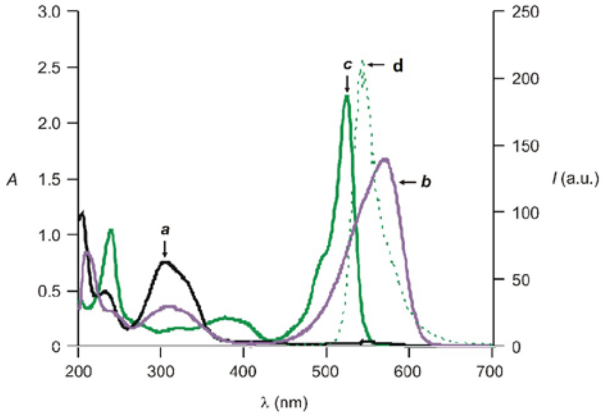

Figure 6.4. Steady-state absorption spectra (0.05 mM, MeCN, 20 °C) of **34a** before (***a***) and after (***b***) the addition of TFA (2 eq.) and **19** (***c***). Steady-state emission spectra (0.05 mM, MeCN, 20 °C) of **19** (***d***, λ_{Ex} = 437 nm).

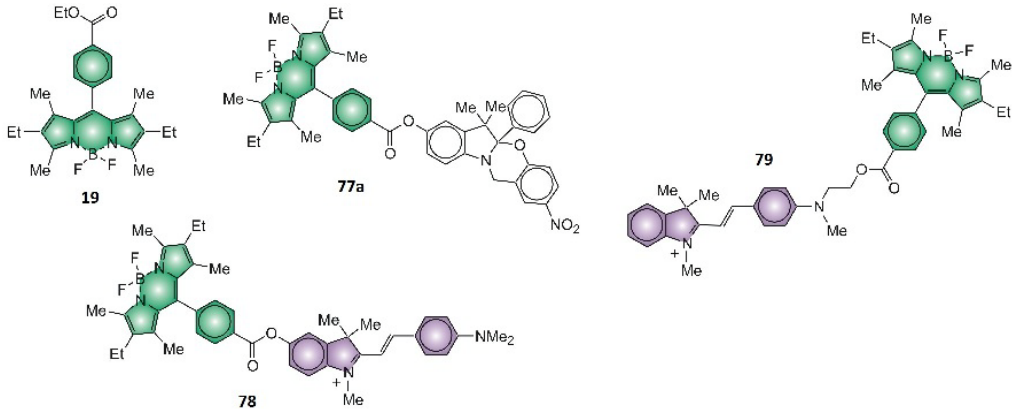

Figure 6.5. Model compounds **19** and **77**–**79**.

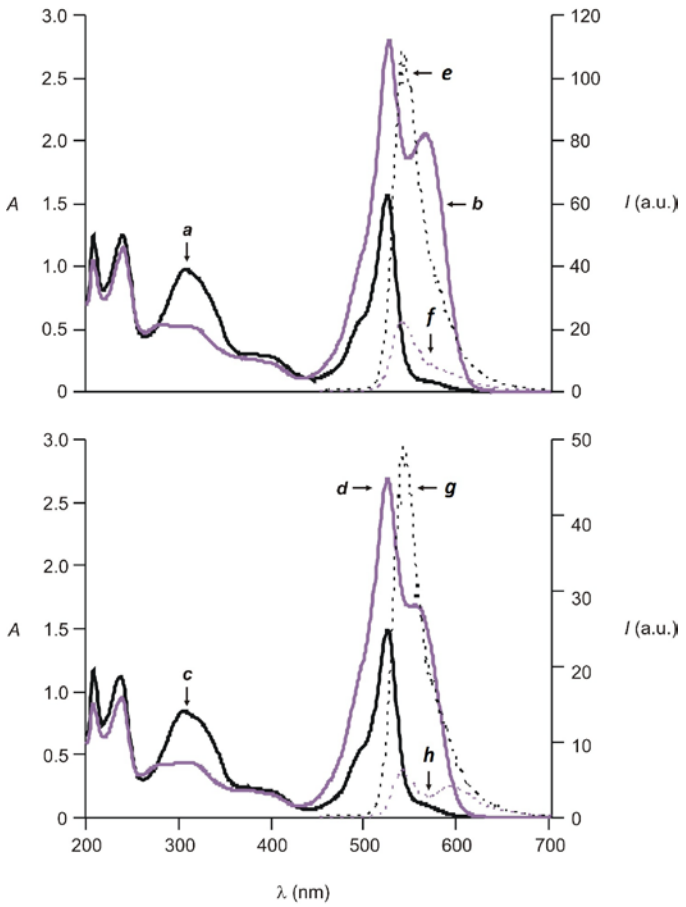

Figure 6.6. Steady-state absorption spectra (0.05 mM, MeCN, 20 °C) of **69a** before (***a***) and after (***b***) the addition of TFA (1 eq.), **70a** before (***c***) and after (***d***) the addition of TFA (1 eq.). Steady-state emission spectra (0.05 mM, MeCN, 20°C) of **69a** before (***e***, λ_{Ex} = 437 nm) and after (***f***, λ_{Ex} = 437 nm) the addition of TFA (1 eq.), **70a** before (***g***, λ_{Ex} = 425 nm) and after (***h***, λ_{Ex} = 425 nm) the addition of TFA (1 eq.).

Upon addition of acid, the [1,3]oxazine ring of the model photochrome **34a** opens to generate **34c** (Figure 6.7) with the concomitant appearance of a band at 569 nm (***b*** in Figure 6.4) in the corresponding spectrum. Indeed, this transformation brings the 2-(4-dimethylaminophenyl)ethynyl appendage in conjugation with the 3*H*-indole heterocycle and the resulting extended chromophore strongly absorbs in the visible region. A similar transformation occurs after the addition of acid to the dyads **69a**–**70a**. Once again, the [1,3]oxazine ring of their photochromic component opens under these conditions to generate **69c**–**70c** (Figure 6.7). Consistently, the corresponding spectra reveal the

appearance of the characteristic absorption of their extended 3*H*-indolium chromophores at *ca.* 560 nm (***b*** and ***d*** in Figure 6.6). In agreement with this interpretation, the spectra of the model fluorophore–photochrome dyad **77a** (Figure 6.5) remain essentially unchanged in the visible region after the addition of acid. In fact, the model compound lacks the 2-(4-dimethylaminophenyl)ethynyl appendage on its photochromic component and, hence, the opening of its [1,3]oxazine ring cannot generate an extended 3*H*-indolium chromophore.

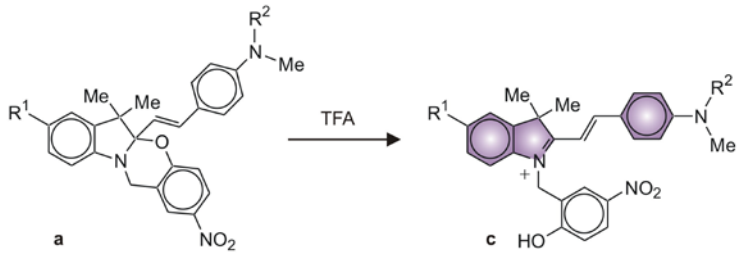

Figure 6.7. Transformation of the [1,3]oxazines **34a** and **69a-70a** into the 3*H*-indolium cations **34c** and **69c-70c** upon addition of acid.

6.2.3. Steady-State Emission Spectroscopy

The model fluorophore **19** emits at *ca.* 540 nm (***e*** in Figure 6.4) upon excitation with quantum yield (ϕ_F in Table 6.1) of 0.40. After its incorporation within the fluorophore–photochrome dyads **69a**–**70a**, this BODIPY fluorophore emits essentially in the same range of wavelengths (***e*** and ***g*** in Figure 6.6), but its ϕ_F is only 0.12 and 0.07 respectively. Thus, the covalent attachment of the fluorescent components to the photochromic components results in partial quenching of their emission. Indeed, the redox potentials of **19** and 4-dimethylaminostyrene suggest that the excited BODIPY components of the dyads **69a**–**70a** can accept an electron from the 2-(4-dimethylaminophenyl)ethynyl appendage of the photochromic components. The emission bands (***d*** in Figure 6.4) of the model fluorophore **19** is positioned in the same range of wavelengths where the extended

3*H*-indolium chromophore of **34c** absorbs (***b*** in Figure 6.4). As a result, the excitation energy of these fluorophores can be transferred to the 3*H*-indolium chromophore, with a concomitant fluorescence quenching, if the two components are sufficiently close to each other. In addition, the redox potentials of these model compounds suggest that the excited BODIPY fluorophores can transfer an electron to the 3*H*-indolium cation of **34c**, if sufficiently close to this component. Consistently, the emission intensity of **69a**–**70a** (***e*** and ***g*** in Figure 6.6) decreases significantly after their transformation into **69c**–**70c** (*f* and ***h*** in Figure 6.6) with contrast ratios (χ in Table 6.1) of 4.5 and 4.9 respectively.

The ability of the 3*H*-indolium cation of **69c**–**70c** to quench the emission of their BODIPY component is further confirmed by the behavior of the model compound **77a** and **78**–**79** (Figure 6.5). The photochromic component of **77a** lacks the 2-(4-dimethylaminophenyl)ethynyl group of **69a**–**70a**. As a result, the opening of the [1,3]oxazine ring of **77a** upon addition of acid is not accompanied by the appearance of the characteristic absorption of the extended 3*H*-indolium cation in the corresponding spectra and, in fact, the emission intensity of their BODIPY fluorophore is essentially unaffected by this transformation. Instead, the 3*H*-indolium chromophore is already in place within **78**–**79** and, consistently, the emission of the fluorescent component is almost completely suppressed in these systems (***a*** and ***b*** in Figure 6.8).

6.2.4. Transient Absorption Spectroscopy

The absorption band at 305 nm (***a*** in Figure 6.4) of the model photochrome **34a** is associated with its 4-nitrophenoxy chromophore. In acetonitrile at 20 °C, laser excitation in the tail on this band results in the opening of the [1,3]oxazine ring with the formation

of **34b** in less than 6 ns with a quantum yield of 0.07 (ϕ_P in Table 6.1). The photogenerated and zwitterionic isomer incorporates a 4-nitrophenoxy anion and a 3*H*-indolium cation, which absorb at 430 and 550 nm respectively. As a result, the absorption spectrum of a solution of **34a**, recorded 0.1 μs after excitation at 355 nm, reveals the characteristic bands of both chromophores (***a*** in Figure 6.9).

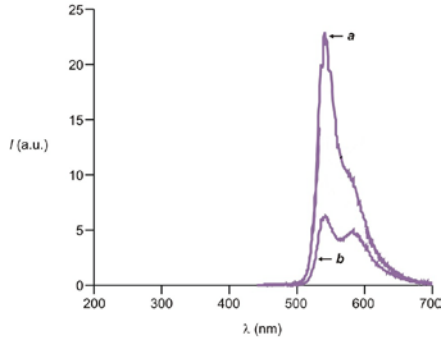

Figure 6.8. Steady-state emission spectra (0.05 mM, 20 °C) of **78** (***a***, λ_{Ex} = 437 nm) and **79** (***b***, λ_{Ex} = 437 nm).

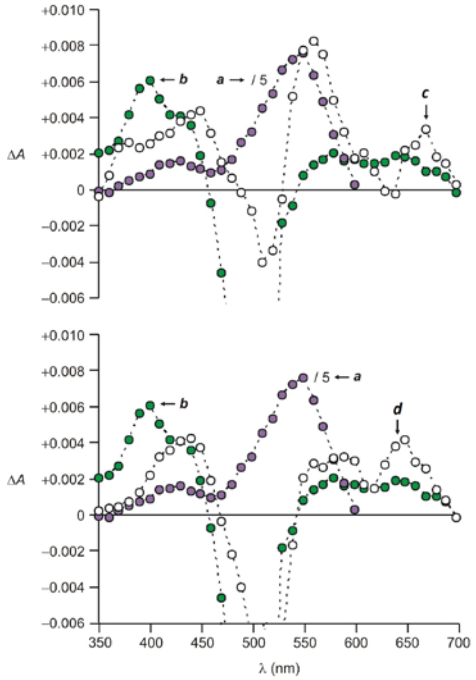

Figure 6.9. Absorption spectra (0.01–0.03 mM, MeCN, 20 °C) of **34a** (***a***), **19** (***b***), **69a** (***c***) and **70a** (***d***) recorded 0.1 μs after laser excitation (355 nm, 6 ns, 15 mJ).

The model fluorophore **19** can also absorb at 355 nm (***c*** in Figure 6.4). In fact, its excitation at this wavelength results in the bleaching of its $S_0 \rightarrow S_1$ transition (***b*** in Figure 6.9), together with the appearance of a band at 430 nm, in the absorption spectra recorded 0.1 μs after laser irradiation. According to literature data,[142] these bands can be assigned to absorptions of the BODIPY chromophores in the triplet manifold.

The illumination of the fluorophore–photochrome dyad **69a** at 355 nm results in the absorption of the exciting radiation by the chromophoric fragments. Consistently, the absorption spectra, recorded 0.1 μs after excitation, show the bleaching of the $S_0 \rightarrow S_1$ transitions of the BODIPY fluorophore and bands for the photochromic component in the ring-opened state (***c*** in Figure 6.9). Specifically, the band at 430 nm corresponds to a ground-state absorption of the 4-nitrophenolate chromophore of **69b** and that at 560 nm is a ground-state absorption of the 3*H*-indolium fragment of this specie. Thus, these observations demonstrate that the photochromic component retains its photochemical behavior after coupling to the fluorescent component. However, the covalent attachment of the two components has a depressive effect on the quantum efficiency of the photoinduced ring-opening process. In particular, the [1,3]oxazine ring of **69a** opens with ϕ_P of 0.05, while **34a** has a ϕ_P 0.07. By contrast, the excitation of the fluorophore–photochrome dyad **70a** does not produce the ring opened isomer **70b**, under otherwise identical experimental conditions. In fact, its transient spectrum (***d*** in Figure 6.9) resembles that of the model fluorophore **19** (***b*** in Figure 6.9) and does not reveal the ground-state absorptions of the ring-opened state of the photochromic fragments (***a*** in Figure 6.9).

The photogenerated isomer **34b** has a lifetime of 2 μs (τ in Table 6.1) and reverts to the original species **34a** with first-order kinetics. As a result, the transient absorptions at 430 and 550 nm decay monoexponentially with the thermal reisomerization of **34b** back to **34a**. The covalent connection of the photochromic component to the fluorescence component in the dyad **69a** has negligible influence on their reisomerization kinetics. In all instances, the transient absorptions at 430 and 560 nm, corresponding to the 4-nitrophenolate anion and 3*H*-indolium cation of the photogenerated isomer **69b** , decay monoexponentially on a microsecond timescale (***a*** in Figure 6.10).

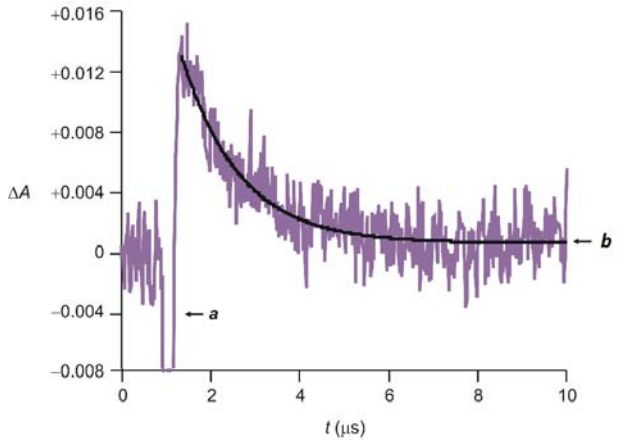

Figure 6.10. Evolution of the absorbance at 560 nm for solutions (0.01–0.03 mM, MeCN, 20 °C) of **69a** (***a***) upon laser excitation (355 nm, 6 ns, 15 mJ) and corresponding curve fitting (***b***).

Specifically, curve fitting (***b*** in Figure 6.10) of the temporal absorbance profile indicates τ of **69b** to be 1 μs (Table 6.1). Thus, a full switching cycle can be completed within few microseconds after excitation with the fluorophore–photochrome dyad. In addition, the system tolerates hundreds of cycles with no sign of degradation, even in the presence of molecular oxygen. Consistently, their steady-state and time-resolved absorption spectra do not change even after 400 excitation cycles.

6.2.5. Transient Emission Spectroscopy.

The steady-state absorption spectra (***a*** in Figure 6.6) of **69a** shows that the band of its fluorescent component extends up to 600 nm. As a result, excitation at 532 nm (λ_{ON}) is accompanied by the characteristic BODIPY fluorescence. Similarly, the absorbance evolution (Figure 6.10) at 560 nm upon excitation at 355 nm (λ_{OFF}) of **69a** indicates that the [1,3]oxazine ring opens within the laser pulse to generate the corresponding isomer **69b**. Thus, the simultaneous illumination of the sample at λ_{ON} and λ_{OFF} with a single pulsed laser can be exploited to probe the emission of the BODIPY component integrated within the photogenerated isomer **69b**. Relying on this irradiation protocol and a long-pass filter (>490 nm) to block and release λ_{OFF}, the influence of the photochromic transformation on the emission intensity of the fluorescent component can be assessed. Indeed, the corresponding plot (***a*** in Figure 6.11) demonstrates that the emission intensity at 580 nm for the fluorophore–photochrome dyad decreases significantly, as the long-pass filter is removed from the optical path to release the beam at λ_{OFF}, and returns to the original value, once the filter is mounted again in the original position. In fact, the fluorescence of the system can be modulated for multiple switching cycles simply by blocking and releasing λ_{OFF}, consistently with the electron and energy transfer processes designed into the photogenerated isomer **69b**. In agreement with these operating principles, the emission intensity (***b*** in Figure 6.11) of the model fluorophore **19**, lacking the photochromic component, remains essentially unaffected under identical illumination conditions.

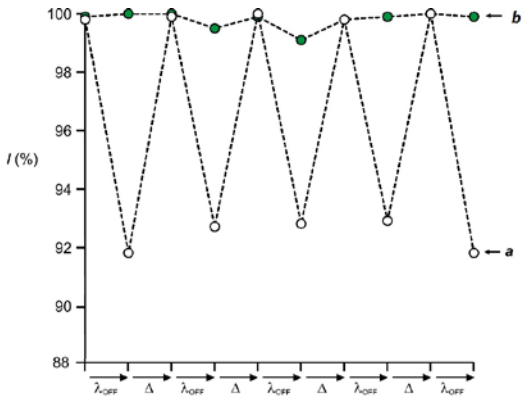

Figure 6.11. Emission intensity at 580 nm of solutions (0.01–0.03 mM, MeCN, 20 °C) of **69a** (***a***) and **19** (***b***) recorded by turning on and off an exciting beam at λ_{OFF} (355 nm, 10 mJ, 6 ns), while illuminating the sample at λ_{ON} (532 nm, 30 mJ, 6 ns).

6.3. Conclusions

Photochromic oxazines can be connected to BODIPY fluorophores in three to five synthetic steps to generate fluorophore–photochrome dyads. In one of the two compounds synthesized, the photochromic fragment retains its photochemical properties, despite the presence of a BODIPY appendage. Specifically, the [1,3]oxazine ring opens upon ultraviolet excitation to generate a zwitterionic isomer in less than 6 ns with quantum yield of 0.05. The photogenerated specie reverts spontaneously back to the original one in few microseconds. In addition, this photoswitchable system is remarkably stable and tolerates hundreds of switching cycles with no sign of degradation. The selective excitation of the BODIPY component at visible wavelengths is accompanied by the emission of light in the form of fluorescence. However, the state of the photochromic component within the fluorophore–photochrome dyad regulates the excitation dynamics of the fluorescent fragment. In particular, the photogenerated state of the photochrome incorporates a 3*H*-indolium cation, which can accept an electron or energy from the

excited BODIPY and quench its fluorescence. Indeed, the emission intensity of the photoswitchable dyad can be modulated with microsecond speeds by photoinducing the interconversion of the photochromic appendage. Hence, this protocol for fluorescence photoswitching with fast speeds and excellent fatigue resistance can evolve into the realization of valuable probes to overcome diffraction in fluorescence imaging and visualize biological samples with nanoscaled resolution.

CHAPTER 7

FLUORESCENCE SWITCHING WITH A PHOTOCHROMIC AUXOCHROME

7.1. Overview

Fluorescent and photochromic components can be paired either covalently or noncovalently and the interconversion of the latters can be invoked to regulate the emission intensity of the formers on the basis of intercomponent electron[143] or energy[144] transfer. The exchange of either an electron or energy between the excited state of a fluorophore and one of the two interconvertible states of a photochrome deactivates the former nonradiatively and causes a decrease in fluorescence quantum yield. The quenching efficiency, however, rarely approaches unity and these processes generally do not result in complete fluorescence suppression. In addition, the ratio (contrast) between the emission intensity measured after the photochromic transformation and that measured before is related to the composition of the photostationary state. In most instances, both interconvertible forms are present at the photostationary state and, hence, modest contrast ratios are generally associated with these photoswitchable systems.[145] In addition, their excitation dynamics can encourage competitive deactivation pathways and the gradual degradation of the fluorescent and/or photochromic components with the number of switching cycles. Thus, the evolution of these molecular and supramolecular switches into functional materials for practical applications requires the identification of innovative operating principles that would ensure fluorescence photoswitching with improved contrast ratios and fatigue resistances. On the basis of these considerations, we devised a general strategy for fluorescence modulation that avoids intercomponent electron or energy transfer and is instead solely based on the photoinduced elongation of

the absorption wavelength of a fluorescent chromophore with the aid of an appended photochromic auxochrome. In this chapter, I report the synthesis of a fluorophore–photochrome dyad, designed around this particular switching mechanism, as well as the photochemical and photophysical properties of this compound.

7.2. Results and Discussion

7.2.1. Design and Synthesis

We designed a fluorophore–photochrome dyad (**80** in Figure 7.1), incorporating coumarin and oxazine fragments within the same covalent skeleton. I prepared this compound and its model (**81** in Figure 7.2) in a single step from known precursors. Specifically, the condensation of a preformed coumarin (**82** in Figure 7.2) with a preformed [1,3]oxazine (**42a** in Figure 7.2), in the presence of trifluoroacetic acid (TFA), gave the target molecule **80a** in a yield of 40 %. Similarly, the reaction of **82** with the iodide salt of a 3*H*-indolium cation (**83** in Figure 7.2), followed by counterion exchange, gave the hexafluorophosphate salt of the model compound **81** in a yield of 82 %.

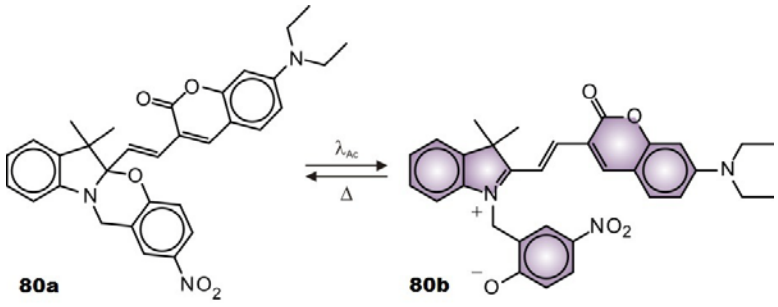

Figure 7.1. Photoinduced and reversible interconversion of **80a** and **80b**.

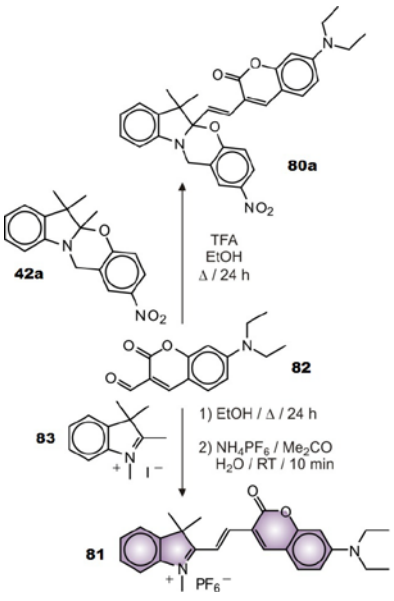

Figure 7.2. Synthesis of the fluorophore–photochrome dyad **80a** and its model **81**.

7.2.2. Absorption Spectroscopy

The steady-state absorption spectrum (***a*** in Figure 7.3) of **80a** shows a band for the coumarin fluorophore at 412 nm. Upon excitation at 355 nm (λ_{Ac}), the [1,3]oxazine ring opens to generate the zwitterionic isomer **80b** (Figure 7.1) in less than 6 ns with a quantum yield of 0.02. This photoinduced isomerization brings the coumarin appendage in conjugation with a 3*H*-indolium cation and generates a *new* chromophoric fragment with an extended π-system. As a result, a *new* band appears at 570 nm in the absorption spectrum (***b*** in Figure 7.3) recorded 0.03 μs after excitation. Consistently, this band resembles that observed in the steady-state absorption spectrum (***c*** in Figure 7.3) of the hexafluorophosphate salt of the model compound **81**. Thus, the photoinduced transformation of one component within the fluorophore–photochrome dyad alters the electronic structure of the other and causes a bathochromic shift in absorption by *ca.* 160 nm. The process, however, is fully reversible and the photogenerated isomer **80b** reverts

to the original state with first-order kinetics in few microseconds with the concomitant decay of its absorption band in the visible region.

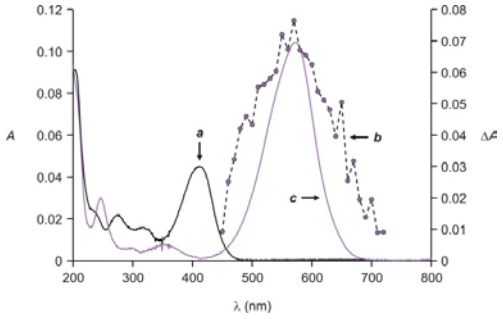

Figure 7.3. Steady-state absorption spectra of solutions (2.5 μM, MeCN, 20 °C) of **80a** (***a***) and the hexafluorophosphate salt of **81** (***c***). Time-resolved absorption spectrum of a solution (0.01 mM, MeCN, 20 °C) of **80a** (***b***) recorded 0.03 μs after excitation at 355 nm (10 mJ, 6 ns).

Nonlinear curve-fitting of the corresponding temporal absorbance profile (Figure 7.4) indicates the lifetime of **80b** to be 0.2 μs. In addition, this fluorophore–photochrome dyad tolerates hundreds of switching cycles with no sign of degradation, even in the presence of molecular oxygen. In fact, the absorbance measured in the visible region 0.03 μs after activation at λ_{Ac} does not change even after 500 switching cycles (***a*** in Figure 7.5).

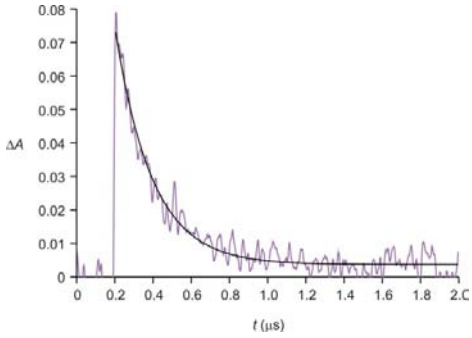

Figure 7.4. Absorbance evolution at 580 nm for a solution (0.01 mM, MeCN, 20 °C) of **80a** upon excitation at 355 nm (10 mJ, 6 ns) and the corresponding monoexponential fitting.

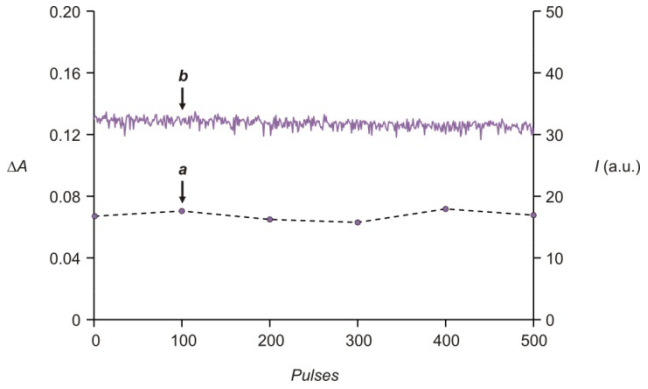

Figure 7.5. Evolution of the absorbance (***a***) measured at 580 nm 0.03 µs after activation at 355 nm (10 mJ, 6 ns) for a solution (0.01 mM, MeCN, 20 °C) of **80a** with the number of excitation pulses. Evolution of the emission intensity (***b***) measured at 645 nm upon excitation at 574 nm for a solution of the hexafluorophosphate salt of **81** (2.5 µM, MeCN, 20 °C) with the number of excitation pulses.

7.2.3. Emission Spectroscopy

The emission spectrum (***a*** in Figure 7.6) of **80a**, recorded within an excitation pulse of 6 ns at 532 nm (λ_{Ex}), does not show any significant fluorescence because the coumarin fluorophore does not absorb at λ_{Ex} (***a*** in Figure 7.3).

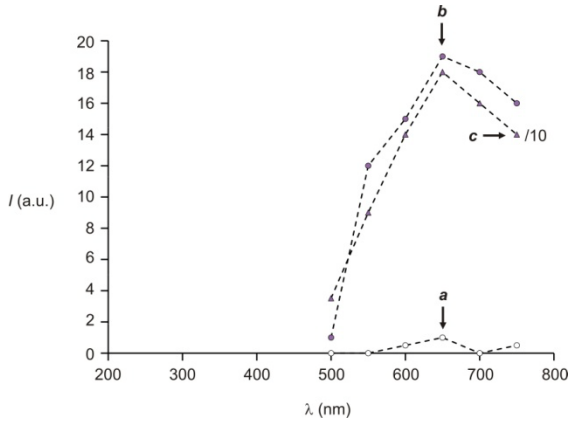

Figure 7.6. Emission spectra of solutions (0.01 mM, MeCN, 20°C) of **80a** illuminated at 532 nm (30 mJ, 6 ns) without (***a***) and with (***b***) simultaneous irradiation at 355 nm (10 mJ, 6 ns) and of the hexafluorophosphate salt of **81** (***c***) recorded upon illumination at 532 nm only.

However, the photoinduced opening of the adjacent [1,3]oxazine ring can be exploited to shift the band of the fluorophore sufficiently to permit absorption at λ_{Ex}. Consistently,

the simultaneous illumination of the sample at λ_{Ac} and λ_{Ex} results in the appearance of an intense emission at 650 nm in the corresponding spectrum (***b*** in Figure 7.6). Indeed, the beam at λ_{Ac} opens the [1,3]oxazine ring of **80a** with the formation of **80b** and that at λ_{Ex} excites the coumarin fragment of the photogenerated isomer with concomitant fluorescence. In agreement with these observations, the emission spectrum (***c*** in Figure 7.6) of the hexafluorophosphate salt of **81**, recorded under identical experimental conditions but exciting sample only at λ_{Ex}, shows essentially the same band. In fact, this model fluorophore has a molar extinction coefficient of 83 mM^{-1} cm^{-1} at 573 nm with a fluorescence quantum yield of 0.09, corresponding to a brightness of 8 mM^{-1} cm^{-1}. In addition, the fluorescence lifetime of the hexafluorophosphate salt of **81** is only 0.3 ns. This value is three orders of magnitude shorter than the lifetime (*cf.*, 0.2 μs) of the photogenerated isomer **80b** and, in principle, offers the opportunity to excite a single dyad at λ_{Ex} tens of times per activation step. Furthermore, this particular fluorophore tolerates multiple excitation cycles without decomposing. Indeed, the emission intensity of the hexafluorophosphate salt of **81** does not change even after 500 excitation pulses at λ_{Ex} (***b*** in Figure 7.5).

7.3. Conclusions

As a conclusion, we designed and implemented a mechanism for fluorescence modulation under optical control based on a photoinduced bathochromic shift in the absorption of a fluorophore connected to a photochrome. The modular character and synthetic accessibility of our design logic offers the opportunity, at least in principle, to photoregulate the electronic structure of a given chromophore with an appended

photochromic auxochrome. Thus, this general strategy can ultimately lead to an entire family of molecular switches with photocontrollable electrochemical and spectroscopic signatures.

CHAPTER 8

EXPERIMENTAL PROCEDURES

7.1. General Methods

Chemicals were purchased from commercial sources and used as received with the exception of MeCN and CH_2Cl_2, which were distilled over CaH_2, and THF, which was distilled over Na and Ph_2CO. All reactions were monitored by thin-layer chromatography, using aluminum sheets coated with silica (60, F_{254}). Fast atom bombardment mass spectra (FABMS) were recorded with a VG Mass Lab Trio-2 in a 3-nitrobenzyl alcohol matrix. High resolution electrospray ionization mass spectra (HRESIMS) were recorded with an Agilent LCTOF spectrometer. Nuclear magnetic resonance (NMR) spectra were recorded with a Bruker Avance 400. Absorption spectra were recorded with a Varian Cary 100 Bio spectrometer, using quartz cells with a path length of 0.5 cm. Time-resolved absorption spectra were recorded with a Luzchem Research mLFP–111 spectrometer, after excitation with a Continuum Surelite II–10 Nd–YAG laser [pulse width = 6 ns (FWHM), wavelength = 355 nm]. Emission spectra were recorded with a Varian Cary Eclipse spectrometer in aerated solutions. Samples were irradiated at 254 nm (0.5 mW cm^{-2}) with a Mineralight UVGL–25 lamp. Cyclic voltammograms were recorded with a CH Instruments 660A in degassed solutions under an atmosphere of Ar. PMMA films doped with **18a**, **19** and **20a** were prepared by spin-coating CH_2Cl_2 solutions of the dopant (1.0 mg mL^{-1}) and polymer (52 mg mL^{-1}) on glass slides at 420 rpm for 9 s, using a Chemat Technologies KW-4A spin coater. The thicknesses of the films were measured with a Tencor Instruments 10-00090 surface profilometer. Images of the film were recorded with an Olympus IM50 inverted

fluorescence microscope, equipped with a 100 W mercury arc lamp and standard fluorescein excitation and emission filters, using the Diagnostic Instruments Spot system (a digital camera/frame grabber/software package) for image acquisition. The doughnut-shaped spot was generated with a Laser Innovations Coherent 90-6 argon ion laser operated at 351 nm and directed (without focusing) at an angle of incidence of *ca.* 4^{o} into a Mitsubishi Cable America ST400E-FV with SL sleeves fused silica optical fiber (core diameter = 400 μm, length = 2 m).

Compounds **18a**, **22a** and **23a** were prepared according to literature procedures[75,117].

7.2. Experimental Procedures

19. A solution of **21** (67 mg, 0.2 mmol), EtOH (15 mL, 0.3 mmol) and 4-dimethylaminopyridine (2 mg, 0.02 mmol) in MeCN (20 mL) was cooled with an ice bath under Ar. After the addition of *N*,*N*'-dicyclohexylcarbodiimide (36 mg, 0.2 mmol), the reaction mixture was allowed to warm up to ambient temperature and stirred under these conditions for 3 days. The solvent was distilled off under reduced pressure and the residue was purified by column chromatography [SiO_2: CH_2Cl_2 / hexanes 1:2 $\rightarrow$ 3:1 (v/v)] to yield **19** (27 mg, 38%) as a pink solid. FABMS: *m/z* = 452 $[M]^+$; ^{1}H NMR (400 MHz, $CDCl_3$): δ 0.99 (6H, t, 8 Hz), 1.30 (6H, s), 1.41 (3H, t, 7 Hz), 2.37 (4H, q, 8 Hz), 2.49 (6H, s), 4.42 (2H, q, 7 Hz), 7.49 (2H, d, 8 Hz), 8.15 (2H, d, 8 Hz); ^{13}C-NMR (100 MHz, $CDCl_3$): δ = 11.5, 12.2, 13.9, 14.3, 16.9, 61.6, 129.3, 130.4, 130.5, 131.6, 133.7, 139.1, 140.0, 140.4, 154.5, 166.2.

20a. A solution of **18a** (63 mg, 0.2 mmol), **21** (89 mg, 0.2 mmol) and 4-dimethylaminopyridine (3 mg, 0.02 mmol) in MeCN (20 mL) was cooled with an ice

bath under Ar. After the addition of *N*,*N*'-dicyclohexylcarbodiimide (43 mg, 0.2 mmol), the reaction mixture was allowed to warm up to ambient temperature and stirred under these conditions for 4 days. The solvent was distilled off under reduced pressure and the residue was purified by column chromatography [SiO_2: CH_2Cl_2 / hexanes 1:3 $\rightarrow$ CH_2Cl_2 / $MeCO_2Et$ 10:1 (v/v)] to yield **20a** (73 mg, 54%) as a pink solid. FABMS: *m/z* = 758 $[M]^+$; ^{1}H NMR (400 MHz, $CDCl_3$): δ = 0.99 (6H, t, 7 Hz), 1.20 (3H, s), 1.25 (6H, s), 1.31 (3H, s), 2.30 (4H, q, 7 Hz), 2.55 (6H, s), 3.53–3.60 (1H, m), 3.66–3.73 (1H, m), 4.54 (2H, t, 6 Hz), 5.90 (1H, d, 10 Hz), 6.78 (2H, d, 9 Hz), 6.90–6.94 (2H, m), 7.12 (1H, d, 7 Hz), 7.22 (1H, t, 8 Hz), 7.40 (2H, d, 8 Hz), 8.02–8.06 (2H, m), 8.13 (2H, d, 8 Hz); ^{13}C-NMR (100 MHz, $CDCl_3$): δ 12.2, 15.0, 17.5, 20.3, 23.0, 26.3, 32.0, 42.9, 53.2, 63.5, 106.9, 107.2, 116.0, 118.8, 120.5, 122.1, 122.3, 123.2, 126.4, 128.3, 128.8, 129.2, 130.6, 130.7, 133.5, 136.1, 141.4, 141.6, 147.0, 154.8, 159.7, 166.2.

21. A solution of 3-ethyl-2,4-dimethylpyrrole (500 mg, 4 mmol), 4-carboxybenzaldehyde (300 mg, 2 mmol) and CF_3CO_2H (10 μL, 0.1 mmol) in CH_2Cl_2 (200 mL) was stirred for 12 h at ambient temperature under Ar. After the addition of a solution of 2,3-dichloro-5,6-dicyano-*p*-benzoquinone (454 mg, 2 mmol) in CH_2Cl_2 (15 mL), the mixture was stirred for a further 30 min. Then, Et_3N (4 mL, 28 mmol) and $BF_3 \cdot Et_2O$ (4 mL, 32 mmol) were added and the mixture was stirred for a further 30 min, washed with H_2O (3 × 100 mL) and dried over Na_2SO_4. The solvent was distilled off under reduced pressure and the residue purified by column chromatography [SiO_2: $MeCO_2Et$ / hexanes 1:1 (v/v)] to yield **21** (492 mg, 58%) as a red powder. FABMS: *m/z* = 424 $[M]^+$; ^{1}H NMR (400 MHz, $CDCl_3$): δ = 0.99 (6H, t, 8 Hz), 1.28 (6H, s), 2.31 (4H, q, 8 Hz), 2.55 (6H, s), 7.47 (2H, d, 8 Hz), 8.25 (2H, d, 8 Hz); ^{13}C-NMR (100 MHz,

$CDCl_3$): δ = 12.2, 12.9, 14.9, 17.4, 129.3, 130.1, 130.6, 131.2, 133.5, 138.4, 138.9, 142.0, 154.8, 170.2.

25a. A solution of benzylidene-bis(tricyclohexylphosphine)dichlororuthenium (2.0 mg, 0.002 mmol) in THF (1 mL) was added dropwise to a solution of **22a** (9 mg, 0.01 mmol) and **24** (190 mg, 0.1 mmol) in THF (4 mL) maintained under Ar. The mixture was stirred at ambient temperature for 23 h and then vinyl ethyl ether (1 mL, 10.4 mmol) was added. After 30 min, the solvent was distilled off under reduced pressure and the residue was dissolved in MeOH (0.5 mL). The addition of Et_2O (10 mL) caused the precipitation of a pink solid, which was isolated to afford **25a** (160 mg) after centrifugation and removal of the supernatant.

26a. A solution of benzylidene-bis(tricyclohexylphosphine)dichlororuthenium (2.0 mg, 0.002 mmol) in THF (1 mL) was added dropwise to a solution of **23a** (5 mg, 0.01 mmol) and **24** (215 mg, 0.1 mmol) in THF (4 mL) maintained under Ar. The mixture was stirred at ambient temperature for 23 h and then vinyl ethyl ether (1 mL, 10.4 mmol) was added. After 30 min, the solvent was distilled off under reduced pressure and the residue was dissolved in MeOH (0.5 mL). The addition of Et_2O (10 mL) caused the precipitation of a pink solid, which was isolated to afford **26a** (164 mg) after centrifugation and removal of the supernatant.

28a. A solution of **36** (381 mg, 1.5 mmol) and 4-nitro-2-chloromethyl-phenol (341 mg, 1.8 mmol) in MeCN (30 mL) was heated for 2 d under reflux and Ar. After cooling down to ambient temperature, the solvent was distilled off under reduced pressure and the residue was dissolved in CH_2Cl_2 (20 mL). The resulting solution was washed with

aqueous $NaHCO_3$ (5 w%, 2 × 30 mL) and H_2O (2 × 20 mL). The solvent of the organic phase was distilled off under reduced pressure and the residue was purified by column chromatography [SiO_2: CH_2Cl_2/hexanes (1:1, v/v)] to afford **28a** (110 mg, 18%) as a yellow solid. FABMS: *m/z* = 402 $[M]^+$; HRESIMS: *m/z* calcd. for $[M + H]^+$ $C_{24}H_{23}N_2O_4$: 403.1658, found 403.1659; ^1H NMR (500 MHz, $CDCl_3$): δ = 0.87 (3H, s), 1.47 (3H, s), 3.77 (3H, s), 4.47 (1H, d, 19 Hz), 4.55 (1H, d, 19 Hz), 6.62 (1H, d, 9 Hz), 6.67 (1H, dd, 2 and 6 Hz), 6.78 (1H, d, 2 Hz), 6.88 (1H, d, 9 Hz), 7.37–7.43 (3H, m), 7.60–7.67 (2H,m), 7.90–7.95 (2H, m); ^{13}C NMR (100 MHz, $CDCl_3$): δ = 19.5, 27.7, 41.2, 50.1, 56.0, 106.0, 109.6, 110.3, 111.7, 118.2, 120.3, 123.4, 123.9, 128.2, 128.8, 129.2, 136.1, 139.5, 140.7, 140.9, 155.0, 159.3.

29a. A solution of **37** (35 mg, 0.1 mmol) and 4-nitro-2-chloromethyl-phenol (27 mg, 0.1 mmol) in MeCN (30 mL) was heated for 2 d under reflux and Ar. After cooling down to ambient temperature, the solvent was distilled off under reduced pressure and the residue was dissolved in CH_2Cl_2 (15 mL). The resulting solution was washed with H_2O (20 mL). The solvent of the organic phase was distilled off under reduced pressure and the residue was purified by column chromatography [SiO_2: CH_2Cl_2/hexanes (1:1, v/v)] to afford **29a** (31 mg, 56%) as a yellow solid. FABMS: *m/z* = 418 $[M + H]^+$; HRESIMS: *m/z* calcd. for $[M + H]^+$ $C_{23}H_{20}N_3O_5$: 418.1403, found 418.1405; ^1H NMR (400 MHz, CD_3CN): δ = 0.84 (3H, s), 1.65 (3H, s), 4.61 (1H, d, 18 Hz), 4.95 (1H, d, 18 Hz), 6.96 (1H, d, 9 Hz), 7.05 (1H, d, 9 Hz), 7.40–7.50 (3H, m), 7.61–7.66 (2H, m), 7.92–8.00 (2H, m), 8.10 (1H, d, 2 Hz), 8.15 (1H, dd, 2 and 9 Hz); ^{13}C NMR (100 MHz, CD_3CN): δ = 17.9, 27.0, 41.2, 49.5, 105.2, 109.0, 118.7, 119.1, 120.7, 123.8, 124.3, 125.9, 128.3, 129.3, 135.0, 139.1, 141.9, 142.1, 153.6, 158.5.

30a. A solution of **38** (153 mg, 0.6 mmol) and 4-nitro-2-chloromethyl-phenol (132 mg, 0.7 mmol) in MeCN (30 mL) was heated for 2 d under reflux and Ar. After cooling down to ambient temperature, the solvent was distilled off under reduced pressure and the residue was dissolved in CH_2Cl_2 (15 mL). The resulting solution was washed with aqueous KOH (0.2 M, 10 mL) and H_2O (10 mL). The solvent of the organic phase was distilled off under reduced pressure and the residue was purified by column chromatography [SiO_2: CH_2Cl_2/hexanes (1:1, v/v)] to afford **30a** (120 mg, 48%) as a white solid. FABMS: *m/z* = 390 $[M]^+$; HRESIMS: *m/z* calcd. for $[M]^+$ $C_{23}H_{20}N_2O_3$: 391.1452, found 391.1460; ^{1}H NMR (400 MHz, $CDCl_3$): δ = 0.87 (3H, s), 1.58 (3H, s), 4.50 (1H, d, 18 Hz), 5.04 (1H, d, 18 Hz), 6.59–6.67 (1H, m), 6.72 (1H, dd, 2 and 8 Hz), 6.94 (1H, d, 9 Hz), 7.40–7.48 (3H, m), 7.60–7.70 (2H,m), 7.92 (1H, d, 3 Hz), 7.98 (1H, dd, 3 and 9 Hz); ^{13}C NMR (75 MHz, $CDCl_3$): δ = 14.5, 27.8, 42.1, 51.3, 103.7, 106.3, 106.5, 118.1, 120.9, 123.4, 124.3, 128.3, 129.2, 129.7, 135.3, 141.4, 142.8, 147.3, 150.4, 156.3, 158.8.

31a. A solution of **39** (191 mg, 0.7 mmol) and 4-nitro-2-chloromethyl-phenol (139 mg, 0.7 mmol) in MeCN (30 mL) was heated for 2 d under reflux and Ar. After cooling down to ambient temperature, the solvent was distilled off under reduced pressure and the residue was dissolved in CH_2Cl_2 (20 mL). The resulting solution was washed with aqueous NaOH (0.01 M, 10 mL) and H_2O (2 × 20 mL). The solvent of the organic phase was distilled off under reduced pressure and the residue was purified by column chromatography [SiO_2: CH_2Cl_2/hexanes (1:1, v/v)] to afford **31a** (172 mg, 57%) as a white solid. FABMS: *m/z* = 409 $[M + H]^+$; HRESIMS: *m/z* calcd. for $[M]^+$ $C_{23}H_{19}N_2O_3$: 409.1358, found 409.1367; ^{1}H NMR (500 MHz, $CDCl_3$): δ = 0.85 (3H, s), 1.56 (3H, s),

4.52 (2H, d, 18 Hz), 4.57 (2H, d, 18 Hz), 6.60–6.63 (1H, m), 6.81–6.92 (3H, m), 7.36–7.44 (3H, m), 7.63 (2H, d, 5 Hz), 7.92–7.97 (2H, m); ^{13}C NMR (100 MHz, $CDCl_3$): δ = 18.6, 27.8, 41.4, 50.2, 106.1, 109.8, 110.7, 113.8, 118.4, 120.2, 123.6, 124.2, 128.3, 129.0, 129.5, 135.9, 140.0, 141.3, 143.0, 157.4, 159.3.

32a. A solution of **40** (670 mg, 2.7 mmol) and 2-chloromethyl-4-nitro-phenol (551 mg, 2.9 mmol) in MeCN (15 mL) was heated for 2 d under reflux and Ar. After cooling down to ambient temperature, the solvent was distilled off under reduced pressure and the residue was dissolved in CH_2Cl_2 (15 mL). The resulting solution was washed with aqueous KOH (0.2 M, 10 mL) and H_2O (10 mL). The solvent of the organic phase was distilled off under reduced pressure and the residue was purified by column chromatography [SiO_2: hexanes/CH_2Cl_2 (2:1, v/v)] to give **32a** (590 mg, 55%) as a white solid. FABMS: *m/z* = 403 $[M + H]^+$; HRESIMS: *m/z* calcd. for $[M + H]^+$ $C_{24}H_{23}N_2O_4$: 442.1658, found 442.1660; ^{1}H NMR ($CDCl_3$, 400 MHz): δ = 0.86 (3H, s), 1.58 (3H, s), 3.82 (3H, s), 4.53 (2H, d, 18 Hz), 4.63 (2H, d, 18 Hz), 6.73 (1H, d, 8 Hz), 6.86–6.95 (4H, m), 7.14–7.18 (2H, m), 7.55 (2H, d, 8 Hz), 7.93 (2H, d, 8 Hz); ^{13}C-NMR ($CDCl_3$, 100 MHz): δ = 18.8, 28.0, 41.1, 50.0, 55.7, 105.7, 109.4, 114.4, 118.5, 120.5, 121.2, 122.8, 123.5, 124.1, 128.0, 128.1, 129.7, 138.2, 141.1, 147.2, 159.6, 160.4.

33a. A solution of **41** (110 g, 0.4 mmol) and 2-chloromethyl-4-nitro-phenol (86 mg, 0.5 mmol) in MeCN (10 mL) was heated for 2 d under reflux and Ar. After cooling down to ambient temperature, the solvent was distilled off under reduced pressure and the residue was dissolved in CH_2Cl_2 (15 mL). The resulting solution was washed with aqueous KOH (0.2 M, 10 mL) and H_2) (10 mL). The solvent of the organic phase was distilled off under reduced pressure and the residue was purified by column chromatography

[SiO_2: hexanes/CH_2Cl_2 (2:1, v/v)] to give **33a** (83 mg, 48%) as a yellow solid. FABMS: *m/z* = 415 $[M]^+$; HRESIMS: *m/z* calcd. for $[M + H]^+$ $C_{25}H_{26}N_3O_3$: 416.1974, found 416.1982; ^1H NMR ($CDCl_3$, 400 MHz): δ = 0.86 (3H, s), 1.57 (3H, s), 2.97 (6H, s), 4.54 (2H, d, 16 Hz), 4.60 (2H, d, 16 Hz), 6.67–6.73 (3H, m), 6.85–6.91 (2H, m), 7.13–7.17 (2H, m), 7.46 (2H, d, 8 Hz), 7.91 (2H, d, 8 Hz); ^{13}C NMR ($CDCl_3$, 100 MHz): δ = 18.8, 28.0, 40.7, 41.2, 50.0, 106.2, 109.4, 112.3, 118.5, 120.6, 121.0, 122.8, 123.5, 124.0, 127.9, 129.3, 138.4, 141.0, 147.3, 151.0, 160.0.

34a. A solution of **42a** (60 mg, 0.2 mmol), 4-dimethylaminobenzaldehyde (145 mg, 1.0 mmol) and CF_3CO_2H (5 μL, 0.06 mmol) in MeCN (30 mL) was heated for 6 d under reflux and Ar. After cooling down to ambient temperature, the solvent was distilled off under reduced pressure and the residue was dissolved in CH_2Cl_2 (4 mL). The addition of hexanes (30 mL) caused the formation of a precipitate, which was filtered off, dissolved in CH_2Cl_2 (15 mL) and washed with aqueous KOH (0.01 M, 5 mL). The solvent of the organic phase was distilled off to afford **34a** (40 mg, 47%) as a purple solid. FABMS: *m/z* = 441 $[M]^+$; HRESIMS: *m/z* calcd. for $[M + H]^+$ $C_{27}H_{28}N_3O_3$: 442.2131, found 442.2134; ^1H NMR (400 MHz, CD_3CN): δ = 1.41 (6H, s), 2.91 (6H, s), 4.77 (2H, s), 6.38 (1H, bd, 16 Hz), 6.68 (2H, d, 9 Hz), 6.84–6.94 (4H, m), 7.13–7.18 (1H, m), 7.23 (1H, d, 7 Hz), 7.39 (2H, d, 9 Hz), 7.95 (1H, dd, 3 and 9 Hz), 8.07 (1H, bs).

35a. A solution of **43** (278 mg, 0.9 mmol) and 2-chloromethyl-4-nitrophenol (169 mg, 0.9 mmol) in MeCN (20 mL) was heated under reflux for 24 h. After cooling to ambient temperature, the solvent was distilled off under reduced pressure and the residue was dissolved in CH_2Cl_2 (3 mL). The addition of Et_2O (20 mL) caused the precipitation of a purple solid. The solid was dissolved in CH_2Cl_2 (30 mL) and washed with H_2O (20

mL). The organic phase was dried over Na_2SO_4 and the solvent was distilled off under reduced pressure to give **35a** (248 mg, 60%) as a purple solid. FABMS: *m/z* = 461 $[M + H]^+$; ^1H NMR (DMSO): δ = 1.34 (6H, s), 2.93 (6H, s), 4.85 (2H, s), 6.42 (1H, d, 16 Hz), 6.67 (2H, d, 9 Hz), 6.88–6.95 (4H, m), 7.20 (1H, d, 8 Hz), 7.44 (2H, d, 8 Hz), 7.95 (1H, d, 9 Hz), 8.10 (1H, s); ^{13}C NMR (DMSO): δ = 23.9, 24.8, 26.2, 45.0, 45.4, 50.8, 111.1, 111.3, 111.9, 112.8, 114.7, 118.3, 121.6, 123.8, 125.4, 130.2, 139.6, 141.9, 142.6, 152.2, 155.0, 157.9, 160.2, 190.7.

37. A solution of *i*-propylphenylketone (0.2 mL, 1.3 mmol) and 4-nitrophenylhydrazine (0.2 g, 1.3 mmol) in EtOH (10 mL) was heated for 15 h under reflux. After cooling down to ambient temperature, the solvent was distilled off under reduced pressure, the residue was dissolved in concentrated HCl (5 mL) and the resulting solution was heated for 12 h under reflux. After cooling down to ambient temperature, the pH was adjusted to *ca.* 8 with a saturated aqueous solution of Na_2CO_3 and the solution was extracted with CH_2Cl_2 (3 × 10 mL). The organic phase was dried ($MgSO_4$), filtered and the solvent was distilled off under reduced pressure. The residue was purified by column chromatography [SiO_2: hexanes/CH_2Cl_2 (2:3, v/v)] to afford **37** (0.1 g, 40%) as a yellow solid. FABMS: *m/z* = 267 $[M + H]^+$; ^1H NMR (400 MHz, $CDCl_3$): δ = 1.68 (6H, s), 7.52–7.57 (3H, m), 7.77 (1H, d, 9 Hz), 8.19–8.22 (2H, m), 8.24 (1H, d, 2 Hz), 8.32 (1H, dd, 2 and 9 Hz); ^{13}C NMR (100 MHz, $CDCl_3$): δ = 24.9, 54.7, 117.3, 121.3, 125.0, 129.2, 131.9, 132.8, 146.3, 149.0, 158.7, 188.7.

38. A solution of *i*-propylphenylketone (0.9 mL, 6 mmol) and 4-fluorophenylhydrazine (1.0 g, 6 mmol) in EtOH (10 mL) was heated for 24 h under reflux. After cooling down to ambient temperature, the solution was diluted with H_2O (20 mL) and the pH was

adjusted to *ca.* 8 with aqueous KOH (0.3 M). Then, the mixture was extracted with CH_2Cl_2 (3 × 15 mL). The organic phase was dried ($MgSO_4$), filtered and the solvent was distilled off under reduced pressure. The residue was purified by column chromatography [SiO_2: hexanes/CH_2Cl_2 (1:1, v/v)] to afford **38** (0.8 g, 55%) as a yellow solid. FABMS: *m/z* = 240 $[M + H]^+$; ^1H NMR (400 MHz, $CDCl_3$): δ = 1.60 (6H, s), 7.04–7.09 (2H, m), 7.48–7.50 (3H, m), 7.64–7.65 (1H, m), 8.12–8.15 (2H, m); ^{13}C NMR (100 MHz, $CDCl_3$): δ = 25.0, 54.5, 109.0, 115.0, 122.1, 128.2, 129.1, 131.0, 133.5, 150.0, 160.8, 163.2, 183.5.

39. A solution of *i*-propylphenylketone (0.9 mL, 6 mmol) and 2,4-difluorophenylhydrazine hydrochloride (1.0 g, 6 mmol) and concentrated H_2SO_4 (5 mL) in EtOH (10 mL) was heated for 24 h under reflux. After cooling down to ambient temperature, the solution was diluted with aqueous NaOH (2 M, 10 mL) and the mixture was extracted with CH_2Cl_2 (4 × 25 mL). The organic phase was dried ($MgSO_4$), filtered and the solvent was distilled off under reduced pressure. The residue was crystallized from MeOH to afford **39** (0.7 g, 51%) as a white solid. FABMS: *m/z* = 258 $[M + H]^+$; ^1H NMR (400 MHz, $CDCl_3$): δ = 1.60 (6H, s), 6.82–6.89 (2H, m), 7.47–7.51 (3H, m), 8.15–8.18 (2H, m); ^{13}C NMR (100 MHz, $CDCl_3$): δ = 25.2, 55.2, 103.6, 105.0, 128.7, 129.1, 131.3, 133.1, 152.3, 155.5, 161.1, 163.2, 183.2.

40. A solution of *i*-propyl-(4-methoxyphenyl)-ketone (1.6 g, 9 mmol) and phenylhydrazine (0.89 mL, 9 mmol) in $MeCO_2H$ (5 mL) was heated for 24 h under reflux. After cooling down to ambient temperature, the solution was diluted with H_2O (20 mL) and the pH was adjusted to *ca.* 8 with aqueous KOH (0.3 M). Then, the mixture

was extracted with CH_2Cl_2 (3 × 15 mL). The organic phase was dried ($MgSO_4$), filtered and the solvent was distilled off under reduced pressure. The residue was purified by column chromatography [SiO_2: hexanes/CH_2Cl_2 (1:2, v/v)] to afford **40** (1.52 g, 67%) as a white solid. FABMS: *m/z* = 252 $[M + H]^+$; ^1H NMR (400 MHz, $CDCl_3$): δ = 1.60 (6H, s), 3.88 (3H, s), 7.02 (2H, d, 9 Hz), 7.24 (1H, d, 8 Hz), 7.33–7.38 (2H, m), 7.68 (1H, d, 8 Hz), 8.16 (2H, d, 9 Hz); ^{13}C NMR (100 MHz, $CDCl_3$): δ = 25.4, 53.6, 55.8, 114.4, 120.8, 121.2, 125.8, 126.3, 128.1, 130.8, 147.9, 153.6, 162.0, 183.0.

41. A solution of *i*-propyl-(4-dimethylaminophenyl)-ketone (0.25 g, 1.3 mmol) and phenylhydrazine (0.13 mL, 1.3 mmol) in $MeCO_2H$ (2 mL) was heated under reflux for 24 h. After cooling down to ambient temperature, the solution was diluted with H_2O (20 mL) and the pH was adjusted to *ca.* 8 with aqueous KOH (0.3 M). Then, the mixture was extracted with CH_2Cl_2 (3 × 15 mL). The organic phase was dried ($MgSO_4$), filtered and the solvent was distilled off under reduced pressure. The residue was purified by column chromatography [SiO_2: hexanes/CH_2Cl_2 (1:3, v/v)] to afford **41** (0.19 g, 55%) as a yellow liquid. FABMS: *m/z* = 265 $[M + H]^+$; ^1H NMR (400 MHz, $CDCl_3$): δ = 1.61 (6H, s), 3.06 (6H, s), 6.78 (2H, d, 9 Hz), 7.23 (1H, d, 7 Hz), 7.31–7.36 (2H, m), 7.66 (1H, d, 8 Hz), 8.14 (2H, d, 9 Hz); ^{13}C NMR (100 MHz, $CDCl_3$): δ = 25.8, 40.5, 53.3, 111.8, 120.2, 121.0, 121.1, 125.1, 127.9, 130.4, 147.9, 152.2, 154.0, 183.4.

43. A solution of 2,3,3'-trimethyl-5-fluoro-3*H*-indole (1.09 g, 6.15 mmol), *N,N*-dimethyl-4-aminobenzaldehyde (0.92 g, 6.15 mmol) and HBr (0.5 mL, 33% in AcOH) in EtOH (10 mL) was heated under reflux for 12 h. After cooling to ambient temperature, the solvent was distilled off under reduced pressure. The residue was dissolved in

CH_2Cl_2 (30 mL) and washed with a saturated aqueous solution of $NaHCO_3$ (2 × 20 mL). The organic phase was dried over Na_2SO_4 and the solvent was distilled off under reduced pressure to give **43** (1.6 g, 85%) as an orange solid. FABMS: *m/z* = 310 $[M + H]^+$; ^1H NMR ($CDCl_3$): δ = 1.44 (6H, s), 2.98 (6H, s), 6.69 (2H, d, 8 Hz), 6.85 (1H, d, 16 Hz), 7.00 (2H, t, 7 Hz), 7.49–7.51 (3H, m), 7.66 (1H, d, 16 Hz); ^{13}C NMR ($CDCl_3$): δ = 24.4, 40.6, 53.4, 109.3, 112.5, 115.0, 121.0, 124.3, 129.4, 139.0, 148.9, 150.7, 151.6, 160.3, 162.7, 184.3.

44. A solution of **36** (0.38 g, 1.5 mmol) and 2-bromoethanol (0.13 mL, 1.8 mmol) in PhMe (30 mL) was heated under reflux for 3 d. After cooling down to ambient temperature, the solvent was distilled off under reduced pressure. The residue was dissolved in CH_2Cl_2 (5 mL), forced to precipitate with the addition of hexanes (30 mL) and filtered off. This procedure was repeated two more times and the resulting solid was dissolved in a mixture of MeCN / H_2O (1:1, v/v, 10 mL) and aqueous KOH (2 M, 1 mL). After stirring for 1 h at ambient temperature, the solution was concentrated under reduced pressure and washed with CH_2Cl_2 (3 × 20 mL). The organic phase was dried ($MgSO_4$) and the solvent was distilled off under reduced pressure. The residue was purified by column chromatography [SiO_2: CH_2Cl_2/$MeCO_2Et$ (1:1, v/v)] to afford **44** (65 mg, 14%) as a yellow solid. FABMS: *m/z* = 295 $[M]^+$; ^1H NMR (500 MHz, $CDCl_3$): δ = 0.79 (3H, s), 1.53 (3H, s), 3.27–3.33 (1H, m), 3.49–3.54 (1H, m), 3.62–3.66 (1H, m), 3.68–3.74 (1H, m), 3.82 (3H, s), 6.70–6.72 (1H, m), 6.75–6.79 (2H, m), 7.37–7.42 (3H, m), 7.66–7.72 (2H, m); ^{13}C NMR (100 MHz, $CDCl_3$): δ = 20.4, 29.3, 48.1, 50.8, 56.1, 63.4, 109.5, 112.2, 112.5, 127.6, 128.1, 138.9 141.0, 144.8, 155.6.

45. A high-pressure tube was loaded with a solution of **37** (300 mg, 1.5 mmol) and 2-bromoethanol (1.0 mL, 14 mmol) in MeCN (4 mL) and exposed to microwave radiations for a total of 10 min in 10 s intervals. After cooling down to ambient temperature, the solvent was distilled off under reduced pressure and the residue was dissolved in CH_2Cl_2 (5 mL). The addition of Et_2O (30 mL) caused the formation of a precipitate, which was filtered off and dissolved in H_2O(5 ml). After the addition of KOH (100 mg, 1.8 mmol), the solution stirred at ambient temperature for 10 min and extracted with Et_2O (3 × 15 mL). The organic phase was dried ($MgSO_4$) and the solvent was distilled off under reduced pressure. The residue was purified by column chromatography [SiO_2: hexanes/CH_2Cl_2 (4:1, v/v)] to afford **45** (41 mg, 11%) as a yellow solid. FABMS: *m/z* = 249 $[M + H]^+$; ^{1}H NMR (400 MHz, $CDCl_3$): δ = 1.21 (3H, s), 1.38 (3H, s), 1.43 (3H, s), 3.54–3.75 (3H, m), 3.87–3.91 (1H, m), 6.74 (1H, d, 9 Hz), 7.92 (1H, d, 2 Hz), 8.11 (1H, dd, 2 and 9 Hz); ^{13}C NMR (100 MHz, $CDCl_3$): δ = 17.4, 21.1, 28.0, 46.9, 49.5, 63.4, 109.3, 111.4, 119.2, 125.5, 141.5, 143.0, 157.4.

46. A high-pressure tube was loaded with a solution of **38** (588 mg, 2.5 mmol) and 2-bromoethanol (1.0 mL, 14 mmol) in MeCN (4 mL) and exposed to microwave radiations for a total of 5 min in 10 s intervals. After cooling down to ambient temperature, the solvent was distilled off under reduced pressure and the residue was dissolved in CH_2Cl_2 (5 mL). The addition of Et_2O (30 mL) caused the formation of a precipitate, which was filtered off and dissolved in H_2O (5 mL). After the addition of KOH (100 mg, 1.8 mmol), the solution stirred at ambient temperature for 10 min and extracted with Et_2O (3 × 15 mL). The organic phase was dried ($MgSO_4$) and the solvent was distilled off under reduced pressure. The residue was purified by column chromatography [SiO_2:

hexanes/CH_2Cl_2 (4:1, v/v)] to afford **46** (21 mg, 3%) as a white solid. FABMS: *m/z* = 283 $[M]^+$; ^{1}H NMR (400 MHz, $CDCl_3$): δ = 0.76 (3H, s), 1.51 (3H, s), 3.28–3.34 (1H, m), 3.51–3.74 (3H, m), 6.72–6.90 (3H, m), 7.33–7.38 (3H, m), 7.64 (2H, d, 7 Hz); ^{13}C NMR (100 MHz, $CDCl_3$): δ = 20.4, 29.3, 30.1, 48.1, 50.8, 63.5, 110.2, 112.7, 114.2, 127.7, 128.4, 138.6, 141.4, 147.2, 158.0, 160.4.

48. A mixture of the iodide salt of **52** (15 mg, 0.04 mmol) and $NaBH_4$ (1.5 mg, 0.04 mmol) in MeOH (5 mL) was stirred for 5 min at ambient temperature, diluted with H_2O (5 mL) and extracted with CH_2Cl_2 (2 × 5 mL). The organic phase was dried ($MgSO_4$), filtered and the solvent was distilled off under reduced pressure. The residue was purified by column chromatography (SiO_2: CH_2Cl_2) to afford **48** (12 mg, 90%) as a white solid. FABMS: *m/z* = 274 $[M + H]^+$; ^{1}H NMR (400 MHz, $CDCl_3$): δ = 0.69 (3H, s), 1.38 (3H, s), 2.80 (3H, s), 3.99 (1H, s), 6.58–6.66 (2H, m), 7.34–7.41 (5H, m); ^{13}C NMR (100 MHz, $CDCl_3$): δ = 25.1, 25.4, 26.2, 37.4, 46.1, 84.0, 103.0, 103.3, 103.5, 105.6, 105.8, 128.1, 128.6, 130.1, 137.3.

49. A solution of **36** (0.69 g, 3.4 mmol) and MeI (0.22 mL, 3.6 mmol) in MeCN (30 mL) was heated for 2 d under reflux and Ar. After cooling down to ambient temperature, the solvent was distilled off under reduced pressure and the residue was dissolved in CH_2Cl_2 (7 mL). The addition of hexanes (30 mL) caused the formation of a precipitate, which was filtered off to afford **49** (0.66 g, 49%) as a dark red solid. FABMS: *m/z* = 266 $[M - I]^+$; ^{1}H NMR (500 MHz, CD_3CN): δ = 1.57 (6H, s), 3.81 (3H, s), 3.93 (3H, s), 7.19 (1H, dd, 3 and 9 Hz), 7.34 (1H, d, 3 Hz), 7.57–7.60 (2H, m), 7.70–7.74 (3H, m), 7.77–7.81 (1H, m); ^{13}C NMR (100 MHz, CD_3CN): δ = 21.5, 36.3, 55.2, 56.0, 109.2, 115.0, 117.0, 125.5, 127.9, 129.6, 132.9, 144.5, 162.1.

50. A solution of **37** (60 mg, 0.2 mmol) and MeI (40 μL, 0.6 mmol) in MeCN (30 mL) was heated for 2 d under reflux and Ar. After cooling down to ambient temperature, the solvent was distilled off under reduced pressure and the residue was dissolved in CH_2Cl_2 (5 mL). The addition of Et_2O (30 mL) caused the formation of a precipitate, which was filtered off to afford **50** (32 mg, 51%) as a yellow solid. FABMS: *m/z* = 281 $[M - I]^+$; ^1H NMR (400 MHz, $CDCl_3$): δ = 1.80 (6H, s), 4.18 (3H, s), 7.64–7.76 (3H, m), 7.93 (2H, d, 7 Hz), 8.10 (1H, d, 10 Hz), 8.41–8.44 (2H, m); ^{13}C NMR (100 MHz, CD_3CN): δ = 22.9, 39.9, 56.9, 119.1, 119.2, 125.2, 126.0, 128.9, 130.2, 134.1, 143.4, 146.8, 149.1, 196.0.

51. A solution of **38** (0.1 g, 0.4 mmol) and MeI (78 μL, 1.2 mmol) in MeCN (30 mL) was heated for 2 d under reflux and Ar. After cooling down to ambient temperature, the solvent was distilled off under reduced pressure and the residue was dissolved in CH_2Cl_2 (5 mL). The addition of Et_2O (30 mL) caused the formation of a precipitate, which was filtered off to afford **51** (69 mg, 43%) as a dark red solid. FABMS: *m/z* = 254 $[M - I]^+$; ^1H NMR (400 MHz, $CDCl_3$): δ = 1.69 (6H, s), 4.12 (3H, s), 7.22–7.32 (2H, m), 7.64–7.70 (3H, m), 7.83–7.89 (3H, m); ^{13}C NMR (100 MHz, CD_3CN): δ = 23.1, 39.2, 56.2, 111.5, 117.3, 119.3, 125.4, 129.0, 130.1, 133.6, 138.4, 144.6, 163.1, 191.3.

52. A high-pressure tube was loaded with a solution of **39** (105 mg, 0.5 mmol) and MeI (1.0 mL, 16.1 mmol) in MeCN (4 mL) and exposed to microwave radiations for a total of 5 min in 10 s intervals. After cooling down to ambient temperature, the solvent was distilled off under reduced pressure and the residue was dissolved in CH_2Cl_2 (7 mL). The addition of hexanes (30 mL) caused the formation of a precipitate, which was filtered off to afford **52** (87 mg, 53%) as a orange solid. FABMS: *m/z* = 272 $[M - I]^+$; ^1H NMR (400 MHz, $CDCl_3$): δ = 1.94 (6H, s), 4.27 (3H, s), 7.01–7.27 (2H, m), 7.76–7.84 (5H, m); ^{13}C

NMR (100 MHz, CD_3CN): δ = 23.0, 41.8, 57.2, 106.2, 107.7, 124.9, 129.1, 130.0, 133.5, 146.7, 150.6, 154.0, 162.7, 192.2.

53. A solution of **40** (0.10 g, 0.4 mmol) and MeI (0.05 mL, 0.8 mmol) in MeCN (10 mL) was heated for 2 d under reflux and Ar. After cooling down to ambient temperature, the solvent was distilled off under reduced pressure and the residue was dissolved in CH_2Cl_2 (4 mL). The addition of Et_2O (30 mL) caused the formation of a precipitate, which was filtered off to afford **53** (70 mg, 44%) as a dark red solid. FABMS: *m/z* = 266 $[M - I]^+$; ^1H NMR (400 MHz, $CDCl_3$): δ = 1.65 (6H, s), 3.95 (3H, s), 4.04 (3H, s), 7.20 (2H, d, 9 Hz), 7.58–7.68 (6H, m); ^{13}C NMR (100 MHz, $CDCl_3$): δ = 23.6, 37.0, 55.8, 56.2, 116.0, 116.2, 117.2, 123.0, 130.1, 131.0, 131.2, 142.0, 142.1, 164.5, 190.9.

54. A solution of **41** (0.10 g, 0.4 mmol) and MeI (0.05 mL, 0.8 mmol) in MeCN (5 mL) was heated for 2 d under reflux and Ar. After cooling down to ambient temperature, the solvent was distilled off under reduced pressure and the residue was dissolved in CH_2Cl_2 (4 mL). The addition of Et_2O (30 mL) caused the formation of a precipitate, which was filtered off to afford **54** (84 mg, 54%) as a dark red solid. FABMS: *m/z* = 279 $[M - I]^+$; ^1H NMR (400 MHz, $CDCl_3$): δ = 1.76 (6H, s), 3.22 (6H, s), 4.34 (3H, s), 6.95 (2H, d, 9 Hz), 7.51–7.59 (3H, m), 7.68 (1H, d, 8 Hz), 8.02 (2H, d, 9 Hz); ^{13}C NMR (100 MHz, $CDCl_3$): δ = 26.5, 39.9, 40.8, 54.3, 111.2, 112.7, 115.2, 122.7, 129.4, 129.9, 134.1, 141.8, 142.7, 155.0, 185.8.

55. A solution of the 1,2,3,3-tetramethyl-3*H*-indolium hexafluorophosphate (31 mg, 0.1 mmol) and 4-dimethylaminobenzaldehyde (22 mg, 0.2 mmol) and CF_3CO_2H (2 μL) in MeCN (25 mL) was heated for 5 d under reflux and Ar. After cooling down to ambient

temperature, the solvent was distilled off under reduced pressure and the residue was dissolved in CH_2Cl_2 (5 mL). The addition of hexanes (30 mL) caused the formation of a precipitate, which was filtered off to afford **55** (36 mg, 82%) a deep purple solid. FABMS: *m/z* = 305 $[M]^+$; ^{1}H NMR (400 MHz, CD_3CN): δ = 1.77 (6H, s), 3.19 (6H, s), 3.87 (3H, s), 6.89 (1H, d, 12 Hz), 7.05 (2H, d, 21 Hz), 7.51–7.66 (4H, m), 7.90 (2H, d, 12 Hz), 8.20 (1H, d, 21 Hz); ^{13}C NMR (75 MHz, CD_3CN): δ = 26.4, 33.2, 40.0, 51.6, 104.9, 112.8, 113.6, 122.4, 122.9, 128.2, 129.3, 134.2, 142.6, 143.0, 155.0, 155.5, 180.5.

56. A solution of **43** (120 mg, 0.39 mmol) and MeI (113 mg, 0.8 mmol) in MeCN (10 mL) was heated under reflux for 48 h. After cooling to ambient temperature, the solvent was distilled off under reduced pressure and the residue was dissolved in CH_2Cl_2 (3 mL). The addition of Et_2O (20 mL) caused the precipitation of a purple solid, which was filtered off to give **56** (141 mg, 80%). FABMS: *m/z* = 323 $[M - I]^+$; ^{1}H NMR ($CDCl_3$): δ = 1.79 (6H, s), 3.19 (6H, s), 4.18 (3H, s), 6.79 (2H, d, 8 Hz), 7.18 (2H, d, 8 Hz), 7.26 (1H, d, 20 Hz), 7.44-–7.47 (1H, m), 8.04–8.08 (3H, m); ^{13}C NMR ($CDCl_3$): δ = 28.0, 36.2, 40.9, 51.4, 105.5, 110.8, 113.1, 114.9, 116.5, 122.9, 135.8, 138.3, 144.4, 155.1, 155.8, 163.9, 179.4.

57a. *N*,*N*′-Dicyclohexylcarbodiimide (DCC, 181 mg, 0.9 mmol) was added to a solution of **62a** (173 mg, 0.4 mmol), (*endo/exo*)-5-norborene-2-carboxylic acid (123 mg, 0.9 mmol) and 4-dimethylaminopyridine (DMAP, 11 mg, 0.09 mmol) in CH_2Cl_2 (25 mL) maintained at 0°C under Ar. The mixture was allowed to warm up to ambient temperature over the course of 18 h. The solvent was distilled off under reduced pressure and the residue was purified by column chromatography [SiO_2: CH_2Cl_2/hexanes (2:1, v/v) → (5:1, v/v) to afford (*endo/exo*)-**57a** (197 mg, 88%) as a white solid. FABMS: *m/z*

= 509 $[M]^+$; ^{1}H NMR (400 MHz, $CDCl_3$): δ = 0.85 (6H, s), 1.29–1.64 (12H, m), 2.00–2.08 (2H, m), 2.45–2.50 (1H, m), 2.98 (2H, s), 3.19–3.22 (2H, m), 3.38 (1H, s), 4.49–4.60 (4H, m), 6.10–6.27 (4H, m), 6.68 (2H, t, 9 Hz), 6.81–6.93 (6H, m), 7.40–7.42 (6H, m), 7.63 (4H, s), 7.88–7.93 (4H, m); ^{13}C NMR (100 MHz, $CDCl_3$): δ =18.7, 27.9, 29.8, 31.0, 41.3, 42.2, 43.1, 43.7, 44.0, 46.3, 46.8, 47.2, 50.2, 105.9, 109.6, 116.7, 118.4, 120.3, 120.6, 123.5, 124.2, 128.3, 129.0, 129.4, 132.6, 136.1, 138.5, 138.7, 139.2, 141.2, 144.6, 144.7, 145.5, 159.3, 174.1, 175.6.

58a. DCC (43 mg, 0.2 mmol) was added to a solution of **64a** (55 mg, 0.1 mmol), (*endo/exo*)-5-norborene-2-carboxylic acid (29 mg, 0.2 mmol) and DMAP (3 mg, 0.02 mmol) in CH_2Cl_2 (20 mL) maintained at 0°C under Ar. The mixture was allowed to warm up to ambient temperature over the course of 18 h. The solvent was distilled off under reduced pressure and the residue was purified by column chromatography [SiO_2: CH_2Cl_2/hexanes (2:1, v/v) → (5:1, v/v) to afford (*endo/exo*)-**58a** (64 mg, 90%) as a white solid. FABMS: *m/z* = 509 $[M]^+$; ^{1}H NMR (400 MHz, $CDCl_3$): δ = 0.85 (3H, s), 0.86 (3H, s), 1.27–1.61 (12H, m), 2.01–2.06 (2H, m), 2.47–2.50 (1H, m), 3.00 (2H, s), 3.20–3.23 (2H, m), 3.37 (1H, s), 4.48–4.66 (4H, m), 6.05–6.27 (4H, m), 6.72 (2H, d, 9 Hz), 6.86–6.93 (4H, m), 7.10 (2H, d, 9 Hz), 7.15–7.18 (6H, m), 7.62–7.66 (4H, m), 7.92–7.96 (4H, m); ^{13}C NMR (100 MHz, $CDCl_3$): δ =18.8, 28.1, 29.8, 31.0, 41.1, 42.2, 43.1, 43.8, 44.0, 46.4, 46.8, 47.2, 50.2, 105.4, 109.5, 118.4, 120.3, 121.3, 122.2, 122.8, 123.6, 124.2, 128.1, 129.5, 132.4, 133.5, 133.6, 136.0, 138.0, 138.8, 141.3, 147.0, 151.8, 159.2, 173.5, 175.1.

59a. A solution of benzylidene-bis(tricyclohexylphosphine)dichlororuthenium (1.5 mg, 0.002 mmol) in THF (1 mL) was added to a solution of **57a** (46 mg, 0.09 mmol) in THF

(2 mL) maintained under Ar at ambient temperature. After 23 h, vinyl ethyl ether (1 mL, 10.5 mmol) was added and the mixture was stirred for a further 30 min. The was distilled off under reduced pressure and the residue was dissolved in THF (0.5 mL). The addition of MeCN (5 mL) caused the precipitation of a white solid, which was filtered off after centrifugation to give **59a** (27 mg). DSC: T_g = 110°C; TGA: T_d = 231°C; GPC: M_n = 26,600, PDI = 1.22.

60a. A solution of benzylidene-bis(tricyclohexylphosphine)dichlororuthenium (2.0 mg, 0.002 mmol) in THF (1 mL) was added to a solution of **58a** (30 mg, 0.06 mmol) in THF (2 mL) maintained under Ar at ambient temperature. After 25 h, vinyl ethyl ether (1 mL, 10.5 mmol) was added and the mixture was stirred for a further 30 min. The was distilled off under reduced pressure and the residue was dissolved in THF (0.5 mL). The addition of MeCN (4 mL) caused the precipitation of a white solid, which was filtered off after centrifugation to give **60a** (20 mg). DSC: T_g = 86°C; TGA: T_d = 206°C; GPC: M_n = 22,100, PDI = 1.66.

62a. A solution of **61** (205 mg, 0.9 mmol) and 4-nitro-2-chloromethyl-phenol (113 mg, 1.3 mmol) in MeCN was heated under reflux and Ar for 5 d. After cooling down to ambient temperature, the solvent was distilled off under reduced pressure. The residue dissolved in CH_2Cl_2 (20 mL) and washed with aqueous $NaHCO_3$ (5% w/v, 15 mL) and (2 × 15 mL). The solvent of the organic phase was distilled off under reduced pressure and the residue was purified by column chromatography [SiO_2: CH_2Cl_2/hexane (1:1, v/v) → CH_2Cl_2/ethylacetate (10:1, v/v)] to afford **62a** (207 mg, 62%) as an orange solid. FABMS: *m/z* = 389 $[M]^+$; ^{1}H NMR (400 MHz, CD_3CN): δ = 0.78 (3H, s), 1.52 (3H, s),

4.41 (1H, d, 16 Hz), 4.67 (1H, d, 16 Hz), 6.53–6.57 (2H, m), 6.63 (1H, d, 8 Hz), 6.70 (1H, d, 2 Hz), 6.93 (1H, d, 9 Hz), 7.39–7.45 (3H, m), 7.67 (2H, m), 7.91 (1H, dd, 3 and 9.0 Hz), 7.96 (1H, d, 3 Hz); ^{13}C NMR (100 MHz, CD_3CN): δ = 41.7, 51.0, 107.2, 111.2, 112.0, 119.1, 122.0, 128.9, 125.0, 129.5, 129.9, 130.4, 137.4, 140.6, 141.3, 142.2, 153.0, 160.3.

64a. A solution of BBr_3 (1M, 0.75 mL) in CH_2Cl_2 was added to a solution of **63a** (230 mg, 0.6 mmol) in CH_2Cl_2 (100 mL) maintained at 0°C under Ar. The reaction mixture was allowed to warm up to ambient temperature over the course of 15 h and washed with aqueous Na_2CO_3 (5 % w/v, 10 mL) and H_2O (20 mL). The solvent of the organic phase was distilled off under reduced pressure and the residue was dissolved in CH_2Cl_2 (3 mL). The addition of hexanes (50 mL) caused the precipitation of a yellowish solid, which was filtered off to afford **64a** (199 mg, 90%). FABMS: *m/z* = 388 $[M + 1]^+$; ^{1}H NMR (500 MHz, CD_3CN): δ = 0.82 (3H, s), 1.54 (3H, s), 4.47 (1H, d, 18 Hz), 4.73 (1H, d, 18 Hz), 6.75–6.88 (3H, m), 6.95 (1H, t, 9 Hz), 7.14–7.35 (3H, m), 7.47–7.52 (2H, m), 7.94–7.97 (1H, m), 8.00–8.01 (1H, m); ^{13}C NMR (100 MHz, CD_3CN): δ =17.8, 26.9, 40.6, 49.9, 105.7, 109.6, 111.5, 115.6, 118.3, 121.0, 122.8, 124.0, 126.1, 126.6, 128.0, 129.9, 130.6, 138.3, 141.0, 146.9, 158.1.

65a. DCC (18 mg, 0.1 mmol) was slowly added to a solution of **62a** (30 mg, 0.08 mmol), 3,6,9-trioxaundecanedioic acid (100 μL, 0.6 mmol) and DMAP (1 mg, 0.08 mmol) in MeCN (25 mL) maintained at 0°C under Ar. The mixture was allowed to warm up to ambient temperature and stirred under these conditions for 3 d. The solvent was distilled off under reduced pressure and the residue was purified by column chromatography [SiO_2: CH_2Cl_2/EtOAc (3:1 → 1:1, v/v) → EtOAc/MeCN (4:1, v/v)] to afford **65a** (26

mg, 57%) as a white solid. FABMS: *m/z* = 593 $[M]^+$; ^{1}H NMR (500 MHz, $CDCl_3$): δ = 0.85 (3H, s), 1.56 (3H, s), 3.70–3.85 (8H, m), 4.17 (2H, s), 4 39 (2H, s), 4.53 (1H, d, 18 Hz), 4.59 (1H, d, 18 Hz), 6.68 (1H, d, 9 Hz), 6.89–6.94 (3H, m), 7.37–7.43 (3H, m), 7.62 (2H, bs), 7.91 (1H, d, 3 Hz), 8.12 (1H, dd, 3 and 9 Hz); ^{13}C NMR (100 MHz, $CDCl_3$): δ = 18.7, 27.9, 32.0, 41.3, 50.2, 69.0, 69.3, 70.6, 71.0, 71.3, 71.8, 105.8, 109.6, 116.5, 118.6, 120.2, 120.5, 123.5, 124.2, 135.9, 139.4, 141.3, 144.6, 145.1, 159.2, 169.9, 172.3.

66a. DCC (31 mg, 0.15 mmol) was slowly added to a solution of **62a** (58 mg, 0.15 mmol), methoxy-PEG-2000-carboxylic acid (378 mg, 0.15 mmol) and DMAP (2 mg, 0.16 mmol) in CH_2Cl_2 (10 mL) maintained at 0°C under Ar. The mixture was allowed to warm up to ambient temperature and stirred under these conditions for 18 h. The solvent was distilled off under reduced pressure and the residue was purified by column chromatography [SiO_2: EtOAc/hexanes (2:1, v/v)] to afford **66a** (67 mg, 15%) as a yellow solid. ^{1}H NMR (300 MHz, $CDCl_3$): δ = 0.82 (3H, s), 1.54 (3H, s), 3.37 (3H, s), 3.54–3.87 (176H, m), 4.37 (2H, s), 4.51 (1H, d, 17 Hz), 4.59 (1H, d, 17 Hz), 6.66 (1H, d, 9 Hz), 6.86–6.91 (3H, m), 7.37–7.41 (3H, m), 7.60 (2H, d, 6 Hz), 7.91 (2H, d, 6 Hz).

67a. A solution of benzylidene-bis(tricyclohexylphosphine)dichlororuthenium (2 mg, 0.002 mmol) in THF (1 mL) was slowly added to a solution of **57a** (28 mg, 0.06 mmol) and **68** (126 mg, 0.06 mmol) in THF (4 mL) maintained at ambient temperature under Ar. After 23 h, vinyl ethyl ether (1 mL, 10.5 mmol) was added and the mixture was stirred for a further 30 min. The solvent was distilled off under reduced pressure and the residue was dissolved in THF (0.5 mL). The addition of MeCN (10 mL) caused the precipitation of a white solid, which was filtered off after centrifugation to give **67a** (75 mg). GPC: M_n = 19,000, PDI = 1.13.

69a. A solution of **74** (100 mg, 0.14 mmol) and 2-chloromethyl-4-nitrophenol (32 mg, 0.17 mmol) in MeCN (20 mL) was heated under reflux for 24 h. After cooling down to ambient temperature, the solvent was distilled off under reduced pressure and the residue was dissolved in CH_2Cl_2 (3 mL). The addition of Et_2O (20 mL) caused the precipitation of a purple solid. The solid was dissolved in CH_2Cl_2 (30 mL) and washed with H_2O (20 mL). The organic phase was dried over Na_2SO_4 and the solvent was distilled off under reduced pressure to give **69a** (72 mg, 60 %) as a purple solid. FABMS: *m/z* = 864 $[M + H]^+$; HRESIMS: calcd. *m/z* for $C_{51}H_{53}BN_5O_5F_2$ = 864.4102 $[M + H]^+$, found *m/z* = 864.4111; ^{1}H NMR ($CDCl_3$): δ = 1.00 (6H, t, 7 Hz), 1.31 (6H, s), 1.42 (6H, s), 2.32 (4H, q, 7 Hz), 2.56 (6H, s), 2.98 (6H, s), 4.63 (4H, s), 6.16 (1H, d, 16 Hz), 6.67 (3H, m), 6.76 (1H, d, 16 Hz), 6.91 (1H, d, 10 Hz), 7.02 (1H, dd, 8 Hz, 2 Hz), 7.08 (1H, d, 2 Hz), 7.32 (2H, d, 9 Hz), 7.48 (2H,d, 8 Hz), 8.01 (2H, d, 7 Hz), 8.31 (2H, d, 8 Hz); ^{13}C NMR ($CDCl_3$): δ = 12.3, 13.0, 14.5, 15.0, 17.5, 24.6, 30.1, 40.6, 40.8, 41.5, 50.5, 53.4, 109.6, 112.5, 112.6, 116.7, 118.2, 120.4, 120.7, 123.7, 124.0, 124.6, 128.8, 129.3, 129.6, 130.5, 130.7, 131.1, 133.6, 138.5, 138.9, 140.4, 140.8, 141.8, 144.6, 151.5, 154.8, 165.4.

70a. A solution of **76** (114 mg, 0.16 mmol) and 2-chloromethyl-4-nitrophenol (35 mg, 0.188 mmol) in MeCN (20 mL) was heated under reflux for 24 h. After cooling down to ambient temperature, the solvent was distilled off under reduced pressure and the residue was dissolved in CH_2Cl_2 (3 mL). The addition of Et_2O (20 mL) caused the precipitation of a purple solid. The solid was dissolved in CH_2Cl_2 (30 mL) and washed with H_2O (20 mL). The organic phase was dried over Na_2SO_4 and the solvent was distilled off under reduced pressure to **70a** (100 mg, 73 %) as a purple solid. FABMS: *m/z* = 878 $[M + H]^+$; HRESIMS: calcd. *m/z* for $C_{52}H_{55}BN_5O_5F_2$ = 878.4259 $[M + H]^+$, found *m/z* = 878.4264;

^{1}H NMR ($CDCl_3$): δ = 0.98 (6H, t, 7 Hz), 1.26 (6H, s), 1.38 (6H, s), 2.31 (4H, q, 7 Hz), 2.57 (6H, s), 3.10 (6H, s), 3.83 (2H, t, 6 Hz), 4.54 (2H, t, 6 Hz), 4.59 (4H, s), 6.22 (1H, d, 13 Hz), 6.69-6.92 (6H, m), 7.12-7.16 (2H, m), 7.35 (4H, d, 8 Hz), 7.95 (2H, d, 7 Hz), 8.01 (2H, d, 8 Hz); ^{13}C NMR ($CDCl_3$): δ = 12.2, 13.0, 14.5, 15.0, 17.5, 24.5, 30.1, 39.1, 41.1, 50.4, 51.4, 52.9, 62.5, 109.5, 112.6, 112.9, 113.2, 118.0, 120.6,121.4, 122.7, 123.7, 124.5, 124.6, 128.1, 129.1, 129.6, 130.6, 130.7, 133.6, 138.4, 138.9, 139.0, 140.7, 141.3, 146.5, 150.2, 154.8, 160.4, 166.3.

71. A solution of (4-methoxyphenyl) hydrazine (500 mg, 3 mmol), 3-methyl-2-butanone (247 mg, 3 mmol) and PTSA (54 mg, 0.3 mmol) in EtOH (30 mL) was heated under reflux for 15 h. After cooling down to ambient temperature, the solvent was distilled off under reduced pressure. The residue was dissolved in CH_2Cl_2 (30 mL) and washed with H_2O (30 mL). The organic phase was dried over Na_2SO_4 and the solvent was evaporated under reduced pressure to give **71** (545 mg, 96 %) as a red solid. FABMS: *m/z* = 190 $[M + H]^+$; ^{1}H NMR ($CDCl_3$): δ = 1.20 (6H, s), 2.16 (3H, s), 3.77 (3H, s), 6.75 (1H, d, 13 Hz), 6.77 (1H, s), 7.37 (1H, d, 8 Hz); ^{13}C NMR ($CDCl_3$): δ = 14.2, 22.2, 52.7, 54.5, 107.3, 111.3, 119.1, 146.1, 146.4, 157.2, 184.7.

72. A mixture of **71** (497 mg, 3 mmol) in EtOH (30 mL) and HBr (0.005M) in AcOH (0.23 mL) was heated under reflux for 15 h. Then, a solution of 4-dimethylamino benzaldehyde (776 mg, 5 mmol) and TFA (0.5 mL, 0.009 mmol) in EtOH (10 mL) was added and the mixture was heated under reflux for a further 24 h. After cooling down to ambient temperature, the solvent was distilled under reduced pressure and the residue was dissolved in CH_2Cl_2 (30 mL) and washed with aqueous Na_2CO_3 (0.01M, 3 × 20 mL). The organic phase was dried over Na_2SO_4 and the solvent was distilled off under

reduced pressure. The solid residue was purified by column chromatography (SiO_2: CH_2Cl_2) to give **72** (578 mg, 60 %) as a white solid. FABMS: *m/z* 321 $[M + H]^+$; ^1H NMR ($CDCl_3$): δ = 1.45 (6H, s), 2.99 (6H, s), 3.85 (3H, s), 5.27 (1H, s), 6.71 (2H, d, 9 Hz), 6.84 (1H, s), 6.88 (2H, d, 7 Hz), 7.48 (1H, s), 7.49 (1H, d, 7 Hz), 7.51 (1H, d, 12 Hz); ^{13}C NMR ($CDCl_3$): δ = 24.7, 40.6, 53.0, 53.9, 56.1, 108.2, 112.5, 112.8, 115.7, 120.8, 124.7, 129.2, 137.8, 148.7, 151.5, 158.4, 182.6.

73. A solution of BBr_3 (1M) in CH_2Cl_2 (11 mL) was added dropwise to a solution of **72** (385 mg, 1 mmol) in CH_2Cl_2 (40 mL) maintained at 0°C under Ar. The mixture was stirred under these conditions for 1 h, allowed to warm up to ambient temperature over 12 h, washed with a aqueous $NaHCO_3$ (0.01M, 3 × 40 mL) and extracted with THF (2 × 35 mL). The organic phase was dried over Na_2SO_4 and the solvent was distilled off under reduced pressure to give **73** (291 mg, 95 %) as a brown solid. FABMS: *m/z* = 307 $[M + H]^+$; ^1H NMR ($CDCl_3$): δ = 1.39 (6H, s), 2.98 (6H, s), 6.72-6.76 (3H, m), 6.82 – 6.89 (2H, m), 7.28 (1H, d, 9 Hz) 7.51 (2H, d, 9 Hz), 7.53 (1H, s); ^{13}C NMR ($CDCl_3$): δ = 24.4, 40.2, 53.6, 56.3, 108.4, 112.8, 113.0, 115.5, 120.4, 124.5, 129.0, 137.6, 148.5, 151.3, 158.6, 182.4.

74. DCC (97 mg, 0.47 mmol) was added to a solution of **73** (100 mg, 0.31 mmol), **21** (200 mg, 0.47 mmol) and DMAP (3.8 mg, 0.03 mmol) in CH_2Cl_2 (160 mL) maintained at 0°C under Ar. The mixture was allowed to warm up to ambient temperature over 12 h and stirred for a further 36 h. The solvent was distilled off under reduced pressure and the residue was purified by column chromatography [SiO_2: CH_2Cl_2/EtOAc (4:1 v/v) to afford **74** (200 mg, 90 %) as a red solid. FABMS: *m/z* = 714 $[M + H]^+$; ^1H NMR ($CDCl_3$): δ = 1.01 (6H, t, 7 Hz), 1.33 (6H, s), 1.50 (6H, s), 2.33 (4H, q, 7 Hz), 2.56 (6H,

s), 3.05 (6H, s), 6.73 (2H, d, 9 Hz), 6.87 (1H, d, 16 Hz), 7.21-7.25 (2H, m), 7.51 (4H, t, 10 Hz), 7.64 (1H, d, 8 Hz), 7.70 (2H, d, 16 Hz), 8.36 (2H, d, 8 Hz); ^{13}C NMR ($CDCl_3$): δ = 12.3, 13.0, 15.0, 17.5, 24.7, 34.3, 40.6, 53.3, 105.3, 112.5, 115.4, 120.5, 121.4, 124.1, 129.4, 130.0, 130.5, 130.7, 131.2, 133.6, 138.9, 138.4, 141.9, 147.2, 149.0, 151.1, 152.0, 154.8, 165.3, 184.8.

75. A solution of 2,3,3-trimethyl-3*H*-indole (587 mg, 2.44 mmol), *N*-methyl-*N*-(2-hydroxyethyl)-4-aminobenzaldehyde (438 mg, 2.44 mmol) and HBr (0.5 mL, 33 % in AcOH) in EtOH (10 mL) was heated under reflux for 12 h. After cooling down to ambient temperature, the solvent was distilled off under reduced pressure and the residue was dissolved in CH_2Cl_2 (30 mL) and washed with a saturated aqueous solution of $NaHCO_3$ (2 × 20 mL). The organic phase was dried over Na_2SO_4 and the solvent was distilled off under reduced pressure to give **75** (743 mg, 95 %) as an orange solid. FABMS: *m/z* = 321 $[M + H]^+$; ^{1}H NMR ($CDCl_3$): δ = 1.43 (6H, s), 2.98 (3H, s), 3.54 (2H, t, 5 Hz), 3.85 (2H, t, 5 Hz), 6.68 (2H, d, 8 Hz), 6.79 (1H, d, 16 Hz), 7.16-7.31 (3H, m), 7.39 (2H, d, 8 Hz), 7.57 (1H, d, 7 Hz), 7.60 (1H, d, 16 Hz); ^{13}C NMR ($CDCl_3$): δ = 24.7, 39.3, 52.8, 55.1, 59.8, 112.4, 114.9, 120.2, 121.5, 124.2, 125.5, 128.2, 139.5, 146.8, 151.0, 154.2, 184.6.

76. DCC (67 mg, 0.32 mmol) was added to a solution of **75** (68 mg, 0.21 mmol), **21** (135 mg, 0.31 mmol) and DMAP (3 mg, 0.024 mmol) in CH_2Cl_2 (80 mL) maintained at 0 °C under Ar. The mixture was allowed to warm up to ambient temperature over 12 h and stirred for a further 36 h. The solvent was distilled off under reduced pressure and the residue was purified by column chromatography [SiO_2: CH_2Cl_2/EtOAc (4:1 v/v)] to afford **76** (110 mg, 72 %) as a red solid. FABMS: *m/z* = 728 $[M + H]^+$; ^{1}H NMR

($CDCl_3$): δ = 0.97 (6H, t, 7 Hz), 1.25 (6H, s), 1.44 (6H, s), 2.29 (4H, q, 7 Hz), 2.53 (6H, s), 3.16 (6H, s), 3.86 (2H, t, 6 Hz), 4.58 (2H, t, 6 Hz), 6.82 (2H, d, 9 Hz), 6.88 (1H, d, 16 Hz), 7.20 (1H, t, 7 Hz), 7.30-7.35 (2H, m), 7.39 (2H, d, 8 Hz), 7.52 (2H, d, 9 Hz), 7.60 (1H, d, 7 Hz), 7.66 (1H, d, 16 Hz), 8.10 (2H, d, 8 Hz); ^{13}C NMR ($CDCl_3$): δ = 12.2, 12.9, 15.0, 17.4, 24.7, 24.8, 25.3, 26.0, 30.1, 34.3, 39.3, 49.6, 51.3, 52.6, 62.6, 109.9, 112.6, 121.6, 122.9, 123.1, 125.9, 128.0, 128.4, 129.2, 130.5, 130.6, 133.5, 138.4, 138.9, 141.4, 154.7, 166.3.

77a. DCC (40 mg, 0.19 mmol) was added to a solution of **62a** (90 mg, 0.23 mmol), **21** (74 mg, 0.18 mmol) and DMAP (2 mg, 0.02 mmol) in MeCN (20 mL) maintained at 0°C under Ar. The mixture was allowed to warm up to ambient temperature over 12 h and stirred for a further 36 h. The solvent was distilled off under reduced pressure and the residue was purified by column chromatography [SiO_2: CH_2Cl_2/hexanes (1:1 → 4:1 v/v)] to afford **77a** (46 mg, 33 %) as a pink solid. FABMS: *m/z* = 794 $[M]^+$; ^1H NMR (400 MHz, $CDCl_3$): δ = 0.87 (3H, s), 0.99 (6H, t, 8 Hz), 1.31 (6H, s), 1.60 (3H, s), 2.33 (4H, q, 8 Hz), 2.55 (6H, s), 4.57 (1H, d, 18 Hz), 4.64 (1H, d, 18 Hz), 6.76 (1H, d, 9 Hz), 6.93 (1H, d, 9 Hz), 7.06 (1H, dd, 2 and 8 Hz), 7.10 (1H, d, 2 Hz), 7.37–7.45 (3H, m), 7.48 (2H, d, 8 Hz), 7.60–7.67 (2H, m), 7.93 (1H, d, 3 Hz), 7.97 (1H, dd, 3 and 9 Hz), 8.31 (2H, d, 8 Hz); ^{13}C NMR (100 MHz, $CDCl_3$): *δ* = 12.3, 15.0, 17.5, 18.8, 28.0, 41.4, 50.2, 105.9, 109.7, 116.8, 118.6, 120.3, 120.8, 123.5, 124.3, 128.3, 129.1, 129.3, 129.5, 130.6, 130.7, 131.1, 133.5, 136.0, 138.4, 138.9, 139.5, 141.3, 141.8, 145.1, 145.4, 154.8, 159.3, 165.5.

78. A solution of **74** (50 mg, 0.07 mmol) and MeI (20 mg, 0.14 mmol) in MeCN (20 mL) was heated under reflux for 48 h. After cooling down to ambient temperature, the solvent

was distilled off under reduced pressure and the residue was dissolved in CH_2Cl_2 (3 mL). The addition of Et_2O (20 mL) caused the precipitation of a purple solid, which was filtered off to give **78** (41 mg, 80 %). FABMS: *m/z* = 729 $[M + H]^+$; ^{1}H NMR ($CDCl_3$): δ = 1.01 (6H, t, 7 Hz), 1.32 (6H, s), 1.84 (6H, s), 2.33 (4H, q, 7 Hz), 2.56 (6H, s), 3.23 (6H, s), 4.25 (3H, s), 6.84 (2H, d, 8 Hz), 7.42-7.54 (6H, m), 8.07 (2H, d, 16 Hz), 8.35 (3H, d, 8 Hz); ^{13}C NMR ($CDCl_3$): δ = 12.3, 13.0, 14.5, 15.0, 17.5, 23.0, 28.2, 32.0, 35.9, 40.9, 51.4, 105.7, 113.2, 114.2, 116.8, 123.1, 129.6, 129.7, 130.6, 131.3, 133.6, 138.3, 140.0, 142.4, 143.6, 150.7, 154.9, 155.4, 155.9, 164.8, 179.5.

79. A solution of **76** (70 mg, 0.1 mmol) and MeI (28 mg, 0.2 mmol) in MeCN (20 mL) was heated under reflux for 48 h. After cooling down to ambient temperature, the solvent was distilled off under reduced pressure and the residue was dissolved in CH_2Cl_2 (3 mL). The addition of Et_2O (20 mL) caused the precipitation of a purple solid, which was filtered off to give **79** (51 mg, 69 %). FABMS: *m/z* = 743 $[M + H]^+$; ^{1}H NMR (CD_3CN): δ = 0.94 (6H, t, 7 Hz), 1.24 (6H, s), 1.70 (6H, s), 2.29 (4H, q, 7 Hz), 2.44 (6H, s), 3.24 (3H, s), 3.86 (3H, s), 4.02 (2H, t, 5 Hz), 4.62 (2H, t, 5 Hz), 7.04 (2H, d, 9 Hz), 7.07 (1H, d, 16 Hz), 7.43 (2H, d, 8 Hz), 7.51–7.55 (3H,m), 7.63 (1H, d, 7 Hz), 7.90 (2H, d, 9 Hz), 8.02 (2H, d, 8 Hz), 8.16 (1H, d, 16 Hz); ^{13}C NMR ($CDCl_3$): δ = 12.3, 12.9, 15.0, 17.4, 28.0, 36.1, 39.9, 51.4, 51.5, 62.4, 106.9, 113.2, 113.5, 122.7, 123.6, 128.5, 129.3, 129.7, 130.3, 130.6, 130.7, 133.5, 135.9, 138.4, 138.9, 141.5, 142.2, 142.5, 154.7, 154.9, 155.3, 166.2, 180.2.

80a. A solution of **82** (233 mg, 1 mmol), **42a** (310 mg, 1 mmol) and TFA (0.5 mL, 6.5 mmol) in EtOH (10 mL) was heated under reflux for 24 h. After cooling down to ambient temperature, the solvent was distilled off under reduced pressure and the residue

was dissolved in CH_2Cl_2 (5 mL). The addition of Et_2O (50 mL) caused the precipitation of a solid, which was filtered off, dissolved in CH_2Cl_2 (20 mL) and washed with H_2O (20 mL). The organic phase was dried over Na_2SO_4 and the solvent was distilled off under reduced pressure to give **80a** (215 mg, 40 %) as a green solid. FABMS: *m*/*z*= 539 $[M + H]^+$; HRESIMS: *m*/*z* = 538.2344 $[M + H]^+$ (*m*/*z* calcd. for $C_{32}H_{32}N_3O_5$ = 538.2336); ^{1}H NMR ($CDCl_3$): δ = 1.21 (6H, t, 7 Hz), 1.39 (6H, bs), 3.42 (4H, q, 7 Hz), 4.61 (2H, s), 6.47 (1H, d, 2 Hz), 6.58 (1H, dd, 2 and 12 Hz), 6.64–6.71 (2H, m), 6.80–6.95 (3H, m), 7.10–7.15 (2H, m), 7.25 (1H, s), 7.55 (1H, s), 7.96 (1H, dd, 3 and 8 Hz), 8.00 (1H, d, 3 Hz); ^{13}C NMR ($CDCl_3$): δ = 12.9, 19.3, 27.6, 41.2, 45.3, 50.5, 97.3, 104.8, 109.0, 109.7, 116.0, 118.1, 119.0, 120.6, 121.0, 122.7, 123.7, 124.4, 126.3, 128.0, 129.6, 131.2, 138.8, 140.9, 141.6, 146.9, 151.4, 156.4, 159.9, 161.2.

81. A solution of **82** (150 mg, 0.6 mmol) and the iodide salt of **83** (184 mg, 0.6 mmol) in EtOH (10 mL) was heated under reflux for 24 h. After cooling down to ambient temperature, the solvent was distilled off under reduced pressure and the residue was dissolved in CH_2Cl_2 (5 mL). The addition of Et_2O (30 mL) caused the precipitation of a solid, which was filtered off and dissolved in Me_2CO (5 mL). After the addition of a saturated aqueous solution of NH_4PF_6 (5 mL), the solution was concentrated under reduced pressure to half of its original volume and the resulting precipitate was filtered off to give the hexafluorophosphate salt of **81** (273 mg, 82 %) as a purple solid. FABMS: *m*/*z*= 402 $[M - PF_6]^+$; ^{1}H NMR ($CDCl_3$): δ = 1.28 (6H, t, 7 Hz), 1.83 (6H, s), 3.52 (4H, q, 7 Hz), 4.29 (3H, s), 6.45 (1H, d, 2 Hz), 6.69 (1H, dd, 2 and 9 Hz), 7.45–7.56 (4H, m), 7.98 (1H, d, 16 Hz), 8.08 (1H, d, 9 Hz), 8.57 (1H, d, 16 Hz), 9.97 (1H, s); ^{13}C NMR

($CDCl_3$): δ = 13.0, 27.9, 36.2, 46.1, 52.1, 97.2, 109.4, 111.4, 111.5, 113.0, 113.8, 123.0, 129.2, 129.8, 134.8, 142.0, 143.1, 151.2, 155.0, 159.2, 161.4, 181.7.

References and Notes

[1] Y. Hirshberg, *Compt. Rend. Acad. Sci.,* Paris, **1950**, *231*, 903–904.

[2] G. H. Dorion, A. F. Wiebe, *Photochromism*, Focal Press, New York, **1970**.

[3] G. H. Brown (Ed.), *Photochromism*, Wiley, New York, **1971**.

[4] A. V. El'tsov (Ed.), *Organic Photochromes*, Consultants Bureau, New York, **1990**.

[5] H. Bouas-Laurent, H. Dürr (Ed.), *Photochromism: Molecules and Systems*, Elsevier, Amsterdam, **1990**.

[6] J. C. Crano, R. Guglielmetti (Eds.), *Organic Photochromic and Thermochromic Compounds*, Plenum Press, New York, **1999**.

[7] C. B. McArdle (Ed.), *Applied Photochromic Polymer Systems*, Blackie, Glasgow, **1992**.

[8] (a) M. Irie (Ed.), *Photo-Refractive Materials for Ultrahigh Density Optical Memory*, Elsevier, Amsterdam, **1994**. (b) M. Irie. (Ed.), *Chem. Rev.* **2000**, *100*, 1683–1890.

[9] (a) F. M. Raymo, M. Tomasulo, *Chem. Eur. J.* **2006**, *12*, 3186–3193. (b) F. M. Raymo, *Angew. Chem. Int. Ed.*, **2006**, *45*, 5249–5251.

[10] H. Bouas-Laurent, H. Dürr, *Pure Appl. Chem.* **2001**, *73*, 639–665.

[11] H. Görner, *Phys. Chem. Chem. Phys.* **2001**, *3*, 416–423.

[12] M. Irie, K. Sakemura, M. Okinaza, K. Uchida, *J. Org. Chem.* **1995**, *60*, 8305–8309.

[13] H. Görner, C. Fischer, S. Gierisch, J. Daub, *J. Phys. Chem.* **1993**, *97*, 4110–4117.

[14] H. Gross, H. Dürr, W. Retting, *J. Photochem.* **1984**, *26*, 165–178.

[15] C. Weber, F. Rustemeyer, H. Dürr, *Adv. Mater.* **1998**, *10*, 1348–1351.

[16] M. Sheepwash, R. H. Mitchell, C. Bohne, *J. Am. Chem. Soc.* **2002**, *124*, 4693–4700.

[17] M. Seibold, H. Port, K. Gustav, *Chem. Phys. Lett.* **1999**, *314*, 65–72.

[18] D. Gegiu, K. A. Muszkat, E. Fischer, *J. Am. Chem. Soc.* **1968**, *90*, 3907–3918.

[19] H. Görner, H. Gruen, D. Schulte-Frohllnde, *J. Phys. Chem.* **1980**, *84*, 3031–3039.

[20] J. A. Delaire, K. Nakatani, in ref. [8b], p. 1817–1845.

[21] F. M. Raymo, M. Tomasulo, *J. Phys. Chem. A* **2005**, *109*, 7343–7352.

[22] M. G. Kuz'min, M. V. Koz'menko, in ref. [4], p. 245–265.

[23] A. K. Chibisov, H. Görner, *J. Phys. Chem.* **1997**, *101*, 4305–4312.

[24] (a) H. Spreitzer, J. Daub, *Liebigs Ann.* **1995**, 1637–1641. (b) J. Daub, M. Beck, A. Knorr, H. Spreitzer, *Pure Appl. Chem.* **1996**, *68*, 1399–1404.

[25] (a) A. Fernández-Acebes, J.-M. Lehn, *Adv. Mater.* **1998**, *10*, 1519–1522. (b) A. Fernández-Acebes, J.-M. Lehn, *Chem. Eur. J.* **1999**, *5*, 3285–3292.

[26] K. Yagi, C. F. Soong, M. Irie, *J. Org. Chem.* **2001**, *66*, 5419–5423.

[27] J. Ern, A. T. Bens, H.-D. Martin, S. Mukamel, S. Tretiak, K. Tsyganenko, K. Kuldova, H. P. Trommsdorff, C. Kryschi, *J. Phys. Chem. A* **2001**, *105*, 1741–1749.

[28] S.-J. Lim, B.-K. An, S. D. Jung, M. A. Chung, S. J. Park, *Angew. Chem. Int. Ed.* **2004**, *43*, 6346–6350.

[29] (a) Y. Liang, A. S. Dvornikov, P. M. Rentzepis, *Opt. Commun.* **2003**, *223*, 61–66. (b) Y. Liang, A. S. Dvornikov, P. M. Rentzepis, *Proc. Natl. Acad. Sci. USA* **2003**, *100*, 8109–8112. (c) Y. Liang, A. S. Dvornikov, P. M. Rentzepis, *J. Phys. Chem. B* **2004**, *108*, 8652–8658. (d) A. S. Dvornikov, Y. Liang, P. M. Rentzepis, *J. Mater. Chem.* **2005**, *15*, 1072–1078.

[30] T. A. Golovkova, D. V. Kozlov, D. C. Neckers, *J. Org. Chem.* **2005**, *70*, 5545–5549.

[31] M. Giraud, A. Léaustic, M.-F. Charlot, P. Yu, M. Césario, C. Philouze, R. Pansu, K. Nakatani, E. Ishow, *New J. Chem.* **2005**, *29*, 439–446.

[32] N. Xie, Y. Chen, *Chem. Commun.* **2006**, 982–985.

[33] M.-S. Kim, T. Kawai, M. Irie, *Opt. Mater.* **2002**, *21*, 271–274.

[34] (a) C.-C. Ko, L.-X. Wu, K. M.-C. Wong, N. Zhu,V. W.-W Yam, *Chem. Eur. J.* **2004**, *10*, 766–776. (b) V. W.-W Yam, C.-C. Ko, N. Zhu, *J. Am. Chem. Soc.* **2004**, *126*, 12734–12735. (c) T.-W. Ngan, C.-C. Ko, N. Zhu, V. W.-W. Yam, *Inorg. Chem.* **2007**, *46*, 1144–1152.

[35] (a) G. M. Tsivgoulis, J.-M. Lehn, *Angew. Chem., Int. Ed. Engl.* **1995**, *34*, 1119–1122. (b) G. M. Tsivgoulis, J.-M. Lehn, *Chem. Eur. J.* **1996**, *2*, 1399–1406.

[36] J. Ern, T. Bens, H.-D. Martin, S. Mukamel, S. Tretiak, K. Tsyganenko, K. Kuldova, H. P. Trommsdorf, C. Kryschi, *J. Phys. Chem. A* **2001**, *105*, 1741–1749.

[37] M. Frigoli, C. Welch, G. Mehl, *J. Am. Chem. Soc.* **2004**, *126*, 15382–15383.

[38] F. M. Raymo, M. Tomasulo, *Chem. Soc. Rev.* **2005**, *34*, 327–336.

[39] A. J. Myles, N. R. Branda, *J. Am. Chem. Soc.* **2001**, *123*, 177–178.

[40] (a) J. Andréasson, G. Kodis, Y. Terazono, P. A. Liddell, S. Bandyopadhyay, R. H. Mitchell, T. A. Moore, A. L. Moore, D. Gust, *J. Am. Chem. Soc.* **2004**, *126*, 15926–15927. (b) Y. Terazono, G. Kodis, J. Andréasson, G. Jeong, A. Brune, T. Hartmann, H. Dürr, T. A. Moore, A. L. Moore, D. Gust, *J. Phys. Chem. B* **2004**, *108*, 1812–1814. (c) S. D. Straight, J. Andréasson, G. Kodis, S. Bandyopadhyay, R. H. Mitchell, T. A. Moore, A. L. Moore, D. Gust, *J. Am. Chem. Soc.* **2005**, *127*, 9403–9409.

[41] L-H. Liu, K. Nakatani, R. Pansu, J.-J. Vachon, P. Tauc, E. Ishow, *Adv. Mater.* **2007**, *19*, 433–436.

[42] M. Berberich, A.-M. Krause, M. Orlandi, F. Scandola, F. Würthner, *Angew. Chem. Int. Ed.* **2008**, *47*, 6616–6619

[43] A. Archut, G. C. Azzellini, V. Balzani, L. De Cola, F. Vögtle, *J. Am. Chem. Soc.* **1998**, *120*, 12187–12191.

[44] T. Saika, T. Iyoda, K. Honda, T. Shimidzu, *J. Chem. Soc., Chem. Commun.* **1992**, 591–592.

[45] S. Tsuchiya, *J. Am. Chem. Soc.* **1999**, *121*, 48–53.

[46] D. R. Reddy, B. G. Maiya, *Chem. Commun.* **2001**, 117–118.

[47] J. Otsuki, A. Suka, K. Yamazaki, H. Abe, Y. Araki, O. Ito, *Chem. Commun.* **2004**, 1290–1291.

[48] J. L. Rodríguez-Redondo, A. Sastre-Santos, F. Fernández-Lazaro, D. Soares, G. Azzellini, B. Ellioyt, L. Echegoyen, *Chem. Commun.* **2006**, 1265–1267.

[49] T. Inada, S. Uchida, Y. Yokoyama, *Chem. Lett.* **1997**, 321–322.

[50] J. L. Bahr, G. Kodis, L. de la Garza, S. Lin, A. L. Moore, T. A. Moore, D. Gust, *J. Am. Chem. Soc.* **2001**, *123*, 7124–7133.

[51] (a) L. Giordano, T. M. Jovin, M. Irie, E. A. Jares-Erijman, *J. Am. Chem. Soc.* **2002**, *124*, 7481–7489. (b) E. A. Jares-Erijman, L. Giordano, C. Spagnuolo, J. Kawior, R. J. Verneij, T. M. Jovin, *Proc. SPIE* **2004**, *5323*, 13–26.

[52] (a) M. Irie, T. Fukaminato, T. Sasaki, N. Tamai, T. Kawai, *Nature* **2002**, *420*, 759–760. (b) M.-S. Kim, T. Kawai, M. Irie, *Opt. Mater.* **2002**, 275–278. (c) T. Fukaminato, T. Sasaki, T. Kawai, N. Tamai, M. Irie, *J. Am. Chem. Soc.* **2004**, *126*, 14843–14849.

[53] M. Jin, R. Lu, C. Y. Bao, T. H. Xu, Y. Y. Zhao, *Opt. Mater.* **2004**, *26*, 85–88.

[54] E. J. Harbron, D. A. Vicente, M. T. Hoyt, *J. Phys. Chem. B* **2004**, *108*, 18789–18792.

[55] (a) M. Bossi, V. Belov, S. Polyakova, S. W. Hell, *Angew. Chem. Int. Ed.* **2006**, *45*, 7462–7465. (b) A. de Meijere, L. Zhao, V. N. Belov, M. Bossi, M. Noltemeyer, S. W. Hell, *Chem. Eur. J.* **2007**, *13*, 2503–2516.

[56] Z. Zhao, Y. Xing, Z. Wang, P. Lu, *Org. Lett.* **2007**, *9*, 547–550.

[57] (a) T. B. Norsten, N. R. Branda, *Adv. Mater.* **2001**, *13*, 347–349. (b) T. B. Norsten, N. R. Branda, *J. Am. Chem. Soc.* **2001**, *123*, 1784–1785. (c) A. Myles, N. R. Branda, *Adv. Funct. Mater.* **2002**, *12*, 167–173.

[58] A. Osuka, D. Fujikane, H. Shinmori, S. Kobatake, M. Irie, *J. Org. Chem.* **2001**, *66*, 3913–3923.

[59] R. T. Jukes, V. Adamo, F. Hartl, P. Belser, L. De Cola, *Inorg. Chem.* **2004**, *43*, 2779–2792.

[60] (a) S. Wang, W. Shen, Y. Feng, H. Tian, *Chem. Commun.* **2006**, 1497–1499. (b) G. Jiang, S. Wang, W. Yuan, L. Jiang, Y. Song, H. Tian, D. Zhu, *Chem. Mater.* **2006**, *18*, 235–237.

[61] G. Jiang, S. Wang, W. Yuan, Z. Zhao, A. Duan, C. Xu, L. Jiang, Y. Song, D. Zhu, *Eur. J. Org. Chem.* **2007**, 2064–2067.

[62] T. Kawai, T. Sasaki, M. Irie, M. *Chem. Commun.* **2001**, 711–712.

[63] X. Guo, D. Zhang, Y. Zhou, D. Zhu, *J. Org. Chem.* **2003**, *68*, 5681–5687.

[64] S. D. Straight, P. A. Liddell, Y. Terazono, T. A. Moore, A. L. Moore, D. Gust, *Adv. Funct. Mater.* **2007**, *17*, 777–785.

[65] (a) J. Walz, K. Ulrich, H. Port, H. C. Wolf, J. Wonner, F. Effenberg, *Chem. Phys. Lett.* **1993**, *213*, 321–324. (b) M. Seibold, H. Port, H. C. Wolf, *Mol. Cryst. Liq. Cryst.* **1996**, *283*, 75–80. (c) H. Port, M. Hennrich, M. Seibold, H. C. Wolf, *Proc. Electrochem. Soc.* **1998**, *98*, 61–70. (d) H. Port, A. Hartschuh, M. Hennrich, H. C. Wolf, J. M. Endtner, F. Effenberger, *Mol. Cryst. Liq. Cryst.* **2000**, *344*, 145–150. (e) I. B. Ramsteiner, A. Hartschuh, H. Port, *Chem. Phys. Lett.* **2001**, *343,* 83–90.

[66] C. B. McArdle (Ed.), *Applied Photochromic Polymer Systems*, Blackie, Glasgow, 1992.

[67] (a) Y. Liang, A. S. Dvornikov, P. M. Rentzepis, *Chem. Commun.*, **2000**, 1641–1642. (b) Y. Liang, A. S. Dvornikov, P. M. Rentzepis, *Macromolecules*, **2002**, 35, 9377–9382.

[68] Y.-C. Jeong, S. I. Yang, E. Kim , K.-H. Ahn, *Macromol. Rapid Commun.*, **2006**, 27, 1769–1773.

[69] H. Cho, E. Kim, *Macromolecules*, **2002**, 35, 8684–8687.

[70] T. Kawai, Y. Nakashima, T. Kunitake, M. Irie, *Curr. Appl. Phys.*, **2005**, 5, 139–1421.

[71] S. Wang, X. Li, B. Chen, Q. Luo, H. Tian, *Macromol. Rapid Commun.*, **2004**, 205, 1497–1507.

[72] (a) E. J. Harbron, D. A. Vicente, M. T. Hoyt, *J. Phys. Chem. B*, **2004**, 108, 18789–18792. (b) E. J. Harbron, D. A. Vicente, D. H. Hadley, M. R. Imm, *J. Phys. Chem. A*, **2005**, 109, 10846–10853. (c) A. F. Grimes, S. E. Call, D. A. Vicente, D. S. English, E. J. Harbron, *J. Phys. Chem. B*, **2006**, 110, 19183–19190. (d) S. M. Lewis, E. J. Harbron, *J. Phys. Chem. C*, **2007**, 111, 4425–4430.

[73] J. Finden, T. K. Kunz, N. R. Branda, M. O. Wolf, *Adv. Mater.* **2008**, 20, 1998–2002.

[74] S. Wang, C. Yu, M.-S. Choi, S. H. Kim, *Dyes and Pigments*, **2008**, 77, 245–248.

[75] M. Tomasulo, E. Deniz, R. J. Alvarado, F. M. Raymo, *J. Phys. Chem. C*, **2008**, 112, 8038–8045.

[76] (a) I. L. Medintz, S. A. Trammell, H. Mattoussi, J. M. Mauro, *J. Am. Chem. Soc.* **2004**, *126*, 30–31. (b) I. L. Medintz, A. R. Clapp, S. A. Trammell, H. Mattoussi, *Proc. SPIE* **2004**, *5593*, 300–307.

[77] L. Zhu, M.-Q. Zhu, J. K. Hurst, A. D. Q. Li, *J. Am. Chem. Soc.* **2005**, *127*, 8968–8970.

[78] (a) E. Jares-Erijman, L. Giordano, C. Spagnuolo, K. A. Lidke, T. M. Jovin, *Mol. Cryst. Liq. Cryst.* **2005**, *430*, 257–265. (b) S. Mikoski, L. Giordano, M. H. Etchelon, G. Menendez, K. A. Lidke, G. M. Hagen, T. M. Jovin, E. Jares-Erijman, *Proc. SPIE* **2006**, *6096*, 60960X-1–60960X-8.

[79] (a) M. Tomasulo, I. Yildiz, F. M. Raymo, *Aust. J. Chem.* **2006**, *59*, 175–178. (b) M. Tomasulo, I. Yildiz, F. M. Raymo, *Inorg. Chim. Acta* **2007**, *360*, 938–944.

[80] W. H. Binder, R. Sachsenhofer, C. J. Straif, R. Zirbs, *J. Mater. Chem.* **2007**, *17*, 2125–2132.

[81] Z. Zhou, H. Hu, H. Yang, T. Yi, K. Huang, M. Yu, F. Li, C. Huang, *Chem. Commun.* **2008**, 4786–4788.

[82] K. M. Yeo, C. J. Gao, K.-H. Ahn, I. S. Lee, *Chem. Commun.* **2008**, 4622–4624.

[83] J. Fölling, S. Polyakova, V. Belov, A. von Blaaderen, M. L. Bossi, S. W. Hell, *Small* **2008**, *4*, 134–142.

[84] S.-J. Lim, B.-K. An, S. D. Jung, M.-A. Chung, S. Y. Park, *Angew. Chem. Int. Ed.* **2004**, *43*, 6346–6350.

[85] S. Rath, M. Heilig, E. Al-Khalisy, T. Klingler, H. Port, *J. Luminesc.* **2004**, *108*, 401–405.

[86] (a) Y. Liu, M. Fan, C. Zhang, X. Sheng, J. Yao, *Chin. J. Chem* **2007**, *25*, 1612–1616. (b) X.-H. Sheng, A. Peng, H. Fu, Y. Liu, Y. Zhao, Y. MA, J. Yao, *Nanotechnology* **2007**, *18*, 145707-1–145707–7.

[87] S. Xiao, Y. Zou, J. Wu, Y. Zhou, T. Yi, F. Li, C. Huang, *J. Mater. Chem.* **2007**, *17*, 2483–2489.

[88] (a) Z. Hu, Q. Zhang, M. Xue, Q. Sheng, Y. Liu, *J. Phys. Chem. Solids* **2008**, *69*, 206–210. (b) Z. Hu, Q. Zhang, M. Xue, Q. Sheng, Y. Liu, *Opt. Mater.* **2008**, *30*, 851–856.

[89] H. Furukawa, M. Misu, K. Ando, H. Kawaguchi, *Macromol. Rapid Commun.* **2008**, *29*, 547–551.

[90] J. Su, J. Chen, F. Zeng, Q. Chen, S. Wu, Z. Tong, *Polym. Bull.* **2008**, *61*, 425–434.

[91] (a) M.-Q. Zhu, L. Zhu, J. J. Han, W. Wu, J. K. Hurst, A. D. Q. Li, *J. Am. Chem. Soc.* **2006**, *128*, 4303–4309. (b) L. Zhu, W. Wu, M.-Q. Zhu, J. J. Han, J. K. Hurst, A. D. Q. Li, *J. Am. Chem. Soc.* **2007**, *129*, 3524–3526.

[92] J. Chen, F. Zeng, S. Wu, Q. Chen, Z. Tong, *Chem. Eur. J.* **2008**, *14*, 4851–4860.

[93] M. W. Berns, T. Krasieva, C.-H. Sun, A. Dvornikov, P. M. Rentzepis, *J. Photochem. Photobiol. B* **2004**, *75*, 51–56.

[94] Zou, Y.; Yi, T.; Xiao, S.; Li, F.; Li, C.; Gao, X.; Wu, J.; Yu, M.; Huang, C. *J. Am. Chem. Soc* **2008**, *130*, 15750–15751.

[95] (a) J. Fölling, V. N. Belov, R. Kunetsky, R. Medda, A Schönle, A. Egner, C. Eggeling, M. Bossi, S. W. Hell, *Angew. Chem. Int. Ed.* **2007**, *46*, 6266–6270. (b) J. Fölling, V. N. Belov, D. Riedel, A Schönle, A. Egner, C. Eggeling, M. Bossi, S. W. Hell, *ChemPhysChem* **2008**, *9*, 321–326. (d) M. Bossi, J. Fölling, V. N. Belov, V. P. Boyarskiy, R. Medda, A. Egner, C. Eggeling, A Schönle, S. W. Hell, *Nano Lett.* **2008**, *8*, 2463–2468.

[96] O. Chen, R. Glaser, G. I. Likhtenshtein, *J. Biochem. Biophys. Methods* **2008**, *70*, 1073–1079.

[97] N. Soh, K. Yoshida, H. Nakajima, K. Nakano, T. Imato, T. Fukaminato, M. Irie, *Chem. Commun.* **2007**, 5206–5208.

[98] S. Mao, R. K. P. Benninger, Y. Yan, C. Petchprayoon, D. Jackson, C. J. Easley, D. W. Piston, G. Marriott, *Biophys. J.* **2008**, *94*, 4515–4524.

[99] H. Liu, Y. Zhou, Y. Yang, W. Wang, L. Qu, C. Chen, D. Liu, D. Zhang, D. Zhu, *J. Phys. Chem. B* **2008**, *112*, 9893–6896.

[100] Pawley, J. B. (Ed.) *Handbook of Biological Confocal Microscopy*; Springer: New York, 2006.

[101] Haugland, R. P. *The Handbook: A Guide to Fluorescent Probes and Labeling Technologies*; Molecular Probes: Eugene, 2005.

[102]Born, M.; Wolf, E. *Principles of Optics*; Cambridge University Press: Cambridge, 2002.

[103] (a) S. W. Hell, *Nat. Biotechnol.* **2003**, *21*, 1347–1355. (b) S. W. Hell, M. Dyba, S. Jakobs, *Curr. Opinion Neurobiol.* **2004**, *14*, 599–609. (c) S. W. Hell, *Phys. Lett. A* **2004**, *326*, 140–145. (d) S. W. Hell, L. Kastrup, *Nachr. Chem.* **2007**, *55*, 47–50. (e) S. W. Hell, *Science* **2007**, *316*, 1153–1158. (f) S. W. Hell, *Nat. Methods* **2009**, *6*, 24–32. (g) S. W. Hell, R. Schmidt, A. Egner, *Nat. Photonics* **2009**, *3*, 381–387.

[104] M. Bates, B. Huang, X. Zhuang, *Curr. Op. Chem. Biol.* **2008**, *12*, 505–514.

[105] M. G. L. Gustafsson, *Nat. Methods* **2008**, *5*, 385–387.

[106] M. Fernández-Suárez, A. Y. Ting, *Nat. Rev. Mol. Cell. Biol.* **2008**, *9*, 929–943.

[107] M. Heilemann, P. Dedecker, J. Hofkens, M.Sauer, *Laser Photon Rev.* **2009**, *3*, 180–202.

[108] J. Lippincott-Schwartz, S. Manley, *Nat. Methods* **2009**, *6*, 21–23.

[109] S. T. Hess, *Nat. Methods* **2009**, *6*, 124–125.

[110] (a) S. W. Hell, J. Wichmann, *Opt. Lett.* **1994**, *19*, 780–782. (b) T. A. Klar, S. Jakobs, M. Dyba, A. Egner, S. W. Hell, *Proc. Natl. Acad. Sci. USA*, **2000**, *97*, 8206–8210. (c) M. Dyba, S. Jakobs, S. W. Hell, *Nat. Biotechnol.* **2003**, *21*, 1303–1304. (d) V. P. Boyarskiy, V. N. Belov, R. Medda, B. Hein, M. Bossi, S. W. Hell, *Chem. Eur. J.* **2008**, *14*, 1784–1792. (e) B. Harke, C. K. Ullal, J. Keller, S. W. Hell, *Nano Lett.* **2008**, *8*, 1309–1313. (f) R. Schmidt, C. A. Wurm, S. Jakobs, J. Engelhardt, A. Egner, S. W. Hell, *Nat. Methods* **2008**, *5*, 539–544. (g) B. Hein, K. I. Willig, S. W. Hell, *Proc. Natl. Acad. Sci. USA* **2008**, *105*, 14271–14276. (h) U. V. Nagerl, K. I. Willig, B. Hein, S. W. Hell, T. Nonhoeffer, *Proc. Natl. Acad. Sci. USA* **2008**, *105,* 18982–18987. (i) V. Westphal, S. O. Rizzoli, M. A. Lauterbach, D. Kamin, R. Jahn, S. W. Hell, *Science* **2008**, *320*, 246–249. (j) L. Meyer, D. Wildanger, R. Medda, A. Punge, S. O. Rizzoli, G. Donnert, S. W. Hell, *Small* **2008**, *4*, 1095–1100. (k) R. Schmidt, C. A. Wurm, A. Punge, A. Egner, S. Jakobs, S. W. Hell, *Nano Lett.* **2009**, *9*, 2508–2510. (l) C. Eggeling, C. Ringemann, R. Medda, G. Scwarzmann, K. Sandhoff, S. Polyakova, V. N. Belov, B. Hein, C. von Middendorff, A. Schönle, S. W. Hell, *Nature* **2009**, *457*, 1159–1163. (m) A. C. Meyer, T. Frank, D. Khimich, G. Hoch, D. Riedel, N. M. Chapochnikov, Y. M. Yarin, B. Harke, S. W. Hell, A. Enger, T. Mose, *Nat. Neurosci.* **2009**, *12*, 444–453. (n) E. Rittweger, K. Y. Han, S. E. Irvine, C. Eggeling, S. W. Hell, *Nat. Photonics* **2009**, *3*, 144–147. (o) K. Kolmakov, V. N. Belov, J. Bierwagen, C. Ringemann, V. Muller, C. Eggeling, S. W. Hell, *Chem. Eur. J.* **2010**, *16*, 158–166.

[111] (a) S. W. Hell, M. Kroug, *Appl. Phys. B* **1995**, *60*, 495–497. (b) S. W. Hell, S. Jakobs, L. Kastrup, *Appl. Phys. A* **2003**, *77*, 859–860. (c) S. Bretschneider, C. Eggeling, S. W. Hell, *Phys. Rev. Lett.* **2007**, *98*, 218103-1–4.

[112] M. Bossi, V. Belov, S. Polyakova, S. W. Hell, *Angew. Chem. Int. Ed.* **2006**, *45*, 7462–7465.

[113] (a) F. M. Raymo, M. Tomasulo, *Chem. Soc. Rev.* **2005**, *34*, 327–336. (b) F. M. Raymo, M. Tomasulo, *J. Phys. Chem. A* **2005**, *109*, 7343–7352. (c) J. Cusido, E. Deniz, F. M. Raymo, *Eur. J. Org. Chem.* **2009**, 2031–2045. (d) I. Yildiz, E. Deniz, F. M. Raymo, *Chem. Soc. Rev.*, **2009**, *38*, 1859–1867.

[114] M. A. Schwentker, H. Bock, M. Hofmann, S. Jakobs, J. Bewersdorf, C. Eggeling, S. W. Hell, *Microsc. Res. Techn.* **2007**, *70*, 269–280.

[115] M. Bossi, J. Fölling, M. Dyba, V. Westphal, S. W. Hell, *New J. Phys.* **2006**, *8*, 275–284.

[116] J. Fölling, S. Polyakova, V. Belov, A. van Blaaderen, M. L. Bossi, S. W. Hell, *Small* **2008**, *4*, 134–142.

[117] (a) F. M. Raymo, S.Giordani, *J. Am. Chem. Soc.* **2001**, *123*, 4651–4652. (b) F. M. Raymo, S. Giordani, A. J. P. White, D. J. Williams, *J. Org. Chem.* **2003**, *68*, 4158–4169.

[118] The free energy changes for the photoinduced electron transfer processes were estimated with the Rehm–Weller equation (Rehm, D.; Weller, A. *Isr. J. Chem.* **1970**, *8*, 259–271), using the redox potentials in Table 2.1 and an energy change of 2.34 eV for the $S_0 \rightarrow S_1$ transition of the BODIPY fluorophore.

[119] The emission spectra of the fluorophore–photochrome conjugates were recorded before and after (***a*** and ***b*** in Figures 2.4 and 2.9) ultraviolet irradiation, exciting the sample at an isosbestic point. Under these conditions, the fluorescent component absorbs the same amount of exciting photons before and after the interconversion of the photochromic component.

[120] R. H. Grubbs, (Ed.) *Handbook of Metathesis*; Wiley–VCH: Weinheim, 2003.

[121] (a) R. C. Bertelson, in ref. 2, p. 45–431. (b) R. C. Bertelson, in ref. 6, vol. 1, p. 11–83.

[122] A. S. Kholmanskii, K. M. Dyumanev, *Russ. Chem. Rev.*, **1987**, 56, 136–151.

[123] R. Guglielmetti, in ref. 5, p. 314–466 and 855–878.

[124] M. Irie, (Ed.) *Chem. Rev.*, **2000**, 100, 1683–1890.

[125] V. I. Minkin, *Chem. Rev.*, **2004**, 104, 2751–2776.

[126] (a) M. Tomasulo, S. Sortino, A. J. P. White , F. M. Raymo, *J. Org. Chem.*, **2005**, 70, 8180–8189. (b) M. Tomasulo, S. Sortino, F. M. Raymo, *Org. Lett.*, **2005**, 7, 1109–1112. (c) M. Tomasulo, S. Sortino, F. M. Raymo, *Asian Chem. Lett.*, **2007**, 11, 219–222. (d) M. Tomasulo, S. Sortino, F. M. Raymo, *Adv. Mater.*, **2008**, 20, 832–835. (e) M. Tomasulo, S. Sortino, F. M. Raymo, *J. Photochem. Photobiol. A*, **2008**, 200, 44–49. (f) M. Tomasulo, S. Sortino, F. M. Raymo, *J. Org. Chem.*, **2008**, 73, 118–126. (g) E. Deniz, M. Tomasulo, S. Sortino , F. M. Raymo, *J. Phys. Chem. C*, **2009**, 113, 8491–8497. (h) M. Åxman Petersen, E. Deniz, M. Brøndsted Nielsen, S. Sortino, F. M. Raymo, *Eur. J. Org. Chem.*, **2009**, 4333–4339. (i) M. Tomasulo, E. Deniz, T. Benelli, S. Sortino, F. M. Raymo, *Adv. Funct. Mater.*, **2009**, 19, 3956-3961.

[127] (a) A. P. de Silva, G. D. McClean, N. D. McClenaghan T. S., Moody, S. M. Weir, *Nachr. Chem.* **2001**, *49*, 602–606. (b) G. J. Brown, A. P. de Silva, S.Pagliari, *Chem. Commun.* **2002**, 2461–2463. (c) A. P. de Silva, N. D. McClenaghan, *Chem. Eur. J.* **2004**, *10*, 574–586. (d) A. P. de Silva, S.Uchiyama, *Nat. Nanotechnol.* **2007**, *2*, 399–410.

[128] M. D. Ward, *J. Chem. Ed.* **2001**, *78*, 321–328.

[129] F. M. Raymo, *Adv. Mater.* **2002**, *14*, 401–414.

[130] D. Steinitz, F. Remacle, R. D. Levine, *ChemPhysChem* **2002**, *3*, 43–51.

[131] (a) V. Balzani, A. Credi, M.Venturi, *ChemPhysChem* **2003**, *4*, 49–59. (b) A.Credi, *Angew. Chem. Intl. Ed.* **2007**, *46*, 5472–5475.

[132] L. W. Tutt, T. F. Boggess, *Prog. Quant. Electr.* **1993**, *17*, 299–338.

[133] J. W. Perry, in *Nonlinear Optics of Organic Molecules and Polymers*; Eds.: Nalwa, H. S.; Miyata, S.; CRC Press: Boca Raton, 1997, p. 813–840.

[134] E. W. Van Stryland, D. J. Hagan, T. Xia, A. A. Said, in *Nonlinear Optics of Organic Molecules and Polymers*; Eds.: Nalwa, H. S.; Miyata, S.; 1997, p. 841–860.

[135] Y.-P. Sun, J. E. Riggs, *Intern. Rev. Phys. Chem.* **1999**, *18*, 43–90.

[136] R. A. Ganeev, *J Opt. A: Pure Appl. Opt.* **2005**, *7*, 717–733.

[137] J. C. Crano, W. S. Kwak, C. N. Welch in ref. 7, p. 31–79.

[138] (a) S. W. Hell, in *Topics in Fluorescence Spectroscopy*; J. R.Lakowicz, , Ed.; Plenum Press: New York, 1997, 361–422. (b) S. W. Hell, *Nat. Biotechnol.* **2003**, *21*, 1347–1355. (c) S. W. Hell, M. Dyba, S.Jakobs, *Curr. Opinion Neurobiol.* **2004**, *14*, 599–609. (d) S. W. Hell, *Phys. Lett. A* **2004**, *326*, 140–145. (e) S. W.Hell, K. I. Willig, M. Dyba, S. Jakobs, L. Kastrup, V.Westphal, in *Handbook of Biological Confocal Microscopy*; J. B.Pawley, , Ed.; Springer: New York, 2006, p. 571–579. (f) S. W. Hell, L. Kastrup, *Nachr. Chem.* **2007**, *55*, 47–50. (g) S. W. Hell, *Science* **2007**, *316*, 1153–1158. (h) S. W. Hell, A.Schönle, *Science of Microscopy*; P. W. Hawkes, J. C. H.Spence, , Eds.; Springer: New York, 2007, vol. 2, p. 790–834. (g) S. W. Hell, *Nat. Methods* **2009**, *6*, 24–32.

[139] M. Bates, B. Huang, , X. Zhuang*Curr. Op. Chem. Biol.* **2008**, *12*, 505–514

[140] M. Fernández-Suárez, A. Y. Ting, *Nat. Rev. Mol. Cell. Biol.* **2008**, *9*, 929–943.

[141] J. Lippincott-Schwartz, S.Manley, *Nat. Methods* **2009**, *6*, 21–23.

[142] M. Galletta, S. Campagna, M. Quesada, G. Ulrich, R.Ziessel, *Chem. Commun.* **2005**, 4222–4224.

[143] (a) A. J. Myles, N. R. Branda, *J. Am. Chem. Soc.* **2001**, *123*, 177–178. (b) S. D. Straight, J. Andréasson, G. Kodis, S. Bandyopadhyay, R. H. Mitchell, T. A. Moore, A. L. Moore, D. Gust, *J. Am. Chem. Soc.* **2005**, *127*, 9403–9409. (c) L-H. Liu, K. Nakatani, R. Pansu, J.-J. Vachon, P. Tauc, E.Ishow, *Adv. Mater.* **2007**, *19*, 433–436. (d) M. Berberich, A.-M. Krause, M. Orlandi, F. Scandola, F. Würthner, *Angew. Chem. Int. Ed.* **2008**, *47*, 6616–6619.

[144] (a) J. L. Bahr, G. Kodis, L. de la Garza, S. Lin, A. L. Moore, T. A. Moore, D.Gust, *J. Am. Chem. Soc.* **2001**, *123*, 7124–7133. (b) A. Myles, N. R. Branda, *Adv. Funct. Mater.* **2002**, *12*, 167–173. (c) L. Giordano, T. M. Jovin, M. Irie, E. A.Jares-Erijman, *J. Am. Chem. Soc.* **2002**, *124*, 7481–7489. (d) E. J. Harbron, D. A. Vicente, M. T. Hoyt, *J. Phys. Chem. B* **2004**, *108*, 18789–18792. (e) M. Bossi, V. Belov, S. Polyakova, S. W. Hell, *Angew. Chem. Int. Ed.* **2006**, *45*, 7462–7465. (f) R. T. Jukes, V. Adamo, F. Hartl, P. Belser, L.De Cola, *Inorg. Chem.* **2004**, *43*, 2779–2792.

[145] (a) M. Irie, T. Fukaminato, T. Sasaki, N. Tamai, T.Kawai, *Nature* **2002**, *420*, 759–760. (b) T. Fukaminato, T. Umemoto, Y. Iwata, M. Irie, *Chem. Lett.* **2005**, *34*, 676–677. (c) T. Fukaminato, T. Umemoto, Y. Iwata, S. Yokojima, M. Yoneyama, S. Nakamura, M.Irie, *J. Am. Chem. Soc.* **2007**, *129*, 5932–5938.